OPEN ACCESS

University of
BRISTOL

This electronic thesis or dissertation has been downloaded from Explore Bristol Research, http://research-information.bristol.ac.uk

Author:
Wiles, Tim C W

Title:
Novel, Low-Cost Computational Methods for Predicting the Electronic Structure of Molecules

Novel, Low-Cost Computational Methods for Predicting the Electronic Structure of Molecules

Timothy Wiles

17 Oct 2019

A dissertation submitted to the University of Bristol in accordance with the requirements for award of the Doctor of Philosophy

in the

Faculty of Science

School of Chemistry

Word count: 41551

Abstract

In this thesis, we search for ways to make density functional theory (DFT) more accurate. Inspired by the $w(r_{12})$ methods developed for coupled cluster theory, we present Unsöld-W12 (UW12): an approximation to the correlation energy of molecules that is an explicit functional of the single-particle reduced density matrix. The approximation resembles one part of modern explicitly-correlated second-order Møller-Plesset (MP2) theory, and is intended as an alternative to MP2 in double-hybrid (rung-5) exchange-correlation functionals. Orbital optimization with UW12 is straightforward, and the UW12 energy is evaluated without a double summation over unoccupied orbitals, leading to a faster basis-set convergence than is seen in double-hybrid functionals. We show that the formal scaling for evaluating the UW12 energy is N^4 (where N represents the size of the system), and describe how UW12 may be implemented in electronic structure codes.

Having defined the UW12 correlation model, we suggest three new hybrid (rung-4) exchange-correlation functionals: XCH-BLYP-UW12, rBLYP-osUW12, and BLYP-osUW12. All three of these new functionals reduce (to varying degrees) the delocalization error present in DFT.

We conclude by suggesting ways in which UW12 functionals could be improved in the future in terms of both accuracy and computational cost. They may soon outperform double-hybrid (rung-5) functionals in both these areas.

Acknowledgments

I wish to thank every member of my research group, in addition to my Center for Doctoral Training,[1] my friendship group, my family, and my church.[2] Their continued support, encouragement, direction, and interest in the work was exactly what I needed at every step. The administration team at Bristol University made everything run smoothly and seamlessly.

I give special thanks to Jesus Christ: My lord (even though I don't always obey him perfectly), my saviour, and my friend. When I started this PhD I didn't believe he even existed. But when I was ready (and asked him to come into my life) he showed me things I never thought were possible. And he gave me a new life of peace, satisfaction, joy, purpose, hope, and rest that he says will last forever.

---

[1]Center for Doctoral Training in Theory and Modelling in Chemical Sciences (TMCS). `http://www.tmcs.ac.uk/`

[2]City Church Bristol `http://www.citychurch.org.uk/`

Declaration of Authorship

I declare that the work in this dissertation was carried out in accordance with the requirements of the University's Regulations and Code of Practice for Research Degree Programmes and that it has not been submitted for any other academic award. Except where indicated by specific reference in the text, the work is the candidate's own work. Work done in collaboration with, or with the assistance of, others, is indicated as such. Any views expressed in the dissertation are those of the author.

Signed: **Date:**

Contents

Contents

List of Figures

List of Tables

List of Listings

Nomenclature

1-RDM	single-particle reduced density matrix
CAM	Coulomb-attentuated method
CEDA	common energy-denominator approximation
DFT	Density-functional theory
GTG	Gaussian-type geminal
GTO	Gaussian-type orbital
HF	Hartree-Fock
KS-DFT	Kohn-Sham density-functional theory
LDA	local (spin-)density approximation
LFX	local-Fock-exchange
MAE	Mean Absolute Error
MP2	Second-order Møller-Plesset theory
MP2-F12	Explicitly-correlated second-order Møller-Plesset theory
nl	non-local
OEP	optimized effective potential
os	opposite-spin
PCG	primitive Cartesian Gaussian
PT2	Second-order perturbation theory.
RMSE	root-mean-square error
SCF	self-consistent-field

SGG   single-Gaussian geminal

STG   Slater-type geminal

UW12   Unsöld-W12

XCH   exchange-and-correlation hybrid

1. Background

1.1. Introduction

Density functional theory (DFT) is a widely-used computational method for predicting the properties of molecules and solids. It has been applied in almost every area of physics and chemistry: from batteries [2], to proteins [3], to light-harvesting molecules [4]. Its success is due to its low scaling in computational complexity with system size, when compared with more accurate (and more expensive) wavefunction-based methods such as coupled cluster theory [5]. This enables chemists to simulate molecules with hundreds or even thousands of atoms [6]. DFT is in principle an exact method for obtaining the ground-state properties of a system of nuclei and electrons. However, in practice, approximations are used, such as the choice of exchange-correlation functional $E_{xc}[\rho]$, and the choice of basis-set $\{\alpha(\mathbf{r})\}$.

Although DFT approximations have been steadily improving in accuracy across chemistry [7, 8], all approximate functionals suffer from non-integer-charge errors (also known as delocalization errors) and non-integer-spin errors (also known as constancy violations). These lead to both quantitatively- and qualitatively-incorrect behavior for some systems [9, 10, 11, 12, 13]. In addition — unlike wavefunction-based methods — DFT approximations are not systematically-improvable. This means that there is no obvious way to derive new correction terms ("ingredients") that are guaranteed to improve the accuracy of a given DFT approximation for all systems

[8, 14]. Nevertheless, it is common to categorize DFT functionals according to the ingredients they contain on a "Jacob's ladder", with more complex (and more accurate) functionals at the top. Functionals on the lower 3 "rungs" of the ladder are known as pure DFT functionals, and functionals on the upper 2 rungs are known as hybrid functionals.

We now proceed to give a brief outline of Kohn-Sham DFT. We review some of the existing hybrid DFT and double-hybrid DFT methods, and discuss their limitations.

1.2. The Born-Oppenheimer Approximation

In this thesis, we use Hartree atomic units throughout (unless otherwise stated), such that $m_{\text{el}} = e = \hbar = 1/(4\pi\epsilon_0) = 1$. Consider the problem of finding the non-relativistic ground-state energy of a molecule with nuclei at positions $\{\mathbf{R}_I\}$ with charges $\{Z_I\}$ and masses $\{M_I\}$, and electrons at positions $\{\mathbf{r}_i\}$. The Hamiltonian can be written as

$$H = -\sum_I \frac{1}{2M_I}\nabla_I^2 + \frac{1}{2}\sum_{I\neq J}\frac{Z_I Z_J}{|\mathbf{R}_I - \mathbf{R}_J|} - \sum_i \frac{1}{2}\nabla_i^2 - \sum_I\sum_i \frac{Z_I}{|\mathbf{R}_I - \mathbf{r}_i|} + \frac{1}{2}\sum_{i\neq j}\frac{1}{|\mathbf{r}_i - \mathbf{r}_j|} \quad (1.1)$$

$$= T_{\text{n}} + U_{\text{n,n}} + \underbrace{T_{\text{el}} + U_{\text{el,n}} + U_{\text{el,el}}}_{H_{\text{el}}(\{\mathbf{R}_I\})}. \quad (1.2)$$

The Coulomb repulsion between the nuclei is given by

$$U_{\text{n,n}} = \frac{1}{2}\sum_{I\neq J}\frac{Z_I Z_J}{|\mathbf{R}_I - \mathbf{R}_J|}. \quad (1.3)$$

In the Born-Oppenheimer approximation, the masses of the nuclei $\{M_I\}$ are assumed to be much larger than the mass of an electron m_{el}. The wavefunction of the whole system is then

written as a parametric product

$$\Psi(\{\mathbf{R}_I\}, \{\mathbf{r}_i\}) \approx \chi(\{\mathbf{R}_I\})\Phi(\{\mathbf{r}_i\} \mid \{\mathbf{R}_I\}) \tag{1.4}$$

where $\chi(\{\mathbf{R}_I\})$ is the nuclear wavefunction, and $\Phi(\{\mathbf{r}_i\} \mid \{\mathbf{R}_I\})$ is the electronic wave-function at a given (fixed) nuclear geometry $\{\mathbf{R}_I\}$. The electronic wave-function satisfies

$$H_{\text{el}}(\{\mathbf{R}_I\})\Phi(\{\mathbf{r}_i\} \mid \{\mathbf{R}_I\}) = E_{\text{el}}(\{\mathbf{R}_I\})\Phi(\{\mathbf{r}_i\} \mid \{\mathbf{R}_I\}) \tag{1.5}$$

and is normalized such that

$$\langle \Phi(\{\mathbf{R}_I\}) | \Phi(\{\mathbf{R}_I\}) \rangle = 1 \tag{1.6}$$

where angle brackets $\langle \rangle$ denote integration over electronic coordinates. Substituting Eqns. 1.2, 1.4, and 1.5 into the Schrödinger equation

$$H\Psi = E\Psi \tag{1.7}$$

and integrating out the electronic coordinates leads to

$$\sum_I -\frac{1}{2M_I}\nabla_I^2\chi(\{\mathbf{R}_I\}) - \frac{1}{2M_I}\left\langle \Phi(\{\mathbf{R}_I\})\middle|\nabla_I^2\Phi(\{\mathbf{R}_I\})\right\rangle \chi(\{\mathbf{R}_I\})$$

$$-2\frac{1}{2M_I}\left\langle \Phi(\{\mathbf{R}_I\})|\nabla_I\Phi(\{\mathbf{R}_I\})\right\rangle \cdot \nabla_I\chi(\{\mathbf{R}_I\})$$

$$+\left[E_{\text{el}}(\{\mathbf{R}_I\}) + U_{\text{n,n}}(\{\mathbf{R}_I\})\right]\chi(\{\mathbf{R}_I\}) = E\,\chi(\{\mathbf{R}_I\}) \tag{1.8}$$

where the notation is such that operators are confined to within angle brackets $\langle \nabla \rangle$. We now use the convention that $|\Phi(\{\mathbf{R}_I\})\rangle$ is normalised for all $\{\mathbf{R}_I\}$ such that

$$\langle \Phi(\{\mathbf{R}_I\}) | \Phi(\{\mathbf{R}_I\}) \rangle = 1. \tag{1.9}$$

Acting on both sides of Eqn 1.9 with the ∇_I operator we see that

$$\langle \Phi(\{\mathbf{R}_I\}) | \nabla_I \Phi(\{\mathbf{R}_I\}) \rangle + \langle \nabla_I \Phi(\{\mathbf{R}_I\}) | \Phi(\{\mathbf{R}_I\}) \rangle = 0. \tag{1.10}$$

If there are no conical intersections, then $\Phi(\{\mathbf{R}_I\})$ may be chosen to be real for all $\{\mathbf{R}_I\}$. Thus

$$\langle \Phi(\{\mathbf{R}_I\}) | \nabla_I \Phi(\{\mathbf{R}_I\}) \rangle = \langle \nabla_I \Phi(\{\mathbf{R}_I\}) | \Phi(\{\mathbf{R}_I\}) \rangle \tag{1.11}$$

and hence

$$\langle \Phi(\{\mathbf{R}_I\}) | \nabla_I \Phi(\{\mathbf{R}_I\}) \rangle = 0 \tag{1.12}$$

everywhere [15].

The $\langle \Phi(\{\mathbf{R}_I\}) | \nabla_I^2 \Phi(\{\mathbf{R}_I\}) \rangle$ term in Eqn 1.8 is known as the diagonal Born-Oppenheimer correction, and is usually small enough in magnitude to be neglected. See Ref [16] for a discussion of the magnitude of the diagonal Born-Oppenheimer correction when applied to small molecules. We thus arrive at an effective Schrödinger equation for the nuclear wavefunction

$$\sum_I -\frac{1}{2M_I} \nabla_I^2 \chi(\{\mathbf{R}_I\}) + V_n(\{\mathbf{R}_I\}) \chi(\{\mathbf{R}_I\}) = E \, \chi(\{\mathbf{R}_I\}) \tag{1.13}$$

where the potential energy surface $V_n(\{\mathbf{R}_I\})$ is defined as

$$V_n(\{\mathbf{R}_I\}) = E_{el}(\{\mathbf{R}_I\}) + U_{n,n}(\{\mathbf{R}_I\}).$$ (1.14)

The total energy E can be decomposed as

$$E = V_n\left(\{\mathbf{R}_I\}_{eq}\right) + E_{ZPE} = E_{el}\left(\{\mathbf{R}_I\}_{eq}\right) + U_{n,n}\left(\{\mathbf{R}_I\}_{eq}\right) + E_{ZPE}$$ (1.15)

where $E_{el}\left(\{\mathbf{R}_I\}_{eq}\right)$ (which we will henceforth refer to simply as E_{el}) is the electronic energy at the equilibrium geometry $\{\mathbf{R}_I\}_{eq}$.

1.3. Zero-Point Energy

E_{ZPE} is the zero-point energy of the nuclei over the potential energy surface, and results from the quantum nature of the nuclei. It can be thought of as the kinetic energy of the nuclei at the equilibrium geometry arising from the ground state vibrational motion of the nuclei. In all the test sets mentioned in this thesis, values for E_{ZPE} have been estimated and subtracted from the reference single-point energy values. Zero-point energies were estimated using highly accurate benchmark electronic structure methods such as the W4 method [17, 18, 19].

1.4. Wavefunction-based Methods

The W4 method is a highly-accurate and highly-parameterised wavefunction-based electronic structure method, and can be used to obtain sub - kJ mol^{-1} accuracy for thermochemistry

[17, 18, 19]. It includes zero-point energy estimation (as discussed briefly in Section 1.3) and basis-set corrections. A discussion of wavefunction-based methods is beyond the scope of this thesis, but we will introduce them briefly since we use them to benchmark our density-functional results later on.

Wavefunction-based methods are so-called because the formulae for estimating the electronic energy E_{el} are derived by considering and operating on the electronic wavefunction

$$\Phi(\{\mathbf{x}_i\} | \{\mathbf{R}_I\}) = \Phi\left(\mathbf{x}_1, \mathbf{x}_2, \ldots, \mathbf{x}_{N_{el}} | \{\mathbf{R}_I\}\right) \tag{1.16}$$

at a particular (fixed) nuclear configuration $\{\mathbf{R}_I\}$, where $\mathbf{x}_i$ represents the space- and spin-coordinates of electron i. From here on in we omit the nuclear coordinates $\{\mathbf{R}_I\}$ from the electronic wavefunction. We see immediately that Φ is a function of $4N_{el}$ variables, where N_{el} is the number of electrons in the molecule, and the factor 4 appears since each electron is free to move in 3-dimensional space and has a spin-variable. Nowadays it is routine to perform ab-initio electronic structure calculations on molecules with hundreds (if not thousands) of electrons, and hence the full wavefunction Φ can be complex to write down and work with. In wavefunction-based methods it is common instead to write Φ as a sum of products of single-particle wavefunctions known as "molecular orbitals" $\phi_i^D(\mathbf{x})$

$$\Phi\left(\mathbf{x}_1, \mathbf{x}_2, \ldots, \mathbf{x}_{N_{el}}\right) = \sum_D c_D \sum_P \epsilon_P \, \phi_1^D\left(\mathbf{x}_{P_1}\right) \phi_2^D\left(\mathbf{x}_{P_2}\right) \ldots \phi_{N_{el}}^D\left(\mathbf{x}_{P_{N_{el}}}\right) \tag{1.17}$$

$$= \sum_D c_D \, |D\rangle \tag{1.18}$$

where $\{c_D\}$ are coefficients, and the intermediate wave-functions $|D\rangle$ are known as "Slater

determinants". The Slater determinants can also be written as

$$|D\rangle = \prod_i \left(a_i^D\right)^\dagger |\rangle \tag{1.19}$$

where $|\rangle$ is the state with no electrons and the $\left(a_i^D\right)^\dagger$ are operators that create an electron in the orbital $\phi_i^D(\mathbf{x})$. The sequences P in Eqn 1.17 are permutations (orderings) of indices from 1 to N_{el}, and the symbol ϵ_P is an anti-symmetrization factor that is either -1 or 1 and takes care of the anti-symmetry of the wavefunction Φ on interchanging two electrons

$$\Phi\left(\mathbf{x}_1, \mathbf{x}_2, \mathbf{x}_3, \ldots, \mathbf{x}_{N_{\text{el}}}\right) = -\Phi\left(\mathbf{x}_2, \mathbf{x}_1, \mathbf{x}_3, \ldots, \mathbf{x}_{N_{\text{el}}}\right). \tag{1.20}$$

For instance, for $N_{\text{el}} = 3$, we have the permutations P

$$P = [1,2,3], [1,3,2], [2,1,3], [2,3,1], [3,1,2], [3,2,1]. \tag{1.21}$$

which have the corresponding ϵ_P values

$$\epsilon_P = 1, -1, 1, -1, 1, -1, 1, -1. \tag{1.22}$$

Each of the single-particle orbitals $\phi_i^D(\mathbf{x})$ can then be either expressed on a grid, or (more commonly for molecules) expanded in terms of a basis-set of single-particle wavefunctions $\{\alpha(\mathbf{r})\}$ known as "atomic-orbitals". The atomic-orbital basis-set $\{\alpha(\mathbf{r})\}$ contains a certain number of basis functions centred on each atom, with larger basis-sets containing more functions per atom – and hence a higher computational cost. Largers basis sets are more able to model the perturbations in the electronic structure that arise from atoms coming together to form molecules. The Dunning correlation-consistent cc-pVDZ and cc-pVTZ Gaussian atomic-orbital basis sets

are used in the W4 method [20, 21, 22, 23]. The W4 method also includes extrapolation methods known as basis-set corrections that estimate the value of the energy that would be obtained with an infinitely-large basis. In Section 1.9, we introduce Gaussian atomic-orbital basis-sets.

In theory, the sum over D in the right-hand-side of Eqn 1.17 is infinite for an infinitely-large atomic-orbital basis $\{\alpha(\mathbf{r})\}$. However, in practice it is found that most properties of molecules can be calculated to high accuracy using only a small set of determinants $|D\rangle$. The simplest wavefunction-based method in common use is the Hartree-Fock method. In the Hartree-Fock method, only the $D = 0$ term is retained and the electronic wavefunction Φ becomes expressed as a single determinant.

$$\Phi = |0\rangle = \prod_i (a_i)^\dagger \; |\rangle \,. \tag{1.23}$$

The occupied single-particle orbitals $\{\phi_i(\mathbf{x})\}$ can then be adjusted to minimize the expectation value of the Hartree-Fock ground-state energy $\langle 0|H_{\mathrm{el}}|0\rangle$ (see Section 1.11). Note that the Slater-determinant $|0\rangle$ is in general *not* an eigenfunction of the many-particle operator H_{el} in the Hilbert-space of all N_{el}-electron wave-functions Φ. It follows by the variational theorem that the Hartree-Fock ground-state energy $\langle 0|H_{\mathrm{el}}|0\rangle$ provides an upper-bound on the true ground-state energy E^0_{exact}

$$\langle 0|H_{\mathrm{el}}|0\rangle > E^0_{\mathrm{exact}}. \tag{1.24}$$

In more accurate methods (such as the coupled-cluster method), the inter-electronic energy $U_{\mathrm{el,el}}$ is estimated by "mixing" excited-state determinants ($D > 0$) with a reference ($D = 0$) Hartree-Fock determinant wavefunction. The success of the coupled-cluster method is in the use of algebraic techniques that enable the estimation of the sum of a large number of

determinants $|D\rangle$ in a single computational step. A detailed discussion of coupled-cluster is not needed here; suffice to say that even the simplest coupled-cluster methods in common use (such as coupled-cluster with singles and doubles, CCSD) involve summing together terms of the form

$$\langle pq|r_{12}^{-1}|rs\rangle \tau_{tu}^{rs} \tag{1.25}$$

where τ_{tu}^{rs} is some amplitude and $\langle pq|r_{12}^{-1}|rs\rangle$ is a molecular electron-electron integral (see Eqn 1.111). Since there are 6 indices in Eqn 1.25 enumerating single-particle orbitals (*pqrstu*), we will be required to perform on the order of N^6 multiplication operations in order to calculate all such terms (where N represents the size of the molecule). We hence say that the "formal scaling" of CCSD for evaluating E_{el} is N^6 [24]. One can see immediately that the number of computational operations required to find the energy of a 100-atom molecule is thus $10^6 = 1000000$ times the number needed for a 10-atom molecule. Although techniques exist for reducing this scaling – which involve neglecting contributions from sets of orbitals *pqrstu* that are spatially distant from one another [25] – an alternative strategy is to bypass Eqns 1.16 and 1.17 altogether, and to work from the outset with quantities involving fewer variables. This is the realm of density-functional theory (DFT).

1.5. Density-Functional Theory

Let us turn our attention to the electronic energy E_{el}, which can be written as

$$E_{el} = E_{T,el} + E_{el,n} + J + Q \ . \tag{1.26}$$

Let us examine each term in Eqn 1.26. The Coulomb attraction between the nuclei and the electrons — where the number of electrons per unit volume is $\rho(\mathbf{r})$ — is given by

$$E_{\text{el,n}} = \int d\mathbf{r} \underbrace{-\sum_I \frac{Z_I}{|\mathbf{R}_I - \mathbf{r}|}}_{V_{\text{el,n}}(\mathbf{r})} \rho(\mathbf{r}). \tag{1.27}$$

All integrals over real space variables $\mathbf{r}$ in this thesis are assumed to be over the whole simulation cell in three spatial dimensions. The (classical) Coulomb repulsion between the electrons in the Hartree approximation is given by

$$J = \frac{1}{2} \int d\mathbf{r}_1 \rho(\mathbf{r}_1) \underbrace{\int d\mathbf{r}_2 \frac{\rho(\mathbf{r}_2)}{|\mathbf{r}_1 - \mathbf{r}_2|}}_{V_J(\mathbf{r}_1)}. \tag{1.28}$$

Note that Eqn 1.28 contains a contribution J_{self} arising from the interaction energy of each electron with itself. This is known as self-interaction error. In practical Hartree approximation calculations, it is common to remove J_{self} orbital-by-orbital using Eqn 1.112, whereas in Hartree-Fock and density-functional theory calculations the self-interaction is removed (partly or fully) by the exchange term E_{x}. See Section 1.17 for a more complete discussion.

We have not yet given formulae for the non-classical electron-electron interaction energy Q and the electronic kinetic energy $E_{T,\text{el}}$. Of these, $E_{T,\text{el}}$ is usually far larger. The basic premise of DFT is that all the information about the many-electron system is contained in the electron density $\rho(\mathbf{r})$. This is known as the "first Hohenberg-Kohn" theorem, and can be stated as [26]

> "In the ground-state the electron density $\rho(\mathbf{r})$ uniquely determines all properties of H, and hence uniquely determines the total energy E."

This theorem has an important corrolary, often referred to as the "second Hohenberg-Kohn

theorem" or the "variational Hohenberg-Kohn theorem", and can be stated as [26]

"The exact ground-state density $\rho(\mathbf{r})$ is the the N-particle density that minimizes

the energy E."

In principle, if one can obtain exact functional forms for Q and $E_{T,\text{el}}$ in terms of $\rho(\mathbf{r})$, then

the problem is solved: one then simply minimizes the energy E with respect to the electron

density. Such an approach is known as orbital-free density-functional theory. However, "exact"

functional forms for Q and $E_{T,\text{el}}$ (yielding accurate energies for any molecular system) remain

elusive [8], and so it is far more common to use the framework of Kohn-Sham density functional

theory (KS-DFT). Due to the popularity of the Kohn-Sham method, all references to DFT in

this thesis henceforth refer to KS-DFT.

1.6. Kohn-Sham Density Functional Theory

In KS-DFT, one obtains Q and $E_{T,\text{el}}$ by using the properties of an imaginary non-interacting

system of electrons known as the Kohn-Sham auxiliary system. The auxiliary system has

the same electron density $\rho(\mathbf{r})$ as the true system but the electrons in the auxiliary system

do not interact with one another directly. Instead, each electron moves in the "mean-field"

potential $V_J(\mathbf{r}) + V_Q(\mathbf{r}, \mathbf{r}')$ generated by the other electrons. Note that in many common density

functionals the interaction of an electron with *itself* is not fully canceled out between the J

and Q terms. The potential $V_J(\mathbf{r}) + V_Q(\mathbf{r}, \mathbf{r}')$ experienced by electron i thus contains a term

that comes from electron i. This is known as "self-interaction-error", and is discussed in

Section 1.17.

The "mean-field" potential $V_J(\mathbf{r}) + V_Q(\mathbf{r}, \mathbf{r}')$ is then optimized self-consistently (using the

procedure outlined in Section 1.10) until convergence is reached. Since the electrons in the

non-interacting (NI) auxiliary system are independent quantum particles, the Hamiltonian for

the NI system can be written as a sum of one-electron operators

$$H_{\text{el}}^{\text{NI}} = \sum_{pq} h_{pq}^{\text{NI}} \, a_p^\dagger a_q \tag{1.29}$$

and the ground state of the auxiliary system is thus a Slater determinant (see Eqn 1.19)

$$|0\rangle = \left(\prod_i a_i^\dagger \right) |\rangle \, . \tag{1.30}$$

The orbitals $\{\phi_i(\mathbf{x})\}$ are known as the occupied Kohn-Sham spin-orbitals. We use spin-orbitals throughout unless otherwise stated, and use $\mathbf{x}$ to refer to both space ($\mathbf{r}$) and spin (σ) coordinates. It is often helpful to characterize the auxiliary system in terms of the single-particle reduced density matrix (1-RDM)

$$\rho(\mathbf{x}|\mathbf{x}') = \sum_i \phi_i^\star(\mathbf{x}) \phi_i(\mathbf{x}') \, . \tag{1.31}$$

Let us now assume that the electronic kinetic energy of the auxiliary system $E_{T,\text{el}}^{\text{NI}}$ is close to the electronic kinetic energy of the true system $E_{T,\text{el}}$, such that

$$E_{T,\text{el}} \approx E_{T,\text{el}}^{\text{NI}} \tag{1.32}$$

$$= \langle 0 | T_{\text{el}} | 0 \rangle \tag{1.33}$$

$$= \sum_i \int d\mathbf{r} \, \phi_i^\star(\mathbf{r}) \left(-\frac{1}{2} \nabla_{\mathbf{r}}^2 \right) \phi_i(\mathbf{r}) \, . \tag{1.34}$$

The error $\left(E_{T,\text{el}} - E_{T,\text{el}}^{\text{NI}} \right)$ made in this approximation is usually combined with the Q term to form the exchange-correlation energy

$$E_{\text{xc}} = Q + \left(E_{T,\text{el}} - E_{T,\text{el}}^{\text{NI}} \right) \tag{1.35}$$

and the total electronic energy can thus be written as

$$E_{\text{el}} = \langle 0 | T_{\text{el}} | 0 \rangle + E_{\text{el,n}} + J + E_{\text{xc}} \tag{1.36}$$

$$= \langle 0 | T_{\text{el}} | 0 \rangle + \int d\mathbf{r} \, V_{\text{el,n}}(\mathbf{r}) \rho(\mathbf{r}) + \frac{1}{2} \int d\mathbf{r} \, V_J(\mathbf{r}) \rho(\mathbf{r}) + E_{\text{xc}} [\rho(\mathbf{r} | \mathbf{r}')] . \tag{1.37}$$

The first 3 terms in Eqn 1.36 can also be written in terms of individual Kohn-Sham orbitals as

$$\langle 0 | T_{\text{el}} | 0 \rangle = \sum_i \int d\mathbf{r} \, \phi_i^\star(\mathbf{r}) \left(-\frac{1}{2} \nabla_{\mathbf{r}}^2 \phi_i(\mathbf{r}) \right) \tag{1.38}$$

$$= \sum_i \left\langle i \left| -\frac{1}{2} \nabla_{\mathbf{r}}^2 \right| i \right\rangle \tag{1.39}$$

$$E_{\text{el,n}} = \sum_i \int d\mathbf{r} \, \phi_i^\star(\mathbf{r}) V_{\text{el,n}}(\mathbf{r}) \phi_i(\mathbf{r}) \tag{1.40}$$

$$= \sum_i \left\langle i \left| V_{\text{el,n}}(\mathbf{r}) \right| i \right\rangle \tag{1.41}$$

$$J = \frac{1}{2} \int d\mathbf{r}_1 \int d\mathbf{r}_2 \, \phi_i^\star(\mathbf{r}_1) \phi_j^\star(\mathbf{r}_2) r_{12}^{-1} \phi_i(\mathbf{r}_1) \phi_j(\mathbf{r}_2) \qquad \text{where } r_{12} = |\mathbf{r}_1 - \mathbf{r}_2|$$
$$\tag{1.42}$$

$$= \sum_{ij} \frac{1}{2} \langle ij | r_{12}^{-1} | ij \rangle \tag{1.43}$$

$$= \sum_{ij} \frac{1}{2} \left(ii | r_{12}^{-1} | jj \right) \qquad \text{Using Mulliken notation.}$$
$$\tag{1.44}$$

Scientists have worked for over half a century [14] developing simple functional forms for $E_{\text{xc}}[\rho]$. Since the exact functional form of E_{xc} is unknown for an arbitrary molecular system, the problem remains to find approximate forms for E_{xc}. It is the choice of approximate form for E_{xc} that leads to the plethora of density functionals available in chemistry and physics today.

Note that the assumption in Eqn 1.32 is not necessary for the Kohn-Sham method to be successful: provided of course that the exchange-correlation functional E_{xc} models well the

difference $\left(E_{T,\text{el}} - E_{T,\text{el}}^{\text{NI}}\right)$ between the true kinetic energy and the non-interacting kinetic energy. If the *exact* functional E_{xc} were known, then the Kohn-Sham method would also yield the exact ground-state energy and density.

1.6.1. The Kohn-Sham Equations

We are now in the position to solve the minimization problem resulting from the variational Hohenberg-Kohn theorem (see Section 1.5), and find the set of orbitals $\{\phi_i(\mathbf{x})\}$ that minimizes the energy E, subject to the constraint that each orbital ϕ_i is normalized

$$\int d\mathbf{r} \, |\phi_i(\mathbf{r})|^2 = 1. \tag{1.45}$$

We introduce Lagrange multipliers $\{\epsilon_i\}$ that ensure that Eqn 1.45 is satisfied, and thus define the Lagrangian X

$$X = E_{\text{el}} - \sum_i \epsilon_i \left(\int d\mathbf{r} \, |\phi_i(\mathbf{r})|^2 - 1\right). \tag{1.46}$$

The orbitals $\{\phi_i\}$ that minimize E_{el} subject to the constraint (Eqn 1.45) thus satisfy (using Eqn 1.37)

$$0 = \frac{\delta X}{\delta \phi_i^\star(\mathbf{r})} \tag{1.47}$$

$$= \left(-\frac{1}{2}\nabla_{\mathbf{r}}^2\right)\phi_i(\mathbf{r}) + V_{\text{el,n}}(\mathbf{r})\phi_i(\mathbf{r}) + V_J(\mathbf{r})\phi_i(\mathbf{r}) + \int d\mathbf{r}' \, V_{\text{xc}}^{\sigma_i}(\mathbf{r}, \mathbf{r}')\phi_i(\mathbf{r}') - \epsilon_i\phi_i(\mathbf{r}) \tag{1.48}$$

where σ_i is the spin of orbital i and where the exchange-correlation potential $V_{\text{xc}}^{\sigma}(\mathbf{r}, \mathbf{r}')$ is defined as

$$V_{\text{xc}}^{\sigma}(\mathbf{r}, \mathbf{r}') = \frac{\delta E_{\text{xc}}}{\delta \rho^{\sigma}(\mathbf{r}|\mathbf{r}')}. \tag{1.49}$$

Rearranging Eqn 1.48 we arrive at the Kohn-Sham equations

$$\left(-\frac{1}{2}\nabla_{\mathbf{r}}^2\right)\phi_i(\mathbf{r}) + V_{\text{el,n}}(\mathbf{r})\phi_i(\mathbf{r}) + V_J(\mathbf{r})\phi_i(\mathbf{r}) + \int d\mathbf{r}' \, V_{\text{xc}}^{\sigma_i}(\mathbf{r}, \mathbf{r}')\phi_i(\mathbf{r}') = \epsilon_i\phi_i(\mathbf{r}). \tag{1.50}$$

The potentials V_J and V_{xc} both depend on $\rho(\mathbf{x}|\mathbf{x}')$, so these equations must be solved self-consistently. We return to this problem in Section 1.10.

1.7. The Local-Density Approximation

The simplest form of E_{xc} is known as the local (spin-)density approximation (LDA)

$$E_{\text{xc}}^{\text{LDA}} = \int d\mathbf{r}\epsilon_{\text{xc}}^{\text{LDA}}\left(\rho^{\uparrow}(\mathbf{r}), \rho^{\downarrow}(\mathbf{r})\right) \tag{1.51}$$

where the two-variable function $\epsilon_{\text{xc}}^{\text{LDA}}\left(\rho^{\uparrow}, \rho^{\downarrow}\right)$ is the exchange-correlation energy per-unit-volume of a fully-interacting uniform-electron-gas with $\rho^{\uparrow}(\rho^{\downarrow})$ spin-up (spin-down) electrons per unit volume. The uniform-electron-gas is simple model system with $\rho^{\uparrow}$ spin-up and $\rho^{\downarrow}$ spin-down electrons per unit volume in an infinitely large box. The electrons are not confined to any external potential and are free to move wherever they wish. Since the density and potential are uniform, the Kohn-Sham orbitals $\phi_{\mathbf{k}}(\mathbf{r})$ are thus solutions to the free-particle Schroedinger

equation

$$-\frac{1}{2}\nabla_{\mathbf{r}}^2 \phi_{\mathbf{k}}(\mathbf{r}) = \epsilon_{\mathbf{k}}\phi_{\mathbf{k}}(\mathbf{r}).$$ (1.52)

The solutions to Eqn 1.52 in a cubic box of side length L with periodic boundary conditions are plane waves of the form

$$\phi_{\mathbf{k}}(\mathbf{r}) = N_{\mathbf{k}}\exp[-i\mathbf{k}\cdot\mathbf{r}]$$ (1.53)

where $\{\mathbf{k}\}$ are vectors in reciprocal space of the form

$$\left(m_x\frac{2\pi}{L}, \quad m_y\frac{2\pi}{L}, \quad m_z\frac{2\pi}{L}\right)$$ (1.54)

with (m_x, m_y, m_z) integers (positive, negative, or zero). The normalisation constant $N_{\mathbf{k}}$ is chosen such that

$$\int_\Omega d\mathbf{r}\, \phi_{\mathbf{k}}^\star(\mathbf{r})\phi_{\mathbf{k}}(\mathbf{r}) = 1$$ (1.55)

where $\Omega = L^3$ is the volume of the box. The orbital eigenvalues (energies) are given by

$$\epsilon_{\mathbf{k}} = -\frac{k^2}{2}.$$ (1.56)

The problem can then be simplified by taking the limit where the box side-length $L \to \infty$. All sums over $\mathbf{k}$ points can then be calculated as integrals.

Note that thus far we have considered the electrons as being non-interacting. A fully-interacting electronic structure method (such as quantum-Monte-Carlo) is needed in order to determine the true ground-state energy of a uniform-electron-gas at a given electron density $(\rho^\uparrow, \rho^\downarrow)$ [27].

The full interacting exchange-correlation energy per unit volume ϵ_{xc}^{LDA} can be decomposed as

$$\epsilon_{xc}^{LDA}\left(\rho^\uparrow, \rho^\downarrow\right) = \epsilon_x^S\left(\rho^\uparrow, \rho^\downarrow\right) + \epsilon_c^{VWN}\left(\rho^\uparrow, \rho^\downarrow\right) \tag{1.57}$$

where ϵ_x^S is the Hartree-Fock exchange energy per unit volume. For this system, the exchange energy ϵ_x^S can be calculated analytically and is given by [28]

$$\epsilon_x^S\left(\rho^\uparrow, \rho^\downarrow\right) = -\frac{3}{2 \times 2^{\frac{2}{3}}}\left(\frac{3}{\pi}\right)^{\frac{1}{3}}\left[\rho_\uparrow^{\frac{4}{3}} + \rho_\downarrow^{\frac{4}{3}}\right]. \tag{1.58}$$

The correlation energy $\epsilon_c^{VWN}\left(\rho^\uparrow, \rho^\downarrow\right)$ is obtained by interpolating between reference quantum-Monte-Carlo calculations on uniform-electron-gases at various densities [27]. We thus have a method to obtain the ground state energy of any system with a density $(\rho^\uparrow(\mathbf{r}), \rho^\downarrow(\mathbf{r}))$ by dividing space $\{\mathbf{r}\}$ into an infinite number of small, non-overlapping boxes of electron density and then summing the exchange-correlation energies of each box together to find the full exchange-correlation energy E_{xc} (see Eqn 1.51). This approximation holds provided that the electron density varies slowly in space. However, we shall see that for most atoms and molecules this approximation does not hold, and the LDA thus gives poor estimates for atomic and molecular total energies.

1.8. Jacob's Ladder of Density Functionals

Despite its inaccuracies, LDA is widely used in both chemistry and solid-state physics to obtain fast estimates of electronic structure properties, due to its low formal computational scaling. A (naïve) self-consistent LDA calculation scales formally as N^3 where N represents the size of the system. As we have already mentioned, LDA is not sufficiently accurate to be used for most routine chemical problems, since the electron density $\rho(\mathbf{r})$ in a real molecule is highly

non-uniform. LDA systematically over-estimates atomization energies, predicts bond lengths that are too short, and over-binds intermolecular interactions [8, 7]. Over the past 30 years, functional developers have thus investigated taking new pieces of information ("ingredients") from the Kohn-Sham auxiliary system (*e.g.* $\nabla\rho(\mathbf{r})$, $\nabla^2\rho(\mathbf{r})$, $\rho(\mathbf{r}|\mathbf{r}')$) and using them to more accurately predict the energy of the true system. The formulae used to combine these ingredients together are developed by considering theoretical models (as in the case of the PBE functional [29]) or by fitting to large data-sets of molecules (as in the case of the M06-L functional [30]).

Gradient corrections use successive derivatives of the density ($\nabla\rho(\mathbf{r})$, $\nabla^2\rho(\mathbf{r})$, ...) to add information on the non-uniformity of the electron density to the exchange and correlation models. The first gradient corrections to be attempted were systematic power-series expansions in $|\nabla\rho|$, $|\nabla\rho|^2$, $|\nabla^2\rho|$, *etc.* known as gradient expansion approximations (GEAs). However, it was found that GEAs at low order led to little or no improvement in accuracy when added to LDA, and they were hence superceded by generalized gradient approximations (GGAs) [28]. GGAs express the exchange-correlation energy in the form

$$E_{\text{xc}}^{\text{GGA}} = \int d\mathbf{r}\, f\left(\rho(\mathbf{r}), \nabla\rho(\mathbf{r})\right) \tag{1.59}$$

where f is some general bivariate function. BLYP[1] and PBE [29] are among the most popular GGA exchange-correlation functionals used in chemistry today. A detailed discussion of GGAs is beyond the scope of this thesis – although following common double-hybrid methods (see Section 1.14) we use GGA ingredients in our proof-of-concept hybrid functionals in Chapters 5 and 6.

We refer to LDA as a "local" exchange-correlation functional since it can be written in the

---

[1]The BLYP functional is the combination of the Lee-Yang-Parr (LYP) correlation functional [31] with Becke's 1988 exchange functional [32].

form

$$E_{\text{xc}} = \int d\mathbf{r} \, \rho(\mathbf{r}) V_{\text{xc}}(\mathbf{r}) \tag{1.60}$$

where the potential V_{xc} at point $\mathbf{r}$ depends only on the electron density ρ at point $\mathbf{r}$. We refer to GGAs as "semi-local" functionals since they have a V_{xc} that depends only on the electron density at point $\mathbf{r}$ and points in the immediate vicinity of $\mathbf{r}$ (such that the gradient $\nabla\rho(\mathbf{r})$ may be calculated). Local and semi-local functionals are simple to implement and can achieve excellent computational scaling using real-space quadrature methods (see Section 1.19.2). However, as we shall see in the remainder of the thesis, there are some correlation effects that GGAs do not capture well.

In 2001, Perdew and Schmidt [39] proposed a "Jacob's ladder" categorization (shown in Table 1.1) of different density functionals based on the ingredients they contain. The functionals at the bottom of the ladder (including LDA) are the least computationally expensive but also the least accurate. Although there are new functionals being developed every year, the ladder reveals that there have been 4 major advances in the range of ingredients available since LDA.
.

Table 1.1.: Conventional Jacob's ladder for the categorization of density functional approx-
imations. Δ^{AE} (in $kcal \cdot mol^{-1}$) is a representative atomization energy error, taken as the
root-mean-square error (RMSE) of the W4-11 atomization energy test set with dispersion
corrections accounted for. Δ^{BH} (in $kcal \cdot mol^{-1}$) is a representative barrier height error, taken
as the RMSE of the BH76 barrier height test set with dispersion corrections accounted for.
Values are taken from the GMTKN55 database [7].
[†] *This functional is among the three most reliable functionals on the given rung according
to the 2017 GMTKN55 survey [7].*
[⋆] *See Footnote 1 on page 18.*
[◇] *See Section 1.7.*
[△] *See Footnote 2 on the next page.*

		Ingredient not present on lower rungs	Exchange model	Correlation model	Examples	Δ^{AE}	Δ^{BH}
rung-5	double-hybrid functionals and RPA functionals	unoccupied orbitals $\{\psi_a(\mathbf{r})\}$	non-local	non-local	B2-PLYP[33], DSD-BLYP[†][34]	2.72, 3.48	2.93, 1.94
rung-4	hybrid functionals	1-RDM $\rho(\mathbf{r}\|\mathbf{r}')$	non-local	semi-local[△]	B3LYP[35], ωB97X[†][36]	5.53, 5.12	6.45, 2.18
rung-3	meta-generalized gradient approximations	kinetic energy density $\tau(\mathbf{r})$	semi-local	semi-local	M06L[†][30], SCAN[†][37]	6.09, 5.76	4.92, 8.48
rung-2	generalized gradient approximations	gradient of the density $\nabla\rho(\mathbf{r})$	semi-local	semi-local	BLYP[⋆], revPBE[†][38]	24.29, 10.09	8.42, 9.21
rung-1	local (spin-)density approximations	density $\rho(\mathbf{r})$	local	local	LDA[◇]	-	-
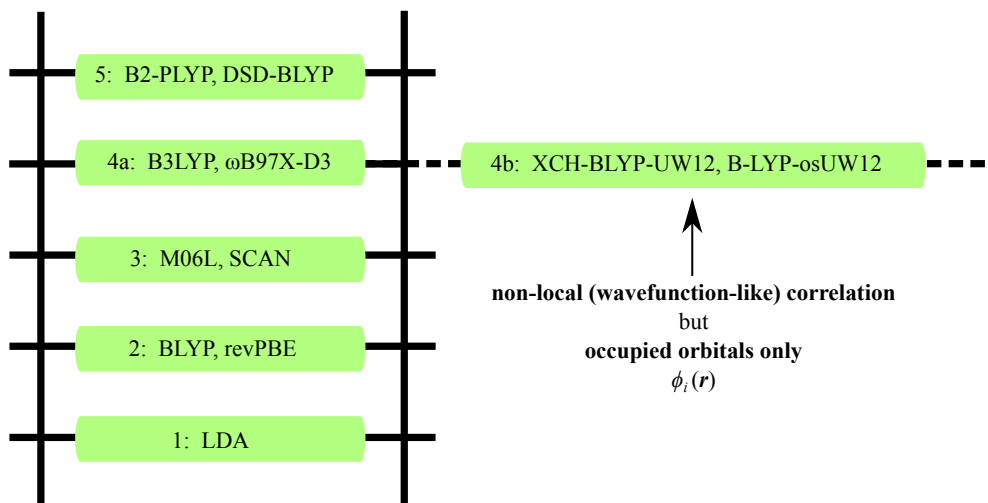
Figure 1.1.: Updated Jacob's ladder showing common examples of functionals on each rung. The new UW12 functionals presented in this thesis are shown on "rung-4b", since they do not fit into the categorization system shown in Table 1.1.

In this thesis, we will seek new functionals that contain non-local correlation (like a rung-5 functional) but only depend on occupied Kohn-Sham orbitals (like a rung-4 functional). The new functionals proposed in this thesis (in Chapters 5 and 6) thus do not fit into any of the categories shown in Table 1.1. We refer to them in this thesis as "rung-4b" hybrid functionals, and our updated Jacob's ladder is shown in Fig 1.1. We refer to conventional hybrid functionals containing only semi-local correlation (such as B3LYP and ωB97X[2]) as "rung-4a" functionals. A "semi-local" functional $E[\rho]$ depends only on the electron (spin-)density $\rho^\sigma(\mathbf{r})$ at the point $\mathbf{r}$ and on derivative quantities at the point $\mathbf{r}$.

---

[2]Note that the related ωB97X-V functional [40] contains the 2-parameter density-dependent VV10 non-local-correlation function [41] to account for dispersion interactions. It is not clear from my reading whether the VV10 correction in ωB97X-V is implemented fully-self-consistently or not, and hence whether or not ωB97X-V should be classed as a rung-4a or rung-4b functional. This is a question for a future student to work out. Note, however, that both ωB97X-D3 and ωB97X-V are far out-performed by BLYP-osUW12 when applied to the SIE4x4 self-interaction error test-set, showing that neither the D3 nor VV10 dispersion corrections cure the self-interaction error problem (see Section 6.5). The RMSE values for the SIE4x4 set are 14.33 and 13.85 kcal mol^{-1} for ωB97X-D3 and ωB97X-V respectively [7], compared to 2.45 kcal mol^{-1} for BLYP-osUW12 (see Table 6.1). We neglect empirical dispersion corrections (density-dependent or otherwise) for the remainder of this thesis, but remark that it would be interesting to investigate adding them in in the future.

In Sections 1.12 and 1.14, we introduce hybrid and double-hybrid functionals (rungs 4 and 5 of the ladder in Table 1.1). It is here that we will focus our attention: can we make a functional with the accuracy benefits of a rung-5 functional, but with excellent basis-set convergence and ease-of-implementation of a rung-4 functional? This is the subject of Chapters 5 and 6.

1.9. Gaussian Basis-Sets

We have seen so far that the computational cost of a practical molecular electronic structure theory calculation depends on the efficiency of calculating each term in the energy expression in Section 1.6, and that these terms can be constructed from molecular integrals over atomic-orbital basis functions such as

$$\left(\alpha\beta|r_{12}^{-1}|\mu\nu\right) = \int d\mathbf{r}_1 \int d\mathbf{r}_2 \, \alpha^\star(r_1)\,\mu^\star(r_2)\,r_{12}^{-1}\beta(r_1)\,\nu(r_1). \tag{1.61}$$

Such integrals are simplified in form if one lets the atomic-orbital basis functions $\{\alpha\}$ be sums of "primitive" Cartesian Gaussian functions (PCGs) of the form

$$g_{\mathbf{a}}\left(\mathbf{r};\,\zeta, \mathbf{A}\right) = (r_x - A_x)^{a_x}\left(r_y - A_y\right)^{a_y}(r_z - A_z)^{a_z}\exp\left[-\zeta\left|\mathbf{r} - \mathbf{A}\right|^2\right] \tag{1.62}$$

where $\mathbf{A} = \left(A_x,\quad A_y,\quad A_z\right)$ and $\mathbf{r} = \left(x,\quad y,\quad z\right)$ are vectors in real-space, and a_x, a_y, a_z are nonegative integers. The simplification of the integral expressions is due to the "Gaussian product theorem", which states that any product of two or more PCGs can itself be expressed as a sum of PCGs. Each atomic-orbital basis function $\alpha(\mathbf{r})$ is then expressed as a sum of PCGs chosen so that $\alpha(\mathbf{r})$ resembles an atomic orbital of an isolated atom located at $\mathbf{A}$. A detailed discussion of Gaussian basis-sets is beyond the scope of this thesis, suffice to say that modern atomic-orbital basis-sets (such as cc-pVTZ [20]) are sufficiently general-purpose that they can

be used in both wavefunction methods and in DFT. We make use of the Gaussian product theorem in Section 4.3 to calculate the modified inter-electron integrals needed for the UW12 model.

1.10. The Self-Consistent-Field Method

Let us now return to the solution of the Kohn-Sham equations (Eqn 1.50). The Kohn-Sham equations must be solved self-consistently to find the orbitals $\{\phi_i(\mathbf{x})\}$ and (equivalently) the 1-RDM $\rho(\mathbf{x}|\mathbf{x}')$. In molecular electronic structure codes – such as the `entos` program (co-developed by the Manby group in the Bristol Centre for Computational Chemistry and the Miller group at the California Institute of Technology [42]) – the orbitals are typically expressed in terms of atomic-orbital basis functions $\{\beta(\mathbf{r})\}$ as

$$\phi_i(\mathbf{r}) = \sum_\beta \phi_i(\beta)\beta(\mathbf{r}) \tag{1.63}$$

where $\phi_i(\beta)$ are known as the "molecular orbital coefficients". The 1-RDM is expressed as

$$\rho^\sigma(\mathbf{r}|\mathbf{r}') = \sum_{\alpha\beta} \alpha(\mathbf{r})D^\sigma_{\alpha\beta}\beta(\mathbf{r}') \tag{1.64}$$

where it is assumed that the atomic-orbitals are real, and that the matrix $\mathbf{D}^\sigma$ (often referred to as the "density kernel") is real and symmetric. If we insert Eqn 1.63 into Eqn 1.50, then multiply with $\alpha(\mathbf{r})$ and integrate over all space, the Kohn-Sham equations become

$$\sum_\beta \underbrace{\left\langle \alpha \left| \left(-\frac{1}{2}\nabla^2_\mathbf{r}\right) + V_{\text{el,n}}(\mathbf{r}) + V_J(\mathbf{r}) + V^{\sigma_i}_{\text{xc}}(\mathbf{r},\mathbf{r}') \right| \beta \right\rangle}_{=:F^{\sigma_i}_{\alpha\beta}} \phi_i(\beta) = \underbrace{\langle \alpha|\beta \rangle}_{=:S_{\alpha\beta}} \epsilon_i \phi_i(\beta). \tag{1.65}$$

Eqn 1.65 can be recognized as a generalized eigenvalue equation by writing it in terms of matrices

$$\mathbf{F}^{\sigma} \mathbf{C}^{\sigma} = \mathbf{S} \mathbf{C}^{\sigma} \epsilon^{\sigma} \qquad (1.66)$$

where $\mathbf{C}^{\sigma}$ has elements

$$C_{\beta i}^{\sigma} = \phi_i(\beta) \qquad (1.67)$$

ϵ^{σ} has elements

$$\epsilon_{ij}^{\sigma} = \delta_{ij} \epsilon_i \qquad (1.68)$$

and the indices i and j run over all occupied Kohn-Sham orbitals with spin σ. The symmetric matrix $\mathbf{F}^{\sigma}$ is known as the Fock matrix and can also be written as

$$F_{\alpha\beta}^{\sigma} = [\partial E / \partial D_{\alpha\beta}^{\sigma} + \partial E / \partial D_{\beta\alpha}^{\sigma}]/2. \qquad (1.69)$$

Note that the density-kernel $\mathbf{D}^{\sigma}$ can also be written as

$$\mathbf{D}^{\sigma} = \mathbf{C}^{\sigma} (\mathbf{C}^{\sigma})^{T}. \qquad (1.70)$$

Since the Fock matrix $\mathbf{F}^{\sigma}$ depends on the density-kernel $\mathbf{D}^{\sigma}$, Eqn 1.66 is typically solved using the self-consistent-field (SCF) method: The Fock matrix $\mathbf{F}^{\sigma}$ is diagonalized and the resulting eigenvectors $\phi_i(\beta)$ (Kohn-Sham orbitals) are used to construct a new density-kernel $\mathbf{D}^{\sigma}$, and the process is repeated until convergence is reached. In `entos`, the SCF is considered

converged when all the elements of the orbital gradient matrix

$$\tilde{\mathbf{G}}^\sigma = \tilde{\mathbf{F}}^\sigma \tilde{\mathbf{D}}^\sigma - \tilde{\mathbf{D}}^\sigma \tilde{\mathbf{F}}^\sigma \tag{1.71}$$

are smaller in magnitude than a certain threshold value (known as the orbital threshold), and when the magnitude of the change in the energy E per iteration falls below a certain threshold (known as the energy threshold).[3] In Eqn 1.71, the matrices $\tilde{\mathbf{D}}^\sigma$ and $\tilde{\mathbf{F}}^\sigma$ are expressed in an orthonormalized basis $\{\tilde{\beta}(\mathbf{r})\}$ such that $\langle \tilde{\alpha} | \tilde{\beta} \rangle = \delta_{\tilde{\alpha}\tilde{\beta}}$.

The procedure to calculate the total energy E of a molecule in the Kohn-Sham framework is thus[4]

1. Begin with the positions of the atoms. Calculate the inter-nuclear repulsion energy $E_{n,n}$.

2. Construct an atomic-orbital basis-set $\{\alpha(\mathbf{r})\}$, a density-fitting basis set $\{A(\mathbf{r})\}$, and a quadrature grid $\{g_\lambda, \mathbf{r}_\lambda\}$. Calculate the values of necessary molecular integrals, eg. $(\alpha\beta|r_{12}^{-1}|A)$.

3. Make an initial guess for the density matrix $\mathbf{D}^\sigma$.

4. Calculate the energy E and Fock matrix $\mathbf{F}^\sigma$.

5. Diagonalize $\mathbf{F}^\sigma$ and use the resulting eigenvectors to construct a new $\mathbf{D}^\sigma$.

6. Return to step 3 and repeat until convergence is reached.

In this thesis, we will only be concerned with the computational expense of step 4, since this is the step that depends on the functional used. We now proceed to discuss how the various terms in E and $\mathbf{F}$ are calculated.

---

[3]There is no guarantee that the SCF procedure will converge to the global minimum in the space of all possible density-kernels $\mathbf{D}^\sigma$. In high-symmetry cases (such as in atoms) the initial guess and the number of electrons with each spin may need to be experimented with in order to find the minimum with the lowest energy E.

[4]In cases (such as hybrid DFT) where the energy depends on the 1-RDM $\rho(\mathbf{r}|\mathbf{r}')$ rather than just on the electron density $\rho(\mathbf{r})$, the Kohn-Sham framework is often referred to as the "generalized" Kohn-Sham framework. Since in this thesis we are concerned exclusively with hybrid DFT, we do not use such terms here.

1.11. Aside - Hartree-Fock Theory as a Functional of the Density Matrix

Recall that in the Hartree-Fock approximation it is assumed that the electronic wavefunction Φ is representable as a single Slater Determinant

$$\Phi \approx |0\rangle. \tag{1.72}$$

The electronic energy can then be written as

$$E_{el} = \langle 0|H_{el}|0\rangle = \langle 0|T_{el}|0\rangle + E_{el,n} + J + E_x^{HF} \tag{1.73}$$

where E_x^{HF} is defined as

$$E_x^{HF} = -\frac{1}{2} \sum_\sigma \int d\mathbf{r}_1 \int d\mathbf{r}_2 \, r_{12}^{-1} \, |\rho^\sigma(\mathbf{r}_1|\mathbf{r}_2)|^2 \tag{1.74}$$

which can be written in terms of individual molecular orbitals $\{\phi_i(\mathbf{r})\}$ as

$$E_x^{HF} = -\frac{1}{2} \sum_{ij} \delta_{\sigma_j \sigma_i} \int d\mathbf{r}_1 \int d\mathbf{r}_2 \, \phi_i^\star(\mathbf{r}_1) \phi_j^\star(\mathbf{r}_2) r_{12}^{-1} \, \phi_j(\mathbf{r}_1) \phi_i(\mathbf{r}_2) \tag{1.75}$$

$$= -\frac{1}{2} \sum_{ij} \langle ij|r_{12}^{-1}|ji\rangle \tag{1.76}$$

$$= -\frac{1}{2} \sum_{ij} \left(ij|r_{12}^{-1}|ji\right) \qquad \text{Using Mulliken Notation.}$$

$$\tag{1.77}$$

The notation in Eqn 1.77 was popularised by Robert Mulliken, who was among the first developers of molecular orbital theory [43, 44].

Comparing Eqn 1.73 with Eqn 1.36, we see that Hartree-Fock (HF) theory can be viewed as a rung-4a density functional approximation (see Table 1.1 and Fig 1.1) where the exchange-correlation energy is approximated as $E_{\mathrm{xc}} = E_{\mathrm{x}}^{\mathrm{HF}}$. In pure HF theory, we see that the Coulomb repulsion between an electron i in the Kohn-Sham auxiliary system and itself is exactly canceled out. For a single-electron system (where the electron resides in the Kohn-Sham orbital $\phi_{i=0}(\mathbf{r})$) we have

$$J + E_{\mathrm{x}}^{\mathrm{HF}} = \frac{1}{2}\left(00|r_{12}^{-1}|00\right) - \frac{1}{2}\left(00|r_{12}^{-1}|00\right) = 0. \tag{1.78}$$

Pure HF theory is thus referred to as a "one-electron-self-interaction-free" model, and $E_{\mathrm{x}}^{\mathrm{HF}}$ is often referred to as "exact exchange". The Hartree-Fock exchange energy $E_{\mathrm{x}}^{\mathrm{HF}}$ is an example of a non-local exchange functional, since the integrand in Eqn 1.74 depends on off-diagonal components of $\rho^{\sigma}(\mathbf{r}|\mathbf{r}')$.

1.12. Hybrid DFT

Despite being free from one-electron-self-interaction error, pure HF theory neglects electron correlation effects entirely and so gives poor estimates of molecular total energies – the assumption in Eqn 1.72 is a poor one. As we shall see, HF is less accurate than even the simplest DFT approximations (such as LDA) for most properties of interest to chemists. Intriguingly, however, the errors are sometimes in the opposite direction to the errors made by pure (semi-local) DFT functionals: For instance, whereas LDA systematically over-estimates atomization energies, HF systematically under-estimates them. One can thus imagine that "mixing" the two methods together would yield better results. Such an approach (known as a hybrid functional) can be theoretically justified by using the adiabatic connection formalism popularised by Becke in 1993 [45]. However, for the purposes of this thesis we will consider

the Hartree-Fock energy E_x^{HF} merely as an additional "ingredient" that can be mixed into our DFT energy expression using some mixing fraction a_x^{nl} that is fitted to match experimental results. This is the approach taken by the most accurate hybrid functionals today.

In this thesis, we generalise the definition of hybrid functionals slightly to include all functionals containing non-local exchange or correlation terms (not only the Hartree-Fock exchange energy E_x^{HF}). Returning to the Jacob's ladder analogy in Fig 1.1, we define rung-4a density-functionals as those where the exchange energy can be expressed as a sum of semi-local (DFT) and non-local (nl) parts, but where the correlation energy remains semi-local[5]

$$E_{xc} = a_x^{DFT} E_x^{DFT} + a_c^{DFT} E_c^{DFT} + a_x^{nl} E_x^{nl}. \tag{1.79}$$

For instance, the B3LYP hybrid functional is defined as [35]

$$E_{xc}^{B3LYP} = (1 - a_x^{HF} - a_x^{B88})E_x^{S} + a_x^{HF} E_x^{HF} + a_x^{B88} E_x^{B88}$$
$$+ (1 - a_c^{LYP})E_c^{VWN} + a_c^{LYP} E_c^{LYP} \tag{1.80}$$

where E_x^{S} is the Slater-Dirac exchange functional, E_c^{VWN} is the Vosko-Wilk-Nusair (VWN) correlation functional [27], E_c^{LYP} is the Lee-Yang-Parr (LYP) correlation functional [31], and E_x^{B88} is the Becke 1988 exchange functional [32].[6]

The adjustable parameters a_x^{HF}, a_x^{B88}, $a_c^{LYP} = 0.20, 0.72, 0.81$ were fit to the 56 atomization energies, 42 ionization potentials, 8 proton affinities, and the 10 first-row total atomic energies

---

[5]For the purposes of this thesis, we choose to include dispersion-corrected functionals such as ωB97X-D3 in the rung-4a category, provided that the dispersion-correction is not included in the self-consistent optimisation of the density. See also Footnote 2 on page 21.

[6]Note that there are multiple variants of the VWN functional presented in Ref [27]. The most commonly used in quantum chemistry are known as VWN(III) and VWN(V). These are used to construct two variants of B3LYP: known as B3LYP3 and B3LYP5. In this thesis, all references to B3LYP refer to B3LYP3 instead of B3LYP5 (unless otherwise stated).

of Ref [46]. To fit the parameters in B3LYP, the energy components in Eqn 1.80 were evaluated using the Kohn-Sham orbitals from a previous self-consistent LDA calculation [35] (we refer to such a method as "post-LDA").

1.12.1. Advantages of B3LYP-like Functionals

In the chemistry community, the B3LYP functional remains the most popular exchange-correlation functional after two decades [47, 14]. Its balance of accuracy and computational simplicity give it distinct advantages over other methods. For instance, we see in Fig 5.4a and Table 1.1 that B3LYP is more than twice as accurate as its pure-DFT counterpart BLYP for estimating the atomization energies of molecules in the W4-11 test set, and is nearing chemical accuracy (1 kcal·mol^{-1}).[7] To produce Fig 5.4a, each self-consistent energy evaluation took a matter of minutes on a 16-core intel CPU. By contrast, wavefunction methods such as W4 are more difficult to set up (since they contain a greater number of tunable parameters), are more difficult to converge numerically, and have a higher formal computational scaling with system size. B3LYP's success for the G2 set arises from the inclusion of 20% exact exchange (a_x^{HF}=0.2), which is effective at canceling-out the self-interaction error for these molecules (see Section 1.17 and Chapters 5 and 6).

1.12.2. Disadvantages of B3LYP-like Functionals

Despite being widely used throughout chemistry, B3LYP systematically under-estimates reaction barrier-heights and over-estimates intermolecular interactions in charge-transfer complexes [48, 49]. This problem is due to an incomplete cancellation of the delocalization error (see

---

[7]It is worth noting that the atomization energies are perhaps not the best benchmark to use when comparing B3LYP to other methods (since B3LYP was parameterised using atomization energies).

Section 1.17). The B-HH-LYP hybrid functional [45]

$$E_{xc}^{\text{B-HH-LYP}} = \frac{1}{2}E_x^{\text{B88}} + \frac{1}{2}E_x^{\text{HF}} + E_c^{\text{LYP}} \tag{1.81}$$

is more accurate than B3LYP for reaction barrier-heights, but systematically under-estimates atomization energies. This phenomenon has been attributed [50] to the larger fraction of exact exchange in B-HH-LYP ($a_x^{\text{HF}} = 0.50$) than in B3LYP ($a_x^{\text{HF}} = 0.20$).

Is it possible to make a functional that is accurate for both reaction barrier-heights and atomization energies?

One approach is to replace E_x^{HF} with a range-corrected version by splitting the r_{12}^{-1} potential in Eqn 1.74 into short-range (sr) and long-range (lr) parts, with the switching taking place over a length scale $1/\omega$. The short-range part is then treated with a modified DFT approximation from rungs 1-3, whereas the long-range part is treated with Hartree-Fock exchange E_x^{HF}. Modern range-corrected hybrid functionals such as M05-2X [51] and ωB97X-V [40] have been shown to out-perform non-range-corrected hybrids (also known as "global hybrids") such as B3LYP in almost all cases [52, 7, 8], albeit at the expense of containing a greater number of adjustable parameters. M05-2X has 20 tunable parameters, and ωB97X-V has 10. In this thesis, we will not concern ourselves with the number of adjustable parameters that each functional contains – Suffice to say that functionals with more adjustable parameters require larger and broader training sets in order to avoid over-fitting their parameters.[8] Rather, we will focus our attention on ingredients themselves.

Another approach is to include a non-local correlation model in the hybrid, as well as a non-local exchange model. This is conventionally done by adding in a fraction of the MP2 correlation energy to make a double-hybrid functional, as we shall see in Section 1.14. Using the double-

---

[8]A helpful discussion on the relevance of the number of parameters can be found in Section 3.2. of Ref [8].

hybrid approach, authors have demonstrated that excellent atomization energy accuracy can be obtained for a wide range of values of the exact exchange fraction a_x^{HF}.

1.13. Second-Order Møller-Plesset theory

We have so far discussed the Hartree-Fock method, and how it can be mixed with DFT to produce hybrid functionals. We now turn our attention to another wavefunction-based method known as Second-order Møller-Plesset theory (MP2). In MP2, the electronic energy E_{el} is approximated as

$$E_{el} \approx \langle 0|H_{el}|0\rangle + E_c^{PT2} \tag{1.82}$$

where $|0\rangle$ is the Hartree-Fock determinant (*i.e.* the determinant that minimises $\langle 0|H_{el}|0\rangle$). The MP2 correlation energy E_c^{PT2} is the second-order correction to the energy that results from including interactions between electrons perturbatively. If H_{el} is the full electronic Hamiltonian, which can be written in the form

$$H_{el} = \sum_{pq} h_{pq} a_p^\dagger a_q + V \tag{1.83}$$

where $\{a_p\}$ are operators that annihilate an electron in the Hartree-Fock orbital $\phi_p(\mathbf{r})$, and V is the interaction between electrons

$$V = \frac{1}{2} \sum_{pqrs} \langle pq|r_{12}^{-1}|rs\rangle a_p^\dagger a_q^\dagger a_s a_r, \tag{1.84}$$

then the $E_{\mathrm{c}}^{\mathrm{PT2}}$ correlation energy can be derived [53] by partitioning the electronic Hamiltonian as follows (with the perturbation parameter $\lambda = 1$)

$$H_{\mathrm{el}} = F + \lambda\left(H_{\mathrm{el}} - F\right). \tag{1.85}$$

The Fock operator F is a sum of single-particle operators[9]

$$F = \sum_{pq} F_{pq} a_p^\dagger a_q = \sum_{pq} \left(h_{pq} + V_{\mathrm{Hxc},pq}\right) a_p^\dagger a_q, \tag{1.86}$$

and the Slater determinant $|0\rangle$ is the the N_{el}-electron ground-state of F with eigenvalue E_0

$$F\,|0\rangle = E_0\,|0\rangle. \tag{1.87}$$

Recall from Eqn 1.24 that $\langle 0|H_{\mathrm{el}}|0\rangle$ is in general greater than the exact ground-state electronic energy E_{el}, so we expect $E_{\mathrm{c}}^{\mathrm{PT2}}$ to be negative. Applying perturbation theory and keeping terms in the energy expression that scale as λ^2 yields

$$E_{\mathrm{c}}^{\mathrm{PT2}} = \left\langle 0 \left| (H_{\mathrm{el}} - F)(1 - |0\rangle\langle 0|)(F - E_0)^{-1}(1 - |0\rangle\langle 0|)(H_{\mathrm{el}} - F) \right| 0 \right\rangle. \tag{1.88}$$

Eqn 1.88 can be written as a sum of contributions from singly-excited determinants $\left|{}_i^a\right\rangle = a_a^\dagger a_i\,|0\rangle$ and doubly-excited determinants $\left|{}_{ij}^{ab}\right\rangle = a_a^\dagger a_b^\dagger a_j a_i\,|0\rangle$

$$\begin{aligned}
E_{\mathrm{c}}^{\mathrm{PT2}} = \ &\sum_{ia} \left\langle 0 \left|(H_{\mathrm{el}} - F)\right|{}_i^a\right\rangle \frac{1}{\epsilon_a - \epsilon_i} \left\langle{}_i^a\left|(H_{\mathrm{el}} - F)\right|0\right\rangle \\
&+ \sum_{i<j}\sum_{a<b} \left\langle 0\left|(H_{\mathrm{el}} - F)\right|{}_{ij}^{ab}\right\rangle \frac{1}{\epsilon_a + \epsilon_b - \epsilon_i - \epsilon_j} \left\langle{}_{ij}^{ab}\left|(H_{\mathrm{el}} - F)\right|0\right\rangle
\end{aligned} \tag{1.89}$$

---

[9]The single-particle operator V_{Hxc} is known as the Hartree-exchange-correlation potential.

where $|i\rangle, |j\rangle \equiv \phi_i, \phi_j$ are Kohn-Sham orbitals that are occupied in $|0\rangle$, and $|a\rangle, |b\rangle \equiv \phi_a, \phi_b$ are unoccupied (virtual) spin-orbitals in an infinite single-particle basis $\{\phi_p\}$. In principle, the set $\{\phi_a\}$ is also infinite. However, in most practical implementations of E_c^{PT2}, finite basis sets are used. Note that the step from Eqn 1.88 to Eqn 1.89 does not rely on $|0\rangle$ being the Hartree-Fock determinant. Replacing $|0\rangle$ in Eqn 1.88 with some other determinant results in an expression that is no longer pure MP2 theory, but is nonetheless useful (see Section 1.14).

1.13.1. Contribution from Singly-Excited Determinants

If F is the Fock operator from HF theory

$$F_{pq}^{HF} = h_{pq} + \left\langle \overline{pj} \middle| r_{12}^{-1} \middle| qj \right\rangle \tag{1.90}$$

where the ket $|\overline{pq}\rangle$ is defined as

$$|\overline{pq}\rangle = |pq\rangle - |qp\rangle \tag{1.91}$$

then the first term in Eqn 1.89 is zero by Brillouin's theorem

$$\left\langle 0 \middle| \left(H_{el} - F^{HF} \right) \middle| {}_i^a \right\rangle = \left\langle 0 \middle| V \middle| {}_i^a \right\rangle - \left\langle 0 \middle| V_{Hxc}^{HF} \middle| {}_i^a \right\rangle \tag{1.92}$$

$$= \sum_j \left\langle \overline{ij} \middle| r_{12}^{-1} \middle| aj \right\rangle - \sum_j \left\langle \overline{ij} \middle| r_{12}^{-1} \middle| aj \right\rangle = 0. \tag{1.93}$$

If $|0\rangle$ is not the HF determinant corresponding to F_{pq}^{HF}, then Brillouin's theorem no longer holds. This is the case for double-hybrid functionals (see Section 1.14). However, most developers of double-hybrid functionals assume that single excitations are accounted for by the overall scaling factor a_c in Eqn 1.99. The contribution from singly-excited determinants is thus

assumed to be small, and proportional to the contribution from doubly-excited determinants [33, 48], and is not calculated explicitly. Since it is so common to ignore the singly-excited term, hereon-in we will use the symbol E_c^{PT2} to mean only the second term in Eqn 1.89.

1.13.2. Contribution from Doubly-Excited Determinants

Using the matrix element

$$\left\langle 0 \middle| (H_{el} - F) \middle| {}_{ij}^{ab} \right\rangle = \left\langle 0 \middle| V \middle| {}_{ij}^{ab} \right\rangle = \left\langle ij \middle| r_{12}^{-1} \middle| \overline{ab} \right\rangle \tag{1.94}$$

the second term in Eqn 1.89 is

$$E_c^{PT2} = -\sum_{i<j} \sum_{a<b} \frac{\langle ij|r_{12}^{-1}|\overline{ab}\rangle \langle \overline{ab}|r_{12}^{-1}|ij\rangle}{\epsilon_a + \epsilon_b - \epsilon_i - \epsilon_j} \tag{1.95}$$

$$= -\frac{1}{4} \sum_{ijab} \frac{\langle ij|r_{12}^{-1}|\overline{ab}\rangle \langle \overline{ab}|r_{12}^{-1}|ij\rangle}{\epsilon_a + \epsilon_b - \epsilon_i - \epsilon_j} \tag{1.96}$$

$$= -\frac{1}{2} \sum_{ijab} \frac{\langle ij|r_{12}^{-1}|\overline{ab}\rangle \langle ab|r_{12}^{-1}|ij\rangle}{\epsilon_a + \epsilon_b - \epsilon_i - \epsilon_j}. \tag{1.97}$$

Eqn 1.97 is the familiar form of the MP2 theory that appears in most textbooks, and is the form used in double-hybrid functionals. It is often helpful to decompose the MP2 energy into same-spin $E_{c,s=1}^{PT2}$ and opposite-spin components $E_{c,s=0}^{PT2}$ as follows

$$E_c^{PT2} = E_{c,s=0}^{PT2} + E_{c,s=1}^{PT2} \tag{1.98}$$

where $E_{c,s=1}^{PT2}$ contains those terms where the orbitals i and j have parallel spins ($\sigma_i = \sigma_a = \sigma_j = \sigma_b$) and $E_{c,s=0}^{PT2}$ contains the terms where the orbitals i and j have anti-parallel spins ($\sigma_i = \sigma_a \neq \sigma_j = \sigma_b$).

1.14. Double-Hybrid DFT

Although pure MP2 theory is widely used in both physics and chemistry, its accuracy can be greatly improved by mixing it with hybrid DFT to make a double-hybrid functional [52, 7]. Just as with hybrid functionals, it is possible to theoretically justify such an approach by using adiabatic connection formulae [54, 55]. However, for the purposes of this thesis we will consider the MP2 energy E_c^{PT2} merely as an additional "ingredient" that can be mixed into our DFT energy expression using some mixing fraction a_c^{PT2} that is fitted to match experimental results. This is the approach taken by the most accurate double-hybrid functionals today.

In this thesis, we generalise the definition of double-hybrid functionals slightly to include all functionals that depend explicitly on the virtual Kohn-Sham orbitals. Returning to our Jacob's ladder analogy in Fig 1.1, we define double-hybrid (rung-5) DFT functionals as those where the exchange-correlation energy is expressed as

$$E_{\text{xc}} = E_{\text{x}}^{\text{DFT}} + E_{\text{c}}^{\text{DFT}} + a_{\text{x}}^{\text{HF}} E_{\text{x}}^{\text{HF}} + a_{\text{xc}}^{\text{virt}} E_{\text{xc}}^{\text{virt}} \tag{1.99}$$

where E_c^{virt} is a non-local model of the correlation energy that depends on the unoccupied (virtual) orbitals and their eigenvalues $\{\phi_a, \epsilon_a\}$, in addition to the occupied orbitals and eigenvalues $\{\phi_i, \epsilon_i\}$. In 2006, Grimme [33] proposed choosing E_c^{virt} to be the second-order Møller-Plesset (MP2) correlation energy E_c^{PT2}, building on the earlier development of Görling-Levy perturbation theory [54, 55] and related composite methods by Truhlar [56]. The B2-PLYP double-hybrid functional is defined as [33]

$$E_{\text{xc}}^{\text{B2-PLYP}} = (1 - a_{\text{x}}^{\text{HF}}) E_{\text{x}}^{\text{B88}} + a_{\text{x}}^{\text{HF}} E_{\text{x}}^{\text{HF}} + (1 - a_{\text{c}}) E_{\text{c}}^{\text{LYP}} + a_{\text{c}} E_{\text{c}}^{\text{PT2}} \tag{1.100}$$

where the empirical parameters $a_{\text{x}}^{\text{HF}}, a_{\text{c}}^{\text{PT2}} = 0.53, 0.27$ are optimized for the heats of formation

of the G2/97 set [33]. To evaluate Eqn 1.100, the Kohn-Sham orbitals $\{\phi_p\}$ are first optimized in a self-consistent manner ignoring the MP2 correlation energy E_c^{PT2} term. The E_c^{PT2} energy is then calculated using the resulting orbitals and eigenvalues $\{\phi_p, \epsilon_p\}$. Such double-hybrid functionals are sometimes referred to as "truncated", since the orbitals are optimized using a part of the full energy expression. In truncated double-hybrid functionals, the computationally-expensive problem of finding the derivatives of E_c^{PT2} with respect to orbital rotations is avoided. In Section 1.14.1, we review some more recent methodologies where E_c^{PT2} is included in the self-consistent optimization of the orbitals.

In 2008, Zhang *et al.* [57] proposed an alternative methodology. They used the orbitals and eigenvalues from a B3LYP calculation to calculate the E_c^{PT2}, E_x^{HF}, and E_{xc}^{DFT} components of the energy, and constructed the XYG3 functional

$$E_{xc}^{XYG3} = (1 - a_x^{HF} - a_x^{S})E_x^{B88} + (1 - a_c^{PT2})E_c^{LYP} + a_x^{S}E_x^{S} + a_x^{HF}E_x^{HF} + a_c^{PT2}E_c^{PT2} \qquad (1.101)$$

where the empirical parameters $a_x^{HF} = 0.8033$, $a_x^{S} = -0.0140$, $a_c^{PT2} = 0.3211$ are optimized for the heats of formation of the G3/99 set. One advantage of XYG3 over B2-PLYP is that the higher exact-exchange fraction $a_x^{HF} \approx 0.8$ in XYG3 correctly models the integer discontinuity for systems with non-integer charge (see Section 1.18) [58]. Methods where B3LYP orbitals are used in the final correlation energy evaluation are termed "post-B3LYP" methods. We do not discuss the relative merits of truncated double-hybrid methods versus post-B3LYP double-hybrid methods; suffice to say that the orbitals used in our UW12 hybrids in Chapters 5 and 6 are optimised without truncation. The full energy expression is thus minimised with respect to the density matrix.

Since B2-PLYP, authors have experimented with using spin-component-scaling in the E_c^{PT2} term. The DSD and DOD class of double-hybrid functionals are similar to B2-PLYP, but

contain more adjustable parameters [34].

$$E_{xc}^{DSD-BLYP} = \left(1 - a_x^{HF}\right) E_x^{B88} + a_x^{HF} E_x^{HF} + a_c^{LYP} E_c^{LYP} + a_{c,s=0}^{PT2} E_{c,s=0}^{PT2} + a_{c,s=1}^{PT2} E_{c,s=1}^{PT2}$$

$$(1.102)$$

$$E_{xc}^{DOD-BLYP} = \left(1 - a_x^{HF}\right) E_x^{B88} + a_x^{HF} E_x^{HF} + a_c^{LYP} E_c^{LYP} + a_{c,s=0}^{PT2} E_{c,s=0}^{PT2}. \tag{1.103}$$

The four (three) parameters in DSD-BLYP (DOD-BLYP) are chosen to achieve high accuracy for various thermochemical and kinetic test sets. DSD-BLYP and DOD-BLYP outperform B2-PLYP for the barrier height and atomization energy test sets mentioned in Chapter 6.

The advantage of DOD-BLYP over DSD-BLYP is that the opposite-spin MP2 component $E_{c,s=0}^{PT2}$ can be evaluated in a computation time that scales formally as N^4 by using the Laplace-transform MP2 algorithm, whereas the scaling for the same-spin component $E_{c,s=1}^{PT2}$ is formally N^5. Spin-opposite-scaled double-hybrids such as DOD-BLYP are becoming more popular, and have proved successful at predicting the atomization energies of both small and large molecules [7]. However, all the rung-5 methods mentioned so far have a slower basis-set convergence (see Section 1.9) than the corresponding rung-4 methods, due to the dependence on unoccupied orbitals.

Just like with hybrid functionals, it is possible to split the r_{12}^{-1} potential in Eqn 1.97 into short- and long-range components and thus form "range-separated" double-hybrid functionals. Such functionals thus contain different amounts of non-local correlation at each length-scale. Toulouse and Savin have demonstrated that such functionals are competitive with standard ("global") double-hybrids, and the added flexibility leads to the possibility of treating static correlation problems more accurately [50]. We do not consider explicit range-separated methods further in this thesis. However, it is worth noting that our UW12 model (introduced in Chapter 2) decays exponentially with a length-scale r_c and thus could be considered a short-

range correlation correction. It would be interesting in the future to experiment with modifying the kernel r_{12}^{-1} used in deriving the E_x^{B88}, E_c^{LYP}, and E_x^{HF} components of the BLYP-osUW12 functional (see Chapter 6 on page 131).

1.14.1. Orbital-Optimization

It is somewhat unsatisfying that the electron density is not optimized using the full energy expression in the double-hybrid methods mentioned so far. This can lead to unphysical behavior when spin-unrestricted calculations are performed on stretched bonds [59, 60, 61]. Not only that, but the calculation of gradients and other first-order response properties is made more involved by the fact that the energy is not minimized (stationary) with respect to orbital rotations. Since 2013, orbital-optimized double-hybrids have been developed to address these issues. Orbital-optimized double-hybrid methods show an improved description of electron affinities, reaction barrier-heights, and radical bond dissociation when compared with conventional double-hybrid methods [62, 63, 64, 65]. Some of these methods directly minimize the E_c^{PT2} energy by optimizing the Kohn-Sham orbitals, whereas others use the optimized effective potential (OEP) method to obtain the orbitals. However, neither case is trivial to implement, and so orbital-optimized double hybrids are not yet (and perhaps never will be) available in most electronic structure codes. For the methods developed in this thesis, we choose to write all our energy expressions as functionals of the 1-RDM $\rho(\mathbf{r}|\mathbf{r}')$ and make the energy stationary with respect to $\rho(\mathbf{r}|\mathbf{r}')$, in a manner similar to in Hartree-Fock theory. We thus avoid the complexities of OEP theory.

Although we do not use OEP theory in this thesis, we make brief mention of it here for comparison with our approach. The standard (exchange-only) OEP method involves minimizing the Hartree-Fock energy $\langle 0|H_{el}|0\rangle$ but subject to the constraint that the orbitals $\{\phi_i\}$ are solutions to the Kohn-Sham equations with a local effective exchange potential $v_\sigma(\mathbf{r}_2)$. A brief

theoretical justification for the OEP method is given in Section 2.2.3. The OEP method – and the related local-Fock-exchange (LFX) method – are commonly used for calculating response properties and band gaps for molecular solids. They eliminate the undesirable band-structure issues of Hartree-Fock theory (which arise from an asymmetric treatment of the occupied and unoccupied orbitals), whilst simultaneously eliminating the delocalization errors of DFT by using a high fraction of exact-exchange (commonly $a_{\mathrm{x}}^{\mathrm{HF}} = 1.0$) in the density optimization [66, 67, 68, 69, 70].

Another advantage to minimizing the energy with respect to the 1-RDM in this way comes in considering the removal or addition of an electron: if E is minimized with respect to $\rho(\mathbf{r}|\mathbf{r}')$ then the derivative of the energy E with respect to the occupation number n_i of each orbital $\partial E / \partial n_i$ is equal to the orbital eigenvalue ϵ_i

$$\partial E / \partial n_i = \epsilon_i. \tag{1.104}$$

If the linearity condition (Eqn 1.118) is satisfied such that

$$\partial E / \partial N_{\mathrm{el}} = E\left(N_{\mathrm{el}} - 1\right) - E\left(N_{\mathrm{el}}\right) = -I \tag{1.105}$$

then the ionization potential I is thus the negative of the highest-occupied molecular orbital energy ϵ_{HOMO}

$$I = -\epsilon_{\mathrm{HOMO}}. \tag{1.106}$$

We do not plot molecular orbital energies for our UW12 hybrid functionals (see Chapter 6), but remark that our functionals are competitive with double-hybrid functionals in terms of linearity condition and ionization potentials for atoms (See upper part of Fig 6.5).

Another issue that has faced developers of orbital-optimized electronic structure methods in the past has been that of degeneracies appearing at the Fermi-level. For pure density-functionals (rungs 1-2 of the Jacob's ladder) it is common for the HOMO-LUMO gap to vanish altogether when the orbitals are perturbed. In this case, the MP2 correlation energy E_c^{PT2} diverges to $-\infty$, since the energy expression gives an unphysically-high amplitude to double excitations from the HOMO to the LUMO. The orbital optimization thus collapses to a spurious minimum in the energy surface $E[\rho(\mathbf{r}|\mathbf{r}')]$. Many authors have found ways around this problem by performing the optimization in an approximate manner, or by constraining the optimization to ensure that the calculation finds the "correct" local minimum [62, 64, 59, 63, 65]. However, the UW12 model E_c^{UW12} proposed in Chapter 2 goes part-way towards curing the problem altogether, since the denominator $1/(\epsilon_a - \epsilon_i)$ has been replaced with a damping function $w(r_{12})$ which ensures that the pseudo-amplitude for the double-excitation is always bounded. It is not known whether spurious minima exist in the energy surface for our UW12 hybrids. Note however that the presence of the high fraction of exact exchange $a_x^{\text{HF}} = 0.75$ in the energy expression of BLYP-osUW12 should prevent band-gap collapse during the self-consistent optimization. It may be interesting to try combining OEP/LFX with our UW12 hybrids in the future, to obtain simultaneously-accurate band-structures and electron-densities for molecular solids.

1.15. Density-Driven and Energy-Driven Errors

We have mentioned that all the exchange-correlation functionals used in chemistry are approximations to the exact functional. The density ρ generated by the SCF procedure is thus an approximation to the exact density. There have been numerous efforts to determine how much of the error in the final energy comes from an incorrect density. Such errors are known as "density-driven" errors, as opposed to "energy-driven" errors.

For a purely energy-driven error, the functional gives an incorrect energy $E^{\text{approx}}[\rho]$ even when the exact density ρ_{exact} is used. This can be seen in the case of applying an approximate exchange-correlation functional (such as LDA) to an infinitely-dissociated H_2^+ molecule (see Section 1.17). In this case, LDA under-estimates the energy of the delocalized $H^{0.5+} \ldots H^{0.5+}$ state relative to the localized $H^+ \ldots H$ state, despite symmetry considerations showing us that these states should be degenerate. Even if we add a constant to the approximate exchange-correlation functional $E^{\text{approx}}[\rho]$ it is thus not possible to get the correct energy $E^{\text{exact}}[\rho]$ for both states [71, 72, 11]. Density-driven errors, on the other hand, result from a spurious minimum $\rho'(\mathbf{x})$ in the $E^{\text{approx}}[\rho]$ landscape for which

$$E^{\text{approx}}[\rho'] \ll E^{\text{approx}}[\rho_{\text{exact}}]. \tag{1.107}$$

The self-consistent optimization then runs away to this minimum ρ' rather than to the correct density ρ_{exact}. Density-driven errors can thus occur even when $E^{\text{approx}}[\rho_{\text{exact}}]$ and $E^{\text{approx}}[\rho_{\text{exact}}]$ are close. Density-driven errors are not seen as commonly as energy-driven errors, but can be important in cases such as reaction barrier-heights, heteronuclear bond-dissociations, and others [73, 74, 75, 76, 77, 13]. We investigate reaction barrier-heights in Sections 5.4 and 6.4. In cases where $E^{\text{approx}}[\rho_{\text{exact}}]$ and $E^{\text{exact}}[\rho_{\text{exact}}]$ are close, a simple solution to density-driven errors is to constrain the self-consistent optimization so that the final ρ is close to ρ_{exact}. Alternatively, one can use different functionals (with different exact exchange fractions a_{x}^{HF}, see Section 1.12) to optimize the orbitals and to evaluate the energy. Such a technique is known as density-corrected DFT [75]. In this thesis, we focus primarily on systems for which DFT shows energy-driven errors. However, since the UW12 functionals we develop in Chapters 5 and 6 have a high fraction of exact exchange a_{x}^{HF} – and enable full self-consistent optimization of the density – we expect them to reduce density-driven errors too. We confirm this hypothesis in Section 5.4.

1.16. Non-Integer Charge and Non-Integer Spin Errors

The H_2^+ problem introduced in Sec 1.15 can also be cast in terms of the inability of an approximate DFT functional to model systems with non-integer charge – since the $H^{0.5+} \ldots H^{0.5+}$ state can also be thought of as two isolated H atom systems each with charge 0.5+. Functionals that fail to treat such systems are hence said to display "non-integer charge errors" (also known as "self-interaction errors" or "delocalization errors"). These are the subject of Sections 1.17 and 1.18. As we shall see, hybrid functionals (introduced in Section 1.12) with a high fraction of Hartree-Fock exchange ($a_x^{HF} > 0.7$) tend to be more effective at reducing non-integer charge errors than pure-DFT functionals.

Another class of error is "non-integer spin errors" (also known as "constancy violations"). Such errors can be cast in terms of the inability of an approximate DFT functional to model systems with integer charge but non-integer spin. These errors are particularly noticeable in systems with static correlation, such as the ground state of the infinitely-dissociated H_2 molecule. In infinitely-dissociated H_2, the high-spin $H^\uparrow \ldots H^\uparrow$ and low-spin $H^\uparrow \ldots H^\downarrow$ spin-states become degenerate. For each isolated H atom, the exact DFT functional should thus give

$$E\left[H^{0.5\uparrow,\, 0.5\downarrow}\right] = E\left[H^\uparrow\right] \tag{1.108}$$

which is known as the "constancy condition" [9, 10, 11, 12, 13]. In general, approximate DFT functionals over-estimate the energy of the non-integer-spin $H^{0.5\uparrow,\, 0.5\downarrow}$ state relative to the integer-spin $H^\uparrow$ state. Static correlation problems such as this one are notoriously difficult to solve in the Kohn-Sham framework, since the Kohn-Sham auxiliary system is expressed as a single Slater-determinant $|0\rangle$. Interestingly, pure-DFT functionals in general have *lower* non-integer spin errors than their corresponding hybrid functionals, since the approximate exchange functional E_x^S (see Eqn1.58) "mixes" some of the high-spin and low-spin wavefunctions

together.

Non-integer charge errors and non-integer spin errors are the two major challenges facing approximate DFT functionals today. Non-integer spin errors are smaller than non-integer charge errors for most systems, and are only of real practical concern when transtion-metal dimers are involved. We will henceforth be concerned only with non-integer charge errors. It is the elimination of these that gives rung-5 functionals the performance edge over existing rung-4 and rung-3 functionals.

1.17. Self-Interaction Error and (De)localization Error

Let us take a more detailed look at self-interaction errors and delocalization errors. In Sections 1.5 and 1.6, we saw that the electron-electron interaction energy is commonly decomposed as

$$E_{\text{el,el}}\left[\rho\left(\mathbf{r},\mathbf{r}'\right)\right] = J\left[\rho\left(\mathbf{r}\right)\right] + E_{\text{xc}}\left[\rho\left(\mathbf{r},\mathbf{r}'\right)\right]. \tag{1.109}$$

The J term can be written in terms of the Kohn-Sham orbitals as

$$J\left[\{\phi_i(\mathbf{x})\}\right] = \sum_{ij} \frac{1}{2} \langle ij|r_{12}^{-1}|ij\rangle \tag{1.110}$$

where

$$\langle pq|r_{12}^{-1}|rs\rangle = \int d\mathbf{x}_1 \int d\mathbf{x}_2\, \phi_p^\star(\mathbf{x}_1)\phi_q^\star(\mathbf{x}_2)\frac{1}{|\mathbf{r}_1-\mathbf{r}_2|}\phi_r(\mathbf{x}_1)\phi_s(\mathbf{x}_2) \tag{1.111}$$

43

and the integrals over $\mathbf{x}$ are assumed to be over both space ($\mathbf{r}$) and spin (σ) coordinates. We see immediately that J contains a spurious contribution

$$J_{\text{self}}[\{\phi_i(\mathbf{r})\}] = \sum_i \frac{1}{2} \langle ii|r_{12}^{-1}|ii \rangle \tag{1.112}$$

that arises from each electron interacting with itself. In Hartree-Fock theory (see Section 1.11), this contribution is cancelled exactly by a matching term in the exchange term

$$E_{\text{x}}^{\text{HF}}[\{\phi_i(\mathbf{r})\}] = -\sum_{ij} \frac{1}{2} \langle ij|r_{12}^{-1}|ji \rangle. \tag{1.113}$$

However, for approximate exchange-correlation functionals E_{xc}, this is not usually the case. This occurs because the classical Coulomb term J is calculated exactly, whereas the exchange term E_{x} is approximated using a uniform-electron-gas model and is hence not exact when the density is non-uniform (in a molecular system). The resulting error in the total energy is known as "self-interaction error", since the electron now interacts with itself.

In Section 1.15, we introduced the problem of the infinitely-dissociated H_2^+ molecule. Hartree-Fock theory is exact for this system (since the system only has one electron), whereas LDA under-estimates the energy of the stretched geometry relative to the energy of the isolated H and H^+. This is because the energy of the state where the electron is delocalized across both H atoms is artificially lowered relative to the state where it is localized on one atom by around 60 kcal mol^{-1} [11] (see also Footnote 9 on page 142). Self-interaction error is used interchangeably with the term "delocalization error" in one-electron systems [12, 13].

A similar effect is seen in many-electron systems, although there it is given the broader term "delocalization error". The effect is particularly visible in radical systems with stretched bonds (such as those in Section 6.5). Specifically, the delocalization error is most visible in molecules made from two fragments A and B, where the electron affinity of fragment A closely matches

the ionization potential of fragment *B* [12, 78]. Other examples of such systems include charge-transfer complexes, and polarizable molecular chains [78]. For systems with many electrons, Hartree-Fock theory is no longer exact, and shows the opposite behavior to LDA. It is thus termed as showing localization error. We refer to localization error and delocalization error collectively as (de)localization error.

1.18. Non-integer Charge

We mentioned in Section 1.15 that (de)localization errors can be cast in terms of the inability of the approximate density-functional to model systems with non-integer charge. Let us take a closer look at how systems with non-integer charge can be treated. In this section, we use the symbol $\rho^{N_{el}}(\mathbf{x}|\mathbf{x}')$ to refer to the 1-RDM of a system with N_{el} electrons. We can define the 1-RDM of a system with a non-integer number of electrons trivially in terms of two identical systems with integer number of electrons [79]. For instance, if N_{el} is half-integer then we can define $\rho^{N_{el}}(\mathbf{x}|\mathbf{x}')$ as

$$\rho^{N_{el}}(\mathbf{x}|\mathbf{x}') = \frac{1}{2}\rho^{\lfloor N_{el} \rfloor}(\mathbf{x}|\mathbf{x}') + \frac{1}{2}\rho^{\lceil N_{el} \rceil}(\mathbf{x}|\mathbf{x}'), \tag{1.114}$$

where

$\lfloor x \rfloor$ is the most positive integer such that $\qquad\qquad \lfloor x \rfloor \leq x \qquad$ (1.115)

$\lceil x \rceil$ is the least positive integer such that $\qquad\qquad \lceil x \rceil \geq x. \qquad$ (1.116)

More generally, we can define[10]

$$\rho^{N_{el}}(\mathbf{x}|\mathbf{x}') = (1 - (N_{el} - \lfloor N_{el} \rfloor))\rho^{\lfloor N_{el} \rfloor}(\mathbf{x}|\mathbf{x}') + (N_{el} - \lfloor N_{el} \rfloor)\rho^{\lceil N_{el} \rceil}(\mathbf{x}|\mathbf{x}').$$ (1.117)

Since DFT functionals on rungs $1 - 4$ of the ladder in Fig 1.1 are functionals of the 1-RDM $\rho(\mathbf{x}|\mathbf{x}')$, the energy with non-integer electron number is also trivial to find: one simply applies Eqn 1.117 in Step 5 of the SCF procedure in Section 1.10.

For the exact functional, it can been shown that the energy $E_{lin}(N_{el})$ of a system with some non-integer number of electrons N_{el} is a linear interpolation between systems with integer number of electrons [71, 72]

$$E_{lin}(N_{el}) = (1 - (N_{el} - \lfloor N_{el} \rfloor))E(\lfloor N_{el} \rfloor) + (N_{el} - \lfloor N_{el} \rfloor)E(\lceil N_{el} \rceil).$$ (1.118)

We say that a functional obeying Eqn 1.118 displays "integer discontinuities", since the derivative of E with respect to N_{el} is discontinuous at the points where N_{el} is an integer. For an approximate DFT functional (and for Hartree-Fock theory), this is not usually the case. Thus one measure of the (de)localization error is the deviation from linearity

$$\Delta_{lin}(N_{el}) = E(N_{el}) - E_{lin}(N_{el}).$$ (1.119)

The deviation from linearity is usually negative (positive) for DFT (Hartree-Fock theory) when N_{el} is non-integer, and thus shows the presence of the delocalization error (localization error). For instance, for the $C^{0.5+}$ system (a single isolated carbon atom with half an electron removed),

---

[10]Note that the occupation numbers n_i (the eigenvalues of ρ) will no longer all be either 0 or 1, but could take any value between 0 and 1. ρ is thus no longer idempotent. Some authors have extended the concept of non-integer occupation numbers to the MP2 energy as well, meaning that one can define the energy of a double-hybrid (rung-5) functional for a system with non-integer number of electrons [80, 58, 13]. Since we are concerned with functionals of occupied orbitals in this thesis, we will not give such formulae for the MP2 energy here.

we can define

$$\Delta_{\text{lin}}(N_{\text{el}} = 5.5) = E(N_{\text{el}} = 5.5) - \frac{1}{2}E(N_{\text{el}} = 5) - \frac{1}{2}E(N_{\text{el}} = 6). \tag{1.120}$$

We can see this graphically in the plot of Δ_{lin} against number of electrons N_{el} in the lower-right panel of Fig 6.4. If we integrate the square of Δ_{lin} over a range of values of N_{el} we can define another (more robust) measure of (de)localization error [78]:

$$\Delta_{\text{frac}}(N_{\text{el},1}, N_{\text{el},2}) = \int_{N_{\text{el},1}}^{N_{\text{el},2}} dN_{\text{el}} \, |\Delta_{\text{lin}}(N_{\text{el}})|^2. \tag{1.121}$$

Note that the quantity

$$\sqrt{\Delta_{\text{frac}}/(N_{\text{el},2} - N_{\text{el},1})} \tag{1.122}$$

is the root-mean-square deviation from linearity for a series of systems with N_{el} between $N_{\text{el},1}$ and $N_{\text{el},2}$. In Section 6.6, we compare the Δ_{lin} and Δ_{frac} values for the new functionals presented in this thesis with those for existing functionals, and show that our new functionals reduce the (de)localization error.

1.19. Computational scaling of DFT methods

Our aim in this thesis is to demonstrate that it is possible to compute accurate estimates of the correlation energy of molecules using methods that scale formally as N^4 where N represents the size of the system (expressed in terms of total number of electrons, total number of atoms, or a similar measure). For comparison, we now show that the formal scaling of self-consistent pure DFT (rung-3) calculations is N^3, and that the scaling of self-consistent rung-4 hybrid

calculations is N^4. Note also that the formal scaling of rung-5 methods is also N^4 provided that only the same-spin ($s = 1$) part of the MP2 energy $E_{c,s=1}^{PT2}$ is included. To achieve this, a Laplace-transform is used to sum out the energy denominator the opposite-spin terms in the MP2 energy expression (Eqn 1.97) [81].

For a self-consistent DFT calculation, we must differentiate each term in the Kohn-Sham energy expression (Eqn 1.36) to obtain the contributions to the Fock matrix. The contributions arising from the non-interacting kinetic energy $\langle 0|T_{el}|0 \rangle$ and electron-nuclear interaction energy $E_{el,n}$ (from differentiating Eqns 1.39 and 1.41)

$$\frac{\partial \langle 0|T_{el}|0 \rangle}{\partial D_{\alpha\beta}^{\sigma}} = \left\langle \alpha \left| -\frac{1}{2}\nabla_{\mathbf{r}}^2 \right| \beta \right\rangle \tag{1.123}$$

$$\frac{\partial E_{el,n}}{\partial D_{\alpha\beta}^{\sigma}} = \left\langle \alpha \left| V_{el,n}(\mathbf{r}) \right| \beta \right\rangle \tag{1.124}$$

both scale formally as N^2.

1.19.1. Evaluating the Hartree-Fock Exchange Energy $E_{\mathsf{x}}^{\mathsf{HF}}$ and Coulomb energy J

Consider now the Fock matrix contributions arising from the Coulomb energy J (defined in Eqn 1.44) and — for functionals on rungs 4 and above of the Jacob's ladder — the Hartree-Fock exchange energy $E_{\mathsf{x}}^{\mathsf{HF}}$ (defined in Eqn 1.77). The contribution from the exchange energy $E_{\mathsf{x}}^{\mathsf{HF}}$ is

$$\frac{\partial E_{\mathsf{x}}^{\mathsf{HF}}}{\partial D_{\alpha\beta}^{\sigma}} = -\sum_j \delta_{\sigma_j\sigma} \left(\alpha j | r_{12}^{-1} | \beta j \right). \tag{1.125}$$

A naïve approach to evaluating $\partial E_{\mathsf{x}}^{\mathsf{HF}}/\partial D_{\alpha\beta}^{\sigma}$ would be to transform the four-index integrals

$(\alpha\gamma|r_{12}^{-1}|\beta\delta)$ using the formula

$$\left(\alpha j|r_{12}^{-1}|\beta j\right) = \sum_{\gamma\lambda} \phi_j^\star(\gamma)\left(\alpha\gamma|r_{12}^{-1}|\beta\delta\right)\phi_j(\delta) \tag{1.126}$$

where the Kohn-Sham orbital $\phi_j(\boldsymbol{r})$ is expressed in terms of atomic-orbitals $\{\alpha(\boldsymbol{r})\}$ as

$$\phi_j(\boldsymbol{r}) = \sum_\alpha \phi_j(\alpha)\alpha(\boldsymbol{r}). \tag{1.127}$$

We can see immediately that the computational cost for evaluating $\partial E_{\mathrm{x}}^{\mathrm{HF}}/\partial D_{\alpha\beta}^\sigma$ in this way for all atomic orbital pairs $\alpha\beta$ scales as[11]

$$N_{\mathrm{AO}}^4 N_{\mathrm{el}} \propto N^5 \tag{1.128}$$

where N_{AO} is the number of atomic orbital basis functions $\{\alpha(\boldsymbol{r})\}$, N_{el} is the number of electrons, and N represents the size of the system. We now show that it is possible to evaluate the exchange Fock matrix contribution in a time that scales as N^4, using density-fitting.[12] We use an auxiliary basis of N_{DF} one-electron functions $\{C(\mathbf{r})\}$ to write the two-electron r_{12}^{-1} integrals as [83, 84, 85, 86]

$$\langle ij|r_{12}^{-1}|kl\rangle \approx \langle ij|r_{12}^{-1}|kl\rangle_{\mathrm{DF}} = \sum_{CD}(ik|r_{12}^{-1}|C)(\mathbf{V}^{-1})_{CD}(D|r_{12}^{-1}|jl)\,, \tag{1.129}$$

$$= \sum_C (ik|r_{12}^{-1}|C)(\tilde{C}|r_{12}^{-1}|jl) \tag{1.130}$$

where $\mathbf{V}$ is the matrix of two-index Coulomb integrals in the density-fitting basis. $\mathbf{V}$ is

---

[11]In estimating the slowest step of the calculation, we assume that $N_{\mathrm{AO}} > N_{\mathrm{el}}$.

[12]Note that older papers use the term "resolution of the identity" (RI) to refer to density-fitting [82]. In this thesis we use the term "density-fitting" throughout.

positive-definite and has elements

$$V_{DC} = (D|r_{12}^{-1}|C).$$ (1.131)

where we use the notation

$$(ik|r_{12}^{-1}|C) = s_{ik} \int d\mathbf{r}_1 \int d\mathbf{r}_2 \; \phi_i^\star(\mathbf{r}_1)\phi_k(\mathbf{r}_1) \; r_{12}^{-1} \; C(\mathbf{r}_2)$$ (1.132)

$$(D|r_{12}^{-1}|C) = \int d\mathbf{r}_1 \int d\mathbf{r}_2 \; D(\mathbf{r}_1) \; r_{12}^{-1} \; C(\mathbf{r}_2).$$ (1.133)

The function $(\tilde{C}|$ in Eqn 1.130 is defined as

$$(\tilde{C}| = \sum_D (\mathbf{V}^{-1})_{CD}(D|.$$ (1.134)

The advantage of the density-fitting method comes from the fact that the number of density-fitting functions N_{DF} scales linearly with the system size N, despite the fact that the number of electron pairs ij scales quadratically. The exchange energy becomes

$$E_{\mathrm{x}}^{\mathrm{HF}} = -\frac{1}{2}\sum_C (ij|r_{12}^{-1}|C)(\tilde{C}|r_{12}^{-1}|ij)$$ (1.135)

and the derivative of the energy with respect to the density matrix becomes

$$\partial E_{\mathrm{x}}^{\mathrm{HF}}/\partial D_{\alpha\beta}^\sigma = -\sum_j \delta_{\sigma_j\sigma} \sum_C (\alpha j|r_{12}^{-1}|C)(\tilde{C}|r_{12}^{-1}|\beta j).$$ (1.136)

The computational scaling of evaluating $\partial E_{\mathrm{x}}^{\mathrm{HF}}/\partial D_{\alpha\beta}^{\sigma}$ for all orbital pairs $\alpha\beta$ is thus[13]

$$N_{\mathrm{DF}}^2 N_{\mathrm{AO}} N_{\mathrm{el}} \propto N^4, \tag{1.137}$$

since we need to evaluate

$$(\tilde{C}|r_{12}^{-1}|\beta j) = \sum_D (\mathbf{V}^{-1})_{CD} (D|r_{12}^{-1}|\beta j). \tag{1.138}$$

By using density-fitting, the computational scaling has been reduced from N^5 to N^4. Note that the choice of r_{12}^{-1} in Eqn 1.131 could be replaced with any positive-definite kernel $v(\mathbf{r}_1, \mathbf{r}_2)$. One obvious choice would be $v(\mathbf{r}_1, \mathbf{r}_2) = \delta(\mathbf{r}_1 - \mathbf{r}_2)$, which leads to $\mathbf{V} = \mathbf{S}$ where $\mathbf{S}$ is the overlap matrix. However, it can be shown that setting $v(\mathbf{r}_1, \mathbf{r}_2) = w(r_{12})$ when approximating $\langle ij|w(r_{12})|kl\rangle$ using Eqn 1.130 leads to a cancellation of the first-order error term [83, 84, 85, 86].

We conclude this section by remarking that the Coulomb energy J (defined in Eqn 1.44) and corresponding derivative can be evaluated using the formulae

$$J = \frac{1}{2} \sum_C \sum_{ij} (ii|r_{12}^{-1}|C)(\tilde{C}|r_{12}^{-1}|jj) \tag{1.139}$$

$$\partial J/\partial D_{\alpha\beta}^{\sigma} = \sum_C (\alpha\beta|r_{12}^{-1}|C) \sum_j (\tilde{C}|r_{12}^{-1}|jj). \tag{1.140}$$

The formal scaling for evaluating all the elements $\partial J/\partial D_{\alpha\beta}^{\sigma}$ in this way is

$$N_{\mathrm{DF}} N_{\mathrm{AO}}^2 \propto N^3. \tag{1.141}$$

---

[13]In estimating the slowest step of the calculation, we assume that $N_{\mathrm{DF}} > N_{\mathrm{AO}} > N_{\mathrm{el}}$.

1.19.2. Evaluating the Density-Functional-Theory Exchange-Correlation Energy E_{xc}^{DFT}

We now turn our attention to the Fock matrix contribution arising from the DFT exchange-correlation energy E_{xc}^{DFT} (defined in Eqn 1.51). For LDA, this is given by

$$\frac{\partial E_{xc}^{LDA}}{\partial D_{\alpha\beta}^{\sigma}} = \int d\mathbf{r} \, V_{xc}^{LDA,\sigma}(\mathbf{r}) \, \frac{\partial \rho^{\sigma}(\mathbf{r})}{\partial D_{\alpha\beta}^{\sigma}} \tag{1.142}$$

$$= \int d\mathbf{r} \, V_{xc}^{LDA,\sigma}(\mathbf{r}) \, \alpha^{\star}(\mathbf{r})\beta(\mathbf{r}) \tag{1.143}$$

where the exchange-correlation potential $V_{xc}^{LDA,\sigma}(\mathbf{r})$ is defined as

$$V_{xc}^{LDA,\sigma}(\mathbf{r}) = \frac{\partial E_{xc}^{LDA}}{\partial \rho^{\sigma}(\mathbf{r})} = \frac{\partial \epsilon_{xc}^{LDA}(\mathbf{r})}{\partial \rho^{\sigma}(\mathbf{r})}. \tag{1.144}$$

Eqn 1.143 is commonly evaluated using a quadrature grid of N_{grid} grid points $\{\mathbf{r}_{\lambda}\}$ with real weights $\{w_{\lambda}\}$

$$\frac{\partial E_{xc}^{LDA}}{\partial D_{\alpha\beta}^{\sigma}} \approx \sum_{\lambda} w_{\lambda} V_{xc}^{LDA,\sigma}(\mathbf{r}_{\lambda}) \, \alpha^{\star}(\mathbf{r}_{\lambda})\beta(\mathbf{r}_{\lambda}), \tag{1.145}$$

an approach developed and popularised by Becke, Handy, and Baerends in the early 1990s [87, 88, 89]. An inspection of Eqn 1.145 reveals that the slowest step in evaluating all the elements of $\partial E_{xc}^{LDA}/\partial D_{\alpha\beta}^{\sigma}$ scales as

$$N_{AO}^2 N_{grid} \propto N^3 \tag{1.146}$$

where N_{AO} is the number of atomic orbital basis functions $\{\alpha(\boldsymbol{r})\}$ and N represents the size of the system.

Since the computational complexity of evaluating the derivatives (Fock matrix contributions) for all the terms in Eqn 1.36 is N^3 or lower, we say that the formal scaling of LDA implemented in the manner described is N^3. A simple extension of this formalism to include GGAs and meta-GGAs allows the evaluation of all functionals on rungs 1-3 of the Jacob's ladder (semi-local functionals) in a time that scales formally as N^3.

1.20. Aims of this thesis

In this chapter, we reviewed some of the hybrid and double-hybrid functionals that are the current state-of-the-art in DFT. We have seen that hybrid functionals contain ingredients that are reminiscent of wavefunction-based methods: the Hartree-Fock exchange energy (in rung-4 functionals) and the MP2 correlation energy (in rung-5 functionals). In this thesis, we aim to develop *new* ingredients that can be added into hybrid functionals in order to improve their accuracy (particularly for systems with delocalization errors), whilst maintaining the simplicity and low computational cost that makes DFT popular. In Chapter 2, we present one such new ingredient, which we term UW12, and compare its performance with that of existing rung-4 and rung-5 functionals.

Having categorized existing functionals using the Jacob's ladder illustration, we observed in Section 1.8 that it should be possible to construct "rung-4b" functionals: functionals which contain non-local correlation models but which only depend on occupied Kohn-Sham orbitals. In principle, such functionals should share all the advantages of conventional rung-4a methods (such as a fast basis-set convergence), but with an accuracy approaching that of rung-5 functionals. In Chapters 5 and 6, we attempt to develop such functionals.

We showed that the formal scaling of a self-consistent DFT calculation was N^3 for the pure-DFT functionals on rungs 1–3 of the Jacob's ladder, and N^4 for the hybrid and double-hybrid

functionals on rungs 4–5 (provided that the same-spin $s = 1$ term of the E_c^{MP2} term is excluded from the double-hybrids). In Chapter 3 we demonstrate that the formal scaling of our new rung-4b functionals is also N^4.

1.21. Outline of Thesis

In Chapter 2, we propose a new correlation model (UW12) that is similar in form to MP2, but which can be written in terms of only occupied Kohn-Sham orbitals.

In Chapter 3, we present algorithms for the evaluation of the UW12 energy using atomic-orbital basis-sets.

In Chapter 4, we describe how the molecular integrals used in the algorithms in Chapter 3 were evaluated.

In Chapters 5 and 6, we combine the UW12 model with DFT to make new hybrid functionals. We apply these functionals to a variety of chemical systems: in particular those where the self-interaction error in DFT is most apparent.

In Chapter 7, we summarize our findings and give an outlook for the future.

2. The UW12 correlation model

2.1. Chapter Aims

In Section 1.14.1, we saw that the dependence on unoccupied Kohn-Sham orbitals $\{\phi_a\}$ in the E_c^{PT2} term makes orbital-optimization of double-hybrid functionals non-trivial. The dependence also gives double-hybrid functionals a slower basis-set convergence (see Section 1.9) than hybrid functionals [48].

In this chapter, we seek new correlation models ("ingredients") that can be included as E_c^{nl}. The new models should have wavefunction-character (be similar to E_c^{PT2}) but should depend only on *occupied* Kohn-Sham orbitals $\{\phi_i\}$. More specifically, we will seek expressions that are explicit functionals of the 1-RDM $\rho(\mathbf{x}|\mathbf{x}')$ defined in Eqn 1.31. The total energy can thus be minimized with respect to $\rho(\mathbf{x}|\mathbf{x}')$ in the usual Kohn-Sham manner (see Section 1.10).

2.1.1. Original Contribution

To our knowledge, no fully-self-consistent Kohn-Sham DFT methods currently exist that contain non-local correlation terms that are explicit functionals of the 1-RDM. The model and approach developed in this chapter are hence entirely novel, as are the algorithms for evaluating the energy and Fock matrix in Chapter 3. These algorithms have been published in the Journal

of Chemical Theory and Computation [1]. The data and graphs of Ref [1] are the work of the author of this thesis. The theory and text of Ref [1] were co-written by the author of this thesis and by Fred Manby.

2.2. The UW12 Correlation Energy

Consider the MP2 energy expression defined in Eqn 1.97. In the Unsöld approximation the denominator is approximated as a single characteristic energy gap Δ to give [90]

$$E_c^U = -\frac{1}{2}\frac{1}{\Delta}\sum_{ijab}\langle ij|r_{12}^{-1}|\overline{ab}\rangle\langle ab|r_{12}^{-1}|ij\rangle. \tag{2.1}$$

The model implicitly expresses the amplitudes for double excitations in the form

$$T_{ab}^{ij} \approx -\frac{1}{\Delta}\langle ij|r_{12}^{-1}|\overline{ab}\rangle \tag{2.2}$$

which, *prima facie*, is a terrible approximation, since the excitation energies $(\epsilon_a + \epsilon_b - \epsilon_i - \epsilon_j)$ could range over several orders of magnitude. In particular, Eqn 2.2 gives the same weighting $1/\Delta$ to excitations from the HOMO to the LUMO as it does to excitations from the HOMO to *any* other virtual orbital, rather than giving a lower weighting to high-energy excitations [53]. But without changing the structure of the theory, we can formulate models of the form

$$T_{ab}^{ij} \approx \langle ij|w_{12}|\overline{ab}\rangle \tag{2.3}$$

where w_{12} is a two-electron operator to be determined. We arrive at the Unsöld-W12 (UW12) correlation energy[1]

$$E_c^{UW12} = \frac{1}{2} \sum_{ijab} \langle ij|w_{12}|\overline{ab}\rangle \langle ab|r_{12}^{-1}|ij\rangle. \tag{2.4}$$

Note that E_c^{UW12} is linear in the operator w_{12}, which we refer to as the "geminal" operator. The w_{12} operator serves the purpose of "screening-out" the excitations into high-lying unoccupied orbitals, thus making Eqn 2.3 into a better model for the double-excitation amplitude.

2.2.1. Removing the Summation over Unoccupied Orbitals

In Eqn 2.4, it appears that calculating E_c^{UW12} requires summing over the (infinite set of) unoccupied orbitals $\{\phi_a\}$. We now show that E_c^{UW12} can be expressed in terms of only the (finite set of) occupied orbitals $\{\phi_i\}$. First recognize that

$$\sum_{ab} |\overline{ab}\rangle\langle ab| = \sum_{pq} |\overline{pq}\rangle\langle pq| + \sum_{ij} |\overline{ij}\rangle\langle ij| - \sum_{ip} |\overline{ip}\rangle\langle ip| - \sum_{ip} |\overline{pi}\rangle\langle pi| \quad (2.5)$$

is an exact identity, where $\{\phi_p\}$ is the (infinite) orthonormal set of all Kohn-Sham orbitals. Now recognize that the operator $\sum_p |p\rangle\langle p|$ is the unit operator in the (infinite) space of single-particle wavefunctions. Substituting Eqn 2.5 into Eqn 2.4, we arrive at

$$E_c^{UW12} = E_{c,2el}^{UW12} + E_{c,3el}^{UW12} + E_{c,4el}^{UW12} \tag{2.6}$$

---

[1]Note that singly-excited determinants are ignored in this theory (see Section 1.13.1). In Appendix B, we show how the singly-excited contribution may be added to the E_c^{UW12} energy.

where

$$E_{c,2el}^{UW12} = \frac{1}{2} \sum_{ijpq} \langle ij|w_{12}|\overline{pq}\rangle \langle pq|r_{12}^{-1}|ij\rangle \tag{2.7}$$

$$= \frac{1}{2} \sum_{ij} \langle \overline{ij}|w_{12}r_{12}^{-1}|ij\rangle \tag{2.8}$$

$$= \frac{1}{2} \sum_{ij} (ii|w_{12}r_{12}^{-1}|jj) - \frac{1}{2} \sum_{ij} (ij|w_{12}r_{12}^{-1}|ji) \quad \text{(Mulliken notation)}$$

$$\tag{2.9}$$

$$E_{c,3el}^{UW12} = -\sum_{ijkq} \langle ij|w_{12}|\overline{kq}\rangle \langle kq|r_{12}^{-1}|ij\rangle \tag{2.10}$$

$$= -\sum_{ijk} \langle \overline{ij}k|w_{12}r_{23}^{-1}|kji\rangle \tag{2.11}$$

$$= -\sum_{ijk} (ik|w_{12}|jj|r_{23}^{-1}|ki) + \sum_{ijk} (jk|w_{12}|ij|r_{23}^{-1}|ki) \quad \text{(Mulliken notation)}$$

$$\tag{2.12}$$

$$E_{c,4el}^{UW12} = \frac{1}{2} \sum_{ijkl} \langle ij|w_{12}|\overline{kl}\rangle \langle kl|r_{12}^{-1}|ij\rangle \tag{2.13}$$

$$= \frac{1}{2} \sum_{ijkl} (ik|w_{12}|jl)(ki|r_{12}^{-1}|lj) - \frac{1}{2} \sum_{ijkl} (il|w_{12}|jk)(ki|r_{12}^{-1}|lj). \quad \text{(Mulliken notation)}$$

$$\tag{2.14}$$

Note that this is an exact relation, and is made possible by the structure of the model in Eqn 2.4. Such a completeness relation is not possible in conventional MP2 theory (Eqn 1.97) due to the energy denominator $1/(\epsilon_a + \epsilon_b - \epsilon_i - \epsilon_j)$. We can also write the components of E_c^{UW12} as

explicit functionals of the 1-RDM:

$$E_{c,2el}^{UW12} = \int d\mathbf{x}_1 \int d\mathbf{x}_2 \, w_{12} \, r_{12}^{-1} \, \Gamma_{12|12}^{(2)} \tag{2.15}$$

$$E_{c,3el}^{UW12} = -2 \int d\mathbf{x}_1 \int d\mathbf{x}_2 \int d\mathbf{x}_3 \, w_{12} \, r_{23}^{-1} \, \rho_{3|1} \, \Gamma_{12|32}^{(2)} \tag{2.16}$$

$$E_{c,4el}^{UW12} = \int d\mathbf{x}_1 \int d\mathbf{x}_2 \int d\mathbf{x}_3 \int d\mathbf{x}_4 w_{12} \, r_{34}^{-1} \, \rho_{3|1} \, \rho_{4|2} \, \Gamma_{12|34}^{(2)} \tag{2.17}$$

where we define the two-particle reduced-density-matrix (2-RDM) $\Gamma_{12|34}^{(2)}$ as[2]

$$\Gamma_{12|34}^{(2)} = \frac{1}{2!} \begin{vmatrix} \rho_{1|3} & \rho_{1|4} \\ \rho_{2|3} & \rho_{2|4} \end{vmatrix} \tag{2.18}$$

and use the notation $\rho_{1|2} \equiv \rho(\mathbf{x}_1|\mathbf{x}_2)$.

The UW12 model relies on the efficient computation of the three-electron integrals in Eqn 2.11, which are defined as

$$\langle pqr|w_{12}r_{23}^{-1}|stu\rangle =$$
$$\int d\mathbf{x}_1 \int d\mathbf{x}_2 \int d\mathbf{x}_3 \, \phi_p^\star(\mathbf{x}_1)\phi_q^\star(\mathbf{x}_2)\phi_r^\star(\mathbf{x}_3) \, w_{12}r_{23}^{-1} \, \phi_s(\mathbf{x}_1)\phi_t(\mathbf{x}_2)\phi_u(\mathbf{x}_3) \,, \tag{2.19}$$

and are sometimes written in a form of Mulliken notation as $(ps|w_{12}|qt|r_{23}^{-1}|ru)$. A direct approach to evaluating these by transforming atomic orbital integrals $(\alpha\beta|w_{12}|\gamma\delta|r_{23}^{-1}|\epsilon\zeta)$ has a computational cost that scales formally as $N_{AO}^6 N_{el} \propto N^7$ (where N_{AO} is the size of the atomic orbital basis-set $\{\alpha(r)\}$, and N is the size of the system). This is far higher than the formal scaling (N^4) of density-fitted Hartree-Fock theory (see Section 1.19.1). Luckily — due to the popularity of F12 methods in quantum chemistry — numerous algorithms have been developed

---

[2]Note that Eqn 2.18 does not hold for general many-electron wavefunctions $\Psi(\mathbf{r}_1,\mathbf{r}_2,\dots)$, but is valid for Slater-determinant wavefunctions like that of the Kohn-Sham auxiliary system.

to reduce the formal scaling for evaluating Eqn 2.11 to N^4. The most popular of these methods either evaluate the integral over $\mathbf{x}_2$ in Eqn 2.19 using a resolution-of-the-identity in some orthonormal basis-set $\{x(\mathbf{r})\}$ [91, 92]

$$\langle pqr|w_{12}r_{23}^{-1}|stu\rangle \approx \sum_x \langle pq|w_{12}|sx\rangle\langle xr|r_{12}^{-1}|tu\rangle , \tag{2.20}$$

or evaluate the $\mathbf{x}_2$ integral directly using a quadrature grid [93, 94]. Since our aim in this work is to produce a method that has a fast basis-set convergence, we choose the quadrature grid method, as outlined in Section 3.2.2.

2.2.2. Relationship to MP2-F12

In explicitly-correlated second-order Møller-Plesset theory (MP2-F12), the correlation energy is given by [95]

$$E_c^{\text{MP2-F12}} = \frac{1}{2}\sum_{ij\tilde{a}\tilde{b}} T_{\tilde{a}\tilde{b}}^{ij}\langle \tilde{a}\tilde{b}|r_{12}^{-1}|ij\rangle$$
$$+ \frac{1}{2}\sum_{ijkl} T_{kl}^{ij}\langle kl|f_{12}\Big[\sum_{ab}|ab\rangle\langle ab| - \sum_{\tilde{a}\tilde{b}}|\tilde{a}\tilde{b}\rangle\langle \tilde{a}\tilde{b}|\Big]r_{12}^{-1}|ij\rangle, \tag{2.21}$$

where the indices $\tilde{a}\tilde{b}$ run over the set $\{\phi_{\tilde{a}}\}$ of all unoccupied orbitals in the given atomic orbital basis, and the indices ab run over the set $\{\phi_a\}$ of all unoccupied orbitals in a complete single-particle basis. Consider the case where the atomic orbital basis is minimal, such that the set $\{\phi_{\tilde{a}}\}$ is empty. The expression then becomes

$$E_c^{\text{MP2-F12}} = \frac{1}{2}\sum_{ijklab} T_{kl}^{ij}\langle kl|f_{12}|ab\rangle\langle ab|r_{12}^{-1}|ij\rangle. \tag{2.22}$$

If we set the MP2-F12 occupied-occupied amplitudes to be[3]

$$T_{kl}^{ij} = -\frac{1}{\Delta}(\delta_{ik}\delta_{jl} - \delta_{il}\delta_{jk}),\tag{2.23}$$

and the geminal $f_{12} = -\Delta w_{12}$ (where Δ is some characteristic energy scale), then Eqn 2.22 reduces to the UW12 correlation energy (Eqn 2.4).[4]

2.2.3. Relationship to the Common Energy-Denominator Approximation

Consider the effective Kohn-Sham exchange potential defined as

$$v_\sigma(\mathbf{r}) = \frac{\delta E_{\mathrm{x}}}{\delta \rho_\sigma(\mathbf{r})}.\tag{2.24}$$

For neutral molecules, it can be shown that far from the molecule $v_\sigma(\mathbf{r})$ should decay as r^{-1} where r is the distance from the centre of the molecule. Qualitatitively, each electron experiences a positive attractive charge $+N_{\mathrm{el}}$ from the nuclei but a negative repulsive charge $-(N_{\mathrm{el}} - 1)$ from the other electrons [96]. However, standard LDA and GGA functionals give a Kohn-Sham potential that decays too quickly (exponentially) with distance from the molecule. This is a symptom of self-interaction error, since electron far from the molecule is effectively being repelled by N_{el} electrons rather than $N_{\mathrm{el}} - 1$ electrons [96]. This gives LDA and many GGA functionals a poor qualitative description of unoccupied orbitals and dipole polarizability tensors [97]. It also causes problems in describing molecular anions [98, 96]. For this reason,

---

[3]This *ansatz* for the T_{kl}^{ij} amplitudes is equivalent to making the *diagonal* approximation (see Section II.I of Ref [95]), and then setting all the amplitudes to a common value $T_{ij}^{ij} = -T_{ji}^{ij} = -1/\Delta$ (*i.e.* the Unsöld approximation). Note that this expression is orbital-invariant.

[4]We choose the letter w (as opposed to f) to refer to the geminal function in our work, since the geminal function serves a different purpose in UW12 theory and F12 theory: The geminal function f_{12} in F12 theory accounts for the finite atomic-orbital basis-set, whereas in UW12 theory the geminal function w_{12} contains all the information on electron correlation, including the energy- and length-scale.

many authors use the optimized effective potential (OEP) method to obtain a local Kohn-Sham effective exchange potential $v_\sigma(\mathbf{r}_2)$ with the correct asymptotic properties. A discussion of the OEP method is beyond the scope of this thesis; suffice to say that the method requires solving equations of the form [99, 100]

$$\sum_i \delta_{\sigma_i \sigma} \int d\mathbf{r}_2 [v_\sigma(\mathbf{r}_2) - v^i(\mathbf{r}_2)] \phi_i^\star(\mathbf{r}_2) \phi_i(\mathbf{r}_1) G_i(\mathbf{r}_1, \mathbf{r}_2) + \text{c.c.} = 0 \qquad (2.25)$$

for the effective exchange potential $v_\sigma(\mathbf{r}_2)$, where the Hartree-Fock orbital potentials are given by

$$v_x^i(\mathbf{r}_2) = -\frac{1}{\phi_i^\star(\mathbf{r}_2)} \int d\mathbf{r}_3 \frac{\rho(\mathbf{r}_2|\mathbf{r}_3)}{r_{13}} \phi_i^\star(\mathbf{r}_3) \qquad (2.26)$$

and the orbital Green's function is given by

$$G_i(\mathbf{r}_1, \mathbf{r}_2) = \sum_{p \neq i} \delta_{\sigma_p \sigma_i} \frac{\phi_p(\mathbf{r}_1) \phi_p^\star(\mathbf{r}_2)}{\epsilon_p - \epsilon_i}. \qquad (2.27)$$

Eqn 2.25 can be simplified by replacing all the $\epsilon_a - \epsilon_i$ denominators with a common value Δ where a is unoccupied. This is the common energy-denominator (CEDA) approximation, and has the same spirit as the Unsöld approximation. Eqn 2.27 becomes [99, 100]

$$G_i(\mathbf{r}_1, \mathbf{r}_2) = \sum_a \delta_{\sigma_a \sigma} \frac{\phi_a(\mathbf{r}_1) \phi_a^\star(\mathbf{r}_2)}{\Delta} + \sum_{j \neq i} \delta_{\sigma_j \sigma} \frac{\phi_j(\mathbf{r}_1) \phi_j^\star(\mathbf{r}_2)}{\epsilon_j - \epsilon_i}. \qquad (2.28)$$

We can use the relations

$$\rho(\mathbf{r}_2|\mathbf{r}_1) = \sum_i \phi_i^\star(\mathbf{r}_2) \phi_i(\mathbf{r}_1) \qquad (2.29)$$

and

$$\sum_p \phi_p^\star(\mathbf{r}_2)\phi_p(\mathbf{r}_1) = \delta(\mathbf{r}_1 - \mathbf{r}_2) \tag{2.30}$$

to remove the summation over a and write the Green's function as

$$G_i(\mathbf{r}_1,\mathbf{r}_2) = \frac{1}{\Delta}\left(\delta(\mathbf{r}_2 - \mathbf{r}_1) - \rho(\mathbf{r}_2|\mathbf{r}_1)\right) + \sum_{j\neq i}\delta_{\sigma_j\sigma}\frac{\phi_j(\mathbf{r}_1)\phi_j^\star(\mathbf{r}_2)}{\epsilon_j - \epsilon_i}. \tag{2.31}$$

Substituting this into Eqn 2.25 gives

$$\sum_i \delta_{\sigma_i\sigma}\int d\mathbf{r}_2[v_\sigma(\mathbf{r}_2) - v^i(\mathbf{r}_2)]\phi_i^\star(\mathbf{r}_2)\phi_i(\mathbf{r}_1)$$
$$\times\left(\frac{1}{\Delta}\left(\delta(\mathbf{r}_2 - \mathbf{r}_1) - \rho(\mathbf{r}_2|\mathbf{r}_1)\right) + \sum_{j\neq i}\delta_{\sigma_j\sigma}\frac{\phi_j(\mathbf{r}_1)\phi_j^\star(\mathbf{r}_2)}{\epsilon_j - \epsilon_i}\right) + \text{c.c.} = 0, \tag{2.32}$$

which can then be solved using iterative means. The advantage of Eqn 2.32 over Eqn 2.25 is that Eqn 2.32 contains no summations over unoccupied orbitals. The method for removing the summation over unoccupied orbitals is similar to that used in deriving the UW12 method (see Section 2.2.1), although the application is very different: in the CEDA it is used to simplify the calculation of the OEP, whereas in UW12 it is used to motivate a new model for the correlation energy. We make no further reference to CEDA in this thesis, and mention it here purely for the reader's interest.

2.2.4. Other Related Work

Since performing the work presented in this thesis, we learned that a method with the same energy expression as the UW12 method was independently suggested by Grüneis in 2015 [101] (where it is referred to as "... an interesting method on its own..."). Although Grüneis

is optimistic about the simplicity and basis-set convergence of such an expression, no mention is made of including the expression in fully-self-consistent Kohn-Sham calculations. We believe this is a major advantage of the UW12 method for molecules and transition states (see Section 1.14.1).

In addition, Grüneis chooses to evaluate the three-electron integrals in Eqn 2.19 on a reciprocal-space grid rather than a real-space grid, reflecting the fact that his paper is primarily concerned with solid-state calculations rather than molecules.

2.3. Choosing the Geminal Operator w_{12}

Motivated by the r_{12} methods of explictly-correlated electronic structure theory [102, 103], let us now choose the operator w_{12} to simply be a function of the distance r_{12} between the two electrons

$$w_{12} = w^{s_{12}}(r_{12}) \tag{2.33}$$

where $s_{12} = \delta_{\sigma_1 \sigma_2}$ is the total spin of the two electrons. Note that E_c^{UW12} is invariant to adding a constant c to $w^s(r_{12})$.

We can choose the $w^s(r_{12})$ to correctly model the correlation at any length scale. Inspired by the work of Ten-no [104], we choose $w^s(r_{12})$ to be a Slater-type function in the inter-electron coordinate r_{12}

$$w^{s_{12}}(r_{12}) = -\frac{1}{2(s_{12} + 1)} r_c e^{-r_{12}/r_c} \tag{2.34}$$

where r_c is a characteristic length scale for electron correlation. Dynamical correlation effects are assumed to be less significant for electrons that are far apart (separated by a distance

greater than r_c) due to the screening effect of the other $N_{el} - 2$ electrons. The pre-factor of r_c in Eqn 2.34 ensures that the "cusp condition" is satisfied [94, 104]

$$\left. \frac{dw^{s_{12}}(r_{12})}{dr_{12}} \right|_{r_{12}=0} = \frac{1}{2(s_{12}+1)}. \tag{2.35}$$

This cusp condition can be motivated by considering length-scaling in theoretical models. However, there is no guarantee that such scaling behaviours should hold for molecules. For the functionals developed in Chapter 6, we relax the cusp condition entirely and allow the prefactory of UW12 correlation a_c^{UW12} to vary freely.

In the F12 community, Slater-type geminals such as that shown in Eqn 2.34 have been shown to be accurate for the Helium atom with a range of r_c values, and have been shown to be just as effective as other functional forms [105, 95]. Slater-type geminals were first proposed by Ten-no [94], and have since become widely used.

An alternative choice of geminal operator (based on the success of spin-opposite-scaled double-hybrids) is to use

$$w^{s_{12}}(r_{12}) = -\frac{1}{2}r_c(1 - s_{12})e^{-r_{12}/r_c} \tag{2.36}$$

which is zero when the electrons have parallel spins (when $s_{12} = 1$). We use Eqn 2.34 for the hybrid functionals presented in Chapter 5. We use Eqn 2.36 for the hybrid functionals presented in Chapter 6.

In the future, studies of model systems may lead to more physically-motivated choices for the geminal $w^s(r_{12})$. Such choices may lead to improved accuracy for UW12 methods. However, in the present thesis we will use the choices given in Eqns. 2.34 and 2.36 throughout.

2.4. Chapter Summary

In this chapter, we motivated a new approximation to the correlation energy (which we named UW12) that depends only on occupied Kohn-Sham orbitals. We showed that UW12 can be viewed as a special case of MP2-F12 theory, but can be written as an explicit functional of the 1-RDM $\rho(\mathbf{r}|\mathbf{r}')$. In Chapter 3, we show how the UW12 correlation energy may be evaluated efficiently for molecules. In Chapters 5 and 6, we assess the performance of hybrid functionals containing UW12. We will refer to these as "rung-4b" functionals, since they do not fit into any of the conventional categories shown in the Jacob's Ladder of Table 1.1.

3. Evaluating the UW12 Energy

3.1. Chapter Aims

In Chapter 2, we defined a new correlation model (UW12) that is an explicit functional of the 1-RDM $\rho(\boldsymbol{r}|\boldsymbol{r}')$. In this chapter, we discuss algorithms for evaluating the UW12 energy of molecules efficiently. We also evaluate matrix $\boldsymbol{F}^{\sigma}$, enabling us to optimize the Kohn-Sham orbitals self-consistently. We describe how each algorithm was implemented in the electronic structure program `entos` [42].

3.1.1. Original Contribution

To our knowledge, the approach used in this work — using wavefunction-like correlation terms that are explicit functionals of the 1-RDM in a fully-self-consistent Kohn-Sham framework — has not been attempted before. This presented a challenge, since new algorithms and techniques needed to be developed; combining ideas from wavefunction theory and density-functional theory. Ideas from the F12 literature were particularly instructive, and the author acknowledges Ten-no [94] for inspiration on grid methods in F12 theories. Without these ideas, the N^3 scaling algorithms presented in Section 3.2.2 would not have been possible

The work to develop, implement, and test the UW12 model (in addition to the XCH-UW12-BLYP and BLYP-osUW12 families of hybrid density functionals) was carried out by the author of this thesis under the supervision of Professor Fred Manby. The UW12 (see Chapters 2 and 3) and XCH-UW12-BLYP (see Chapter 5) work has been published in the Journal of Chemical Theory and Computation [1].

The remainder of this chapter is concerned with the design of efficient algorithms for evaluating the UW12 energy and Fock matrix. The algorithms were designed in order to obtain the optimal formal scaling for practical molecular electronic structure calculations. The work presented here demonstrates that UW12 approaches are feasible in practical electronic structure calculations and could in the future be made competitive in computational cost with standard approaches such as B3LYP.

Another noteworthy intellectual contribution is the N^4 scaling algorithm for the indirect UW12 term (see Section 3.2.4 and Appendix 3.22).[1] This was a development that was not anticipated at the start of the project, and was praised by the reviewers of the original XCH-UW12-BLYP paper (Ref [1]) in a private communication.

The `entos` code (in its final, production-quality form) takes the form of a library of C++11 files in the `entos` source code directory. The library can be found in the `unsoldw12` folder of the entos source directory, and is entirely the work of the author of this thesis. The library is included in all standard `entos` builds, and UW12 corrections can thus be included fully-self-consistently in any Kohn-Sham DFT calculation.

The `unsoldwr` library of the `intception` molecular integral package is also the work of the author of this thesis, and is included in all standard `entos` builds. See Section 4.1.1 for a full description.

---

[1]The author gives credit to the Holy Spirit for this idea, since it came to him in a dream following a late-night bible study.

In total, the `unsoldw12` library of the `entos` package contains 3930 lines of production-level code. The `unsoldwr` library of the `intception` package contains 666 lines of production-level code. The code is fully unit-tested. Application-level tests are also provided for the UW12 functionality and can be found in the `test/unsoldw12*.in` files. These files provide examples of how input files can be written and total 963 lines of executable code.[2]

Calculations on molecular test sets were submitted to supercomputer clusters using a suite of python packages shown in Table 3.1. These packages can be found in the `unsoldpaper` repository, and are entirely the work of the author of this thesis. The suite automates the submission of large numbers of input files to supercomputer clusters using a cacheing mechanism, and is used to produce all the data in Chapters 5 and 6 (unless otherwise stated).

Table 3.1.: Description of the python packages used to produce the graphs and tables in Chapters 5 and 6.

Package	Contents	Lines of production-level python code
`unsoldpaper/` `UW12_double_hybrid_paper`	Code for running calculations and generating the graphs / tables in Chapter 5	2496
`unsoldpaper/` `UW12_derivative` `_discontinuity_paper/`	Code for running calculations and generating the graphs / tables in Chapter 6	906
`unsoldpaper/` `tools`	Utilities for calculating geminal expansion coefficients (see Section), reading and writing input files, and submitting files to clusters	3527
`unsoldpaper/` `testsetdata/`	Code for extracting and collating test set data and molecular geometries from web servers	903

---

[2]These numbers were obtained by checking-out `entos` version `e5ab50ddb6655cff0fc1c50e3850c980372bc69c` (20 April 2019)

3.1.2. Algorithmic Complexity

The library evaluates each of the nine terms in the UW12 Fock matrix expression using the most efficient algorithm for that term. The current implementation scales as N^4 for the opposite-spin ($s = 0$) component of E_c^{UW12}, and scales as N^5 for the same-spin ($s = 1$) component.[3] However, since the algorithms and code presented in this chapter are in the proof-of-concept stage, we provide no timing comparisons with other more established DFT methods – although we do make comments about the relative formal scaling of the methods.

3.2. Constructing the UW12 Energy and Fock matrix

In Chapter 2 we defined the components of the UW12 energy E_c^{UW12} (see Eqns. 2.8, 2.11, and 2.13). In this chapter, we separate the direct $(+, |\overline{pq}\rangle = |pq\rangle)$ and indirect $(-, |\overline{pq}\rangle = -|qp\rangle)$ components of E_c^{UW12} such that

$$E_{c,2el}^{\mathrm{UW12}} = E_{c,2el,+}^{\mathrm{UW12}} + E_{c,2el,-}^{\mathrm{UW12}} \tag{3.1}$$

$$E_{c,3el}^{\mathrm{UW12}} = E_{c,3el,+}^{\mathrm{UW12}} + E_{c,3el,-}^{\mathrm{UW12}} \tag{3.2}$$

$$E_{c,4el}^{\mathrm{UW12}} = E_{c,4el,+}^{\mathrm{UW12}} + E_{c,4el,-}^{\mathrm{UW12}} \; . \tag{3.3}$$

Note that $E_{c,+}^{\mathrm{UW12}}$ contains both opposite-spin ($s = 0$) and same-spin ($s = 1$) terms, whereas $E_{c,-}^{\mathrm{UW12}}$ contains only same-spin ($s = 1$) contributions. In Chapter 6 we neglect the same-spin terms altogether, and thus in Chapter 6 we calculate only the direct $E_{c,+}^{\mathrm{UW12}}$ component.

Listing 3.1: An example input file for `entos`, with the UW12 correlation model.

[3]In Appendix A.1 we propose an N^4-scaling algorithm for the same-spin component. This has not yet been implemented in entos, since our most recent functionals (see Chapter 6) do not depend on the same-spin component.

```
1  ! example_UW12_entos_input_file.in
2
3  dft(
4
5    structure (
6      formula='HF'
7      bond_length=1.73286972296764 bohr
8    )
9
10   ! Use 100% exact exchange
11   xc='HF'
12
13   ! Atomic Orbital basis-set
14   basis = 'cc-pVTZ'
15
16   ! Turn off Schwarz integral screening
17   schwarz_threshold=0.0
18
19   ! Density-fitting basis set
20   density_fitting=true
21   df_basis='cc-pVDZ-JKFIT'
22
23   ! Spin-restricted self-consistent-field
24   ansatz='r'
25
26   ! Use 100% UW12 correlation
27   unsoldw12_factor = 1.0
28
29   ! Use the single-Gaussian geminal function for UW12
30   unsoldw12_coeffs = [ -1.0 ]
31   unsoldw12_exponents = [ 1.0 ]
32   unsoldw12_scale_samespin = 0.5
33
34 )
```

The UW12 energy and Fock matrix were implemented in entos by the author of this thesis.

The code can be found in the src/unsoldw12 directory in the entos source directory.[4]

---

[4]Note that all references to the "exchange term" of UW12 in the code in the src/unsoldw12 directory actually refer to the "indirect term" $E_{c,-}^{UW12}$ of UW12. In this thesis, we prefer to use the term "indirect", since it is reduces confusion with the "exchange energy" E_x.

The UW12 energy can be added to a DFT calculation by using the option `unsoldw12_factor`. For example, the input file shown in Listing 3.1 runs a self-consistent calculation on the HF molecule with the exchange-correlation functional

$$E_{xc} = E_x^{HF} + E_c^{UW12}. \tag{3.4}$$

Note that, for simplicity, Listing 3.1 uses the single-Gaussian geminal (SGG) function

$$w_{SGG}(r_{12}) = -\frac{1}{s_{12+1}}e^{-r_{12}^2} \tag{3.5}$$

for the UW12 energy as opposed to the more complex Gaussian-Type-Geminal function $w_{GTG}(r_{12})$ used in practical calculations (see Eqn 4.4).

We now present algorithms for the efficient evaluation of each term in E_c^{UW12}. From here on in, summation symbols are written in the positions that lead to the most efficient algorithm.

3.2.1. Evaluating the Two-Electron Term

The algorithms in this section were implemented in the
`src/unsoldw12/two_el_term_density_fitting.cpp`
file in the entos source directory.

We observe that the direct two-electron term $E_{c,2el,+}^{UW12}$ is similar to the Coulomb energy E_J (defined in Eqn 1.44), and that the indirect Hartree-Fock exchange term $E_{c,2el,-}^{UW12}$ is similar to the Hartree-Fock exchange energy E_x^{HF} (defined in Eqn 1.77). In each case, the r_{12}^{-1} inter-electron potential is replaced with $w_{12}r_{12}^{-1}$. The direct (+) and indirect (−) energies and corresponding

derivatives (using density-fitting) are thus

$$E_{\text{c,2el,+}}^{\text{UW12}} = \frac{1}{2} \sum_C \sum_{ij} (ii|w_{12}^{s_{ij}} r_{12}^{-1}|C)(\tilde{C}|w_{12}^{s_{ij}} r_{12}^{-1}|jj) \tag{3.6}$$

$$\partial E_{\text{c,2el,+}}^{\text{UW12}} / \partial D_{\alpha\beta}^{\sigma} = \sum_C \sum_j (\alpha\beta|w_{12}^{\delta_{\sigma_j\sigma}} r_{12}^{-1}|C)(\tilde{C}|w_{12}^{\delta_{\sigma_j\sigma}} r_{12}^{-1}|jj), \tag{3.7}$$

which has computational scaling[5]

$$N_{\text{DF}} N_{\text{AO}}^2 \propto N^3, \tag{3.8}$$

and

$$E_{\text{c,2el,-}}^{\text{UW12}} = -\frac{1}{2} \sum_C (ij|w_{12}^1 r_{12}^{-1}|C)(\tilde{C}|w_{12}^1 r_{12}^{-1}|ij) \tag{3.9}$$

$$\partial E_{\text{c,2el,-}}^{\text{UW12}} / \partial D_{\alpha\beta}^{\sigma} = -\sum_j \delta_{\sigma_j\sigma} \sum_C (\alpha j|w_{12}^1 r_{12}^{-1}|C)(\tilde{C}|w_{12}^1 r_{12}^{-1}|\beta j), \tag{3.10}$$

which has computational scaling

$$N_{\text{DF}}^2 N_{\text{AO}} N_{\text{el}} \propto N^4. \tag{3.11}$$

In the above, the transformed integrals $(\tilde{C}|w_{12} r_{12}^{-1}|\beta j)$ are defined as

$$(\tilde{C}|w_{12} r_{12}^{-1}|\beta j) = \sum_D (\mathbf{X}^{-1})_{CD} (D|w_{12} r_{12}^{-1}|\beta j), \tag{3.12}$$

---

[5]In estimating the slowest step of the calculation, we assume that $N_{\text{DF}} > N_{\text{AO}} > N_{\text{el}}$.

where the negative-definite matrix $\mathbf{X}$ has elements[6]

$$X_{DC} = (D|w_{12}r_{12}^{-1}|C). \tag{3.13}$$

Note once again (as discussed in Section 1.19.1) that the choice of kernel $w_{12}r_{12}^{-1}$ in Eqn 3.13 is not unique – but that choosing it in this way enables the cancellation of the first-order error term. All that remains is to evaluate the molecular integrals $(\alpha\beta|w_{12}r_{12}^{-1}|C)$ and $(D|w_{12}r_{12}^{-1}|C)$. These are computed using a modified version of the `intception` library, as outlined in Section 4.3.4. An alternative algorithm that does not involve using modified two-electron integrals is proposed in Appendix A.1, but has not yet been implemented in `entos`.

3.2.2. Evaluating the Three-Electron Term

The algorithms in this section were implemented in the
`src/unsoldw12/three_el_term_on_grid.cpp`
file in the `entos` source directory.

We evaluate the three-electron integrals in Eqn 2.11 through a quadrature in the electron coordinate $\boldsymbol{r}_2$ that couples the w_{12} and r_{23}^{-1} operators together, as proposed by Boys and Handy [93] and independently rediscovered by Ten-no [94]. Thus we evaluate Eqn 2.19 using the formula

$$\langle ijk|w_{12}r_{23}^{-1}|lmn\rangle = s_{jm}\int d\mathbf{r}_2\ \phi_j^\star(\mathbf{r}_2)\phi_m(\mathbf{r}_2)\langle i|w^{s_{ij}}(\mathbf{r}-\mathbf{r}_2)|l\rangle\langle k|v(\mathbf{r}-\mathbf{r}_2)|n\rangle \tag{3.14}$$

where $s_{pq} = \delta_{\sigma_p\sigma_q}$, and $v(\mathbf{r}-\mathbf{r}_2) = 1/|\mathbf{r}-\mathbf{r}_2|$. The integral over $\mathbf{r}_2$ is then performed numerically using the SG-1 quadrature grid [106]. The three-electron energies and corresponding

---

[6]Recall that the definition of $w(r_{12})$ in Eqn 2.34 contains a negative sign. The matrix $\mathbf{X}$ is thus negative-definite.

derivatives are thus

$$E_{c,3el,+}^{UW12} = -\sum_{\lambda} g_{\lambda} \, \rho(\mathbf{r}_{\lambda}) \sum_{jk} (\mathbf{r}_{\lambda}|w_{12}^{\delta_{\sigma_j\sigma}}|jk)(\mathbf{r}_{\lambda}|r_{12}^{-1}|kj) \Big] \tag{3.15}$$

$$\partial E_{c,3el,+}^{UW12}/\partial D_{\alpha\beta}^{\sigma} = -2\sum_{jk} \langle \alpha jk|w_{12}r_{23}^{-1}|kj\beta\rangle - \sum_{jk} \langle j\alpha k|w_{12}r_{23}^{-1}|k\beta j\rangle \tag{3.16}$$

$$= -2\sum_{\lambda} g_{\lambda} \left[\sum_{j} \phi_j^{\star}(\mathbf{r}_{\lambda})\phi_j(\mathbf{r}_{\lambda}) \right] \left[\sum_{k} \delta_{\sigma_k\sigma}(\mathbf{r}_{\lambda}|w_{12}^{\delta_{\sigma_j\sigma}}|\alpha k)(\mathbf{r}_{\lambda}|r_{12}^{-1}|k\beta) \right]$$

$$- \sum_{\lambda} g_{\lambda} \left[\alpha^{\star}(\mathbf{r}_{\lambda})\beta(\mathbf{r}_{\lambda}) \right] \left[\sum_{jk} (\mathbf{r}_{\lambda}|w_{12}^{\delta_{\sigma_j\sigma}}|jk)(\mathbf{r}_{\lambda}|r_{12}^{-1}|kj) \right] \tag{3.17}$$

and

$$E_{c,3el,-}^{UW12} = \sum_{\lambda} g_{\lambda} \sum_{i} \phi_i^{\star}(\mathbf{r}_{\lambda}) \sum_{k} \left[\sum_{j} \delta_{\sigma_j\sigma}\phi_j(\mathbf{r}_{\lambda})(\mathbf{r}_{\lambda}|w_{12}^1|jk) \right] (\mathbf{r}_{\lambda}|r_{12}^{-1}|ki)$$

$$\partial E_{c,3el,-}^{UW12}/\partial D_{\alpha\beta}^{\sigma} = \sum_{jk} \langle j\alpha k|w_{12}r_{23}^{-1}|kj\beta\rangle + \sum_{jk} \langle \alpha jk|w_{12}r_{23}^{-1}|k\beta j\rangle \tag{3.18}$$

$$+ \sum_{jk} \langle jk\alpha|w_{12}r_{23}^{-1}|\beta jk\rangle \tag{3.19}$$

$$= \sum_{\lambda} g_{\lambda} \left[\alpha^{\star}(\mathbf{r}_{\lambda}) \right] \left[\sum_{j} \delta_{\sigma_j\sigma}\phi_j(\mathbf{r}_{\lambda}) \sum_{k} (\mathbf{r}_{\lambda}|w_{12}^1|jk)(\mathbf{r}_{\lambda}|r_{12}^{-1}|k\beta) \right]$$

$$+ \sum_{\lambda} g_{\lambda} \left[\beta(\mathbf{r}_{\lambda}) \right] \left[\sum_{j} \phi_j^{\star}(\mathbf{r}_{\lambda})\delta_{\sigma_j\sigma} \sum_{k} (\mathbf{r}_{\lambda}|w_{12}^1|\alpha k)(\mathbf{r}_{\lambda}|r_{12}^{-1}|kj) \right]$$

$$+ \sum_{\lambda} g_{\lambda} \left[\sum_{j} \phi_j(\mathbf{r}_{\lambda})(\mathbf{r}_{\lambda}|w_{12}^1|j\beta) \right] \left[\sum_{k} \phi_k^{\star}(\mathbf{r}_{\lambda})(\mathbf{r}_{\lambda}|r_{12}^{-1}|\alpha k) \right] \tag{3.20}$$

where

$$(\mathbf{r}_{\lambda}|w_{12}|\beta j) = \langle \beta| \, w(\mathbf{r} - \mathbf{r}_{\lambda}) \, |j\rangle \tag{3.21}$$

and where λ refers to a grid point at position $\mathbf{r}_{\lambda}$ with grid weight g_{λ}. The formal scaling for

evaluating the three-electron term is

$$N_{\text{grid}} N_{\text{AO}}^2 N_{\text{el}} \propto N^4 \tag{3.22}$$

where N_{grid} is the number of grid points.[7] All that remains is to evaluate the molecular integrals $(\mathbf{r}_\lambda | w_{12} | \alpha\beta)$ and $(\mathbf{r}_\lambda | r_{12}^{-1} | \alpha\beta)$. These are computed on-the-fly using the `intception` library, as outlined in Section 4.4.

3.2.2.1. Prefactor for the Three-Electron Term

Note that although the formal scaling is N^4, the prefactor for the computational cost of the algorithms in Section 3.2.2 is high, since N_{grid} is typically far larger than N_{AO} and N_{DF} [93, 94]. To avoid this problem, it has been proposed to return to Kutzelnigg's method (see Eqn 2.20) for expressing the $\mathbf{r}_2$ electron using a resolution of the identity in some auxiliary basis $\{|x\rangle\}$. This avoids the use of the quadrature grid entirely, but means that the accuracy now depends on the quality of the auxiliary basis $\{|x\rangle\}$. However, if the frozen-core approximation (see Section 3.4) is also employed, it may be possible to use a small auxiliary basis $\{|x\rangle\}$. This has not yet been investigated, but is the next stage of development of efficient UW12 algorithms.

3.2.3. Evaluating the Four-Electron Term

The algorithms in this section were implemented in the
`src/unsoldw12/four_el_term_density_fitting.cpp`
file in the entos source directory.

In a similar manner to the two-electron term, the direct four-electron term can be evaluated

---

[7]In estimating the slowest step of the calculation, we assume that $N_{\text{grid}} > N_{\text{AO}} > N_{\text{el}}$.

using density-fitting. The direct term is

$$E_{\text{c,4el,}+}^{\text{UW12}} = \frac{1}{2} \sum_{ijkl} (ik|w_{12}^{s_{ij}}|jl)(ki|r_{12}^{-1}|lj) \tag{3.23}$$

$$= \frac{1}{2} \sum_{Cik} (ik|w_{12}^{s_{ij}}|C) \sum_{D} (ki|r_{12}^{-1}|D) \sum_{jl} (\tilde{D}|r_{12}^{-1}|lj)(\tilde{C}|w_{12}^{s_{ij}}|jl) \tag{3.24}$$

$$\partial E_{\text{c,4el,}+}^{\text{UW12}}/\partial D_{\alpha\beta}^{\sigma} = 2 \sum_{Ck} (\alpha k|w_{12}^{s_{ij}}|C) \sum_{D} (k\beta|r_{12}^{-1}|D) \sum_{jl} (\tilde{D}|r_{12}^{-1}|lj)(\tilde{C}|w_{12}^{s_{ij}}|jl) \tag{3.25}$$

which scales as

$$N_{\text{DF}}^2 N_{\text{AO}} N_{\text{el}} \propto N^4. \tag{3.26}$$

The indirect term is

$$E_{\text{c,4el,}-}^{\text{UW12}} = \frac{1}{2} \sum_{ijkl} (il|w_{12}^{1}|jk)(ki|r_{12}^{-1}|lj) \tag{3.27}$$

$$\partial E_{\text{c,4el,}-}^{\text{UW12}}/\partial D_{\alpha\beta}^{\sigma} = -2 \sum_{ijkl} \delta_{\sigma_j \sigma} (\alpha l|w_{12}^{1}|jk)(k\beta|r_{12}^{-1}|lj) \tag{3.28}$$

which scales as

$$N_{\text{AO}}^2 N_{\text{el}}^3 \propto N^5. \tag{3.29}$$

In the above, the transformed integrals $(\tilde{D}|r_{12}^{-1}|lj)$ and $(\tilde{C}|w_{12}^{s_{ij}}|jl)$ are defined as

$$(\tilde{D}|r_{12}^{-1}|lj) = \sum_{D} (\mathbf{X}^{-1})_{CD} (D|r_{12}^{-1}|lj), \tag{3.30}$$

$$(\tilde{C}|w_{12}^{s_{ij}}|jl) = \sum_{C} (\mathbf{Y}^{-1})_{DC}. \tag{3.31}$$

The positive-definite matrix $\mathbf{X}$ and negative-definite matrix $\mathbf{Y}^{s_{ij}}$ have elements[8]

$$X_{DC} = (D|r_{12}^{-1}|C) \tag{3.32}$$

$$Y_{CD}^{s_{ij}} = (C|w_{12}^{s_{ij}}|D). \tag{3.33}$$

Note once again (as discussed in Section 1.19.1) that the choice of density-fitting kernels in Eqns 3.13 and 3.33 is not unique – but that choosing them in this way enables the cancellation of the first-order error term.

We observe that the algorithm for the indirect four-electron term derivative $\partial E_{\text{c,4el,}-}^{\text{UW12}}/\partial D_{\alpha\beta}^{\sigma}$ has N^5 scaling, whereas the algorithms for all the other terms in the energy expression have N^4 scaling or lower. The indirect four-electron term is thus the bottle-neck in any calculation for which the UW12 same-spin prefactor $a_{\text{c,}s=1}^{\text{UW12}}$ is non-zero. An alternative algorithm for evaluating $\partial E_{\text{c,4el,}-}^{\text{UW12}}/\partial D_{\alpha\beta}^{\sigma}$ in a computation time that scales as N^4 is proposed in Appendix A.2, but has not yet been implemented in `entos`. In Chapter 6, we choose to neglect the same-spin ($s = 1$) term altogether. We thus do not calculate $E_{\text{c,4el,}-}^{\text{UW12}}$ in Chapter 6.

3.2.4. Using a Quadrature Grid for All Three Terms

We have seen so far that each term in the UW12 energy expression is calculated in `entos` using a different method

- The $(pq|w(r_{12})|rs)$ integrals in the two-electron term $E_{\text{c,2el}}^{\text{UW12}}$ are approximated using a *density-fitting basis*.

- The $(pq|w(r_{12})|rs)$ integrals in the three-electron term $E_{\text{c,3el}}^{\text{UW12}}$ are approximated using a *quadrature grid*.

---

[8]Recall that the definition of $w(r_{12})$ in Eqn 2.34 contains a negative sign. The matrix $\mathbf{Y}^{s_{ij}}$ is thus negative-definite.

- The $(pq|w(r_{12})|rs)$ integrals in the four-electron term $E_{c,4el}^{UW12}$ are approximated using a *density-fitting basis*.

An alternative method (outlined in Appendix A.2) involves using a quadrature grid to approximate the $(pq|w(r_{12})|rs)$ integrals in all three terms. Such a method does not involve any of the complex two-index and three-index $(\alpha\beta|w(r_{12})|A)$ modified electron-repulsion integrals derived in Section 4.3. Furthermore, it may lead to better error cancellation between the three terms. This has never been investigated, but would be an interesting subject for future research. Although the effect of changing the density-fitting basis and quadrature grid in the practical calculations we have undertaken is small (as we will see in Section 3.3), the error-cancellation between the terms in the method of Appendix A.2 may lead to us being able to use a smaller quadrature grid – thus reducing the prefactor of our calculations.

Although this is an interesting avenue of research, we believe that the method outlined in Section 3.2.2.1 is a more promising route – provided it is coupled with the frozen-core approximation and with a well-motivated choice of auxiliary basis $\{|x\rangle\}$ – since it removes the quadrature grid entirely.

3.2.5. Evaluating the Energy and Fock Matrix

The UW12 energy is evaluated by calling the `form_fock()` routine in the `src/unsoldw12/unsoldw12.cpp` file in the `entos` source directory and passing the parameter `calculate_fock = false` to disable Fock matrix calculation. This routine then calls

- `form_fock_two_el_term_density_fitting()` to calculate $E_{c,2el}^{UW12}$

- `form_fock_three_el_term_on_grid()` to calculate $E_{c,3el}^{UW12}$

- `form_fock_four_el_term_density_fitting()` to calculate $E_{c,4el}^{UW12}$.

In practical calculations of the kind descibed in Chapter 6 (where only the direct component $E_{c,+}^{UW12}$ of the energy is calculated) on small organic molecules, the most expensive term in the calculation is the three-electron term $E_{c,3el}^{UW12}$. Let us proceed to discuss how this term is calculated efficiently in terms of memory management and processor usage. We see from Eqn 3.15 that the $(\mathbf{r}_\lambda | w_{12}^{\delta_{\sigma_j\sigma}} | jk)$ and $(\mathbf{r}_\lambda | r_{12}^{-1} | kj)$ potentials for a product of molecular orbitals $\phi_k^\star(\mathbf{r}_1)\phi_j(\mathbf{r}_1)$ must be calculated at every point on the quadrature grid $\mathbf{r}_\lambda$. The quadrature grid is first split into batches $\{\mathbf{r}_\lambda\}_n \subset \{\mathbf{r}_\lambda\}$ enumerated by index n each containing $N_{grid,n}$ grid-points, such that

$$\sum_n N_{grid,n} = N_{grid}. \tag{3.34}$$

The $(\mathbf{r}_\lambda | h_{12} | \alpha\beta)$ integrals (where $h_{12} = w_{12}^{\delta_{\sigma_j\sigma}}$ or r_{12}^{-1}) are computed in an in-core fashion for each batch and then deleted. The step to transform $(\mathbf{r}_\lambda | h_{12} | \alpha\beta)$ into molecular-orbital space using the formulae

$$(\mathbf{r}_\lambda | h_{12} | \alpha j) = \sum_\beta (\mathbf{r}_\lambda | h_{12} | \alpha\beta)\phi_j(\beta) \tag{3.35}$$

$$(\mathbf{r}_\lambda | h_{12} | ij) = \sum_\alpha \phi_i^\star(\alpha)(\mathbf{r}_\lambda | h_{12} | \alpha j) \tag{3.36}$$

clearly has a formal scaling of $N_{grid}N_{AO}^2 N_{el} \propto N^4$. Since N_{grid} is typically large, this step becomes the bottleneck for our UW12 calculations. However, the efficiency remains adequate for benchmarking the UW12 method against the test sets in Chapters 5 and 6. The methods shown in this thesis for the UW12 evaluation are all in their infancy of development. It is hoped that a method such as that proposed in Section 3.2.2.1 will far reduce the prefactor and make the method competitive in efficiency with conventional rung-4 hybrid functionals.

The UW12 Fock matrix is evaluated by calling the `form_fock()` routine in the `src/`

unsoldw12/unsoldw12.cpp file in the `entos` source directory and passing the parameter `calculate_fock = true` to enable Fock matrix calculation. The Fock matrix components $F^{\sigma}_{\alpha\beta,n}$ are accumulated for each grid point batch n, then summed together using the parallel reduction functions in the Intel Threaded Building Blocks C++ template library [107] to form the full Fock matrix $\mathbf{F}^{\sigma}$.

3.3. Choice of Density-Fitting Basis-Set and Quadrature Grid

We have so far presented algorithms for evaluating the UW12 energy and Fock matrix efficiently. Let us now consider the choice of density-fitting basis-set and quadrature grid.[9]

3.3.1. Convergence With Respect to Quadrature Grid

Table 3.2.: Convergence of the UW12 energy of the HF molecule (with a bond length of 91.7 pm [108]) with respect to quadrature grid, following the work of Ten-no [94]. N_{rad} (shown for the custom grids only) is the number of radial grid points. $\min\{l_{\text{tar}}\}$ is representative of the number of angular grid points associated with each radial grid point.

	H atom		F atom			$E_{\text{c}}^{\text{UW12}}/\text{kcal mol}^{-1}$
Grid	$\min\{l_{\text{tar}}\}$	N_{rad}	$\min\{l_{\text{tar}}\}$	N_{rad}	N_{grid}	
Default (SG-1)					7568	-250.620189
Custom Grid A	5	70	5	85	21598	-250.626035
Custom Grid B	7	70	7	85	22138	-250.626036
Custom Grid C	7	100	7	115	55618	-250.626030

In Table 3.2, we compare the results from using the SG-1 grid to the results using three

---

[9]We save the more complex discussion of convergence with respect to atomic-orbital basis-set for Section 5.4.

custom grids of varying sizes. Custom grids are generated in `entos` by using the `PRUNED` grid type. Calculations were performed self-consistently with the exchange correlation functional $E_{\text{xc}} = E_{\text{x}}^{\text{HF}} + E_{\text{c}}^{\text{UW}12(r_{\text{c}}=a_0)}$. A cc-pVTZ atomic orbital basis-set was used, and a cc-pVDZ-JKFIT density-fitting basis-set.[10] We see that the UW12 correlation energy is converged to an accuracy of $< 6 \times 10^{-3}$ kcal mol^{-1}, which is well within chemical accuracy (1 kcal mol^{-1}).[11]

We conclude that the standard quadrature grid (SG-1) [106] used in `entos` is sufficient for evaluating the UW12 energy to a degree of accuracy that makes it useful for practical electronic structure calculations. This is unsuprising, as quadrature-grid methods with a Slater-gype geminal $w(r_{12})$ (see Eqns 2.34 and 2.36) are already widely used in the literature for calculating MP2-F12 correlation energies to far higher degrees of accuracy than we are aiming for in this work [94]. We make a final remark that there is no guarantee that standard quadrature grids will also be sufficient for modelling other choices of geminal function $w(r_{12})$.

3.3.2. Convergence with Respect to Density-Fitting Basis-Set

The popular "exchange-fitting" (JKFIT) density-fitting basis-sets are optimized to minimize the error in the exchange and Coulomb energies of atoms and small molecules [82, 109]. They are thus generally assumed to be effective at approximating products of pairs of occupied orbitals

$$\phi_i^\star(\mathbf{r})\phi_j(\mathbf{r}) \approx \sum_D d_D^{ij} D(\mathbf{r}) \tag{3.37}$$

---

[10]The cc-pVTZ-JKFIT basis-set was also investigated for this molecule and deemed to be unnecessarily large for calculations at chemical accuracy (1 kcal mol^{-1}) level. We thus use the (smaller) cc-pVDZ-JKFIT density-fitting basis-set in this section, enabling us to run calculations with very large grids and demonstrate quadrature-grid convergence.

[11]In atomic units, 6×10^{-3} kcal mol^{-1} is around 1×10^{-5} E$_{\text{h}}$.

Table 3.4.: Density-fitting basis-set convergence for various methods for the cyclobutane (C_4H_8) molecule. Δ_{DF} is the change in the energy on changing the density-fitting basis-set from Def2-SVP-JKFIT (444 functions) to aug-cc-pVTZ-JKFIT(784 functions) [82, 109]. The atomic-orbital basis-set was aug-cc-pVTZ.

E_{xc}	a_x^{HF}	$\Delta_{DF}/kcal\,mol^{-1}$
BLYP	0	0.01
LDA	0	0.09
BHandHLYP	0.50	0.07
HF	1.00	0.03
DH-BLYP-UW12	0.55	0.08

where d_D^{ij} are fitting parameters. Since (by design) the UW12 method depends only on occupied orbitals, we will assume that these basis-sets are sufficient for our purposes. It should be noted that "MP2-fitting" (MP2FIT) density-fitting basis-sets also exist for modelling products of occupied and unoccupied orbitals $\phi_i^\star(\mathbf{r})\phi_a(\mathbf{r})$ [110].

In Table 3.4, we show the result of increasing the size of the density-fitting basis-set on the energy of a small organic molecule. In the table, DH-BLYP-UW12 refers to a simple hybrid functional (similar to those presented in Chapter 5) defined as

$$
\begin{aligned}
E_{xc}^{\text{DH-BLYP-UW12}} = {} & \left(1 - a_x^{HF}\right) E_x^{B88} + a_x^{HF} E_x^{HF} \\
& + \left(1 - \left(a_x^{HF}\right)^2\right) E_c^{LYP} + \left(a_x^{HF}\right)^2 E_c^{UW12(r_c=1.75\,a_0)}, \quad (3.38)
\end{aligned}
$$

where the parameter $a_x^{HF} = 0.55$ is chosen to match the value for 1DH-BLYP in Ref [50].

We conclude from Table 3.4 that the UW12 hybrid is no more sensitive to density-fitting basis-set than other common electronic structure methods. In addition, the density-fitting basis-set is converged to well within chemical accuracy of 1 kcal mol^{-1}. It is well-known that density-fitting basis-set errors are far smaller than atomic-orbital basis-set errors in general [110].

From here on in we will use the widely-accepted Def2-SVP-JKFIT density-fitting basis-set throughout, unless otherwise stated [82].

3.4. Frozen-Core Approximation

All the electrons (both valence and core) were correlated in the UW12 calculations in this thesis. In future, the frozen-core approximation (where the sum over ij in Eqn 2.4 only runs over valence orbitals) could be implemented to speed up the implementation further [111]. The UW12 correlation energy would thus model only the valence-electron-valence-electron (v-v) correlation. The core-electron-core-electron (c-c) and valence-electron-core-electron (v-c) correlation would no longer need to be treated by the UW12 geminal $w(r_{12})$. Since the first draft of this thesis was submitted, others in the Manby research group have attempted to apply the frozen-core approximation to UW12 hybrids. They have found that using the frozen-core approximation actually *improves* the accuracy of UW12 for the G2RC reaction energies in Chapter 6.

3.5. Natural-Blocking, Integral-Screening, and Quadrature Truncation

In practice, the values of molecular integrals $(\alpha\beta|r_{12}^{-1}|C)$ can be ignored if the atomic orbitals $\alpha(\boldsymbol{r})$ and $\beta(\boldsymbol{r})$ are sufficiently far apart. This is known as Schwarz integral screening [112, 113], and is commonly used in density-fitted Hartree-Fock implementations to reduce the scaling further. However – since our aim in this thesis is to demonstrate the feasibility of UW12 methods – we do not discuss these more advanced computational methods further; Suffice to

say that all the techniques used in the literature to speed up the evaluation of wavefunction-like exchange-correlation models can also be applied to UW12. For a helpful introduction to some of the techniques that can be used to reduce the computational expense (both scaling and prefactor) of wavefunction-like correlation models, see the section labeled "Summary of local OS PT2 approximations" in the Supporting Information of Ref [81]. The next stage in improving the efficiency of the UW12 method is to determine the most efficient algorithm for evaluating the opposite-spin 3-electron component $E_{c,s=0}^{\text{UW12}}$.

3.6. Self-Consistent Orbital Optimization

The UW12 Fock matrix contribution was evaluated using Eqn 1.69, and added to the Kohn-Sham Fock matrix in the `form_fock()` routine in the `scf/fock_builders.h` file in the `entos` source directory. The Kohn-Sham SCF procedure outlined in Section 1.10 was then applied.

Note that for some atoms and molecules it was necessary to apply different SCF convergence settings to make the SCF algorithm converge to the lowest-energy solution.[12]

3.7. Chapter Summary

In this chapter, we constructed the UW12 energy and Fock matrix efficiently from ingredients that are already present in many electronic structure programs. We demonstrated that standard quadrature grids and density-fitting basis-sets are sufficient for practical UW12 calculations on molecules.[13]

---

[12]These special cases can be found in the `tools/entos.py` file in the `unsoldpaper` repository http://bitbucket.org/tim_wiles/unsoldpaper.

[13]Convergence with respect to atomic-orbital basis-set is discussed in Section 5.4.

The algorithms in this chapter were implemented in the electronic structure code `entos`. In Chapter 4, we show how the molecular integrals required for the algorithms presented in this chapter were calculated.

4. Evaluating molecular integrals for UW12

4.1. Chapter Aims

In Chapter 3, we suggested algorithms for evaluating the UW12 correlation energy. These algorithms required F12-like molecular integrals of the form

$$(\mathbf{r}_\lambda|h_{12}|\alpha\beta) = \int d\mathbf{r}_2 \, h(\mathbf{r}_2 - \mathbf{r}_\lambda) \, \alpha^\star(\mathbf{r}_2)\beta(\mathbf{r}_2) \tag{4.1}$$

which we refer to as "modified electron-nuclear integrals", and

$$(\alpha\beta|h_{12}|C) = \int d\mathbf{r}_1 \int d\mathbf{r}_2 \, \alpha^\star(\mathbf{r}_1)\beta(\mathbf{r}_1) \, h_{12} \, C(\mathbf{r}_2) \tag{4.2}$$

$$(D|h_{12}|C) = \int d\mathbf{r}_1 \int d\mathbf{r}_2 \, D(\mathbf{r}_1) \, h_{12} \, C(\mathbf{r}_2) \tag{4.3}$$

which we refer to as "modified electron-electron integrals". Note that the "nucleus" at point $\mathbf{r}_\lambda$ in Eqn 4.1 is not a physical nucleus, but a grid-point. The above formulae contain the arbitrary geminal function h_{12}, which can refer to w_{12}, r_{12}^{-1}, or $w_{12}r_{12}^{-1}$.

4.1.1. Original Contribution

Our aim in the present project was not only to demonstrate that UW12 methods are theoretically plausible, but also to demonstrate that they can be implemented in practical, high-performance electronic structure codes. However, since F12 methods are primarily used by the wavefunction community (as opposed to the DFT community), F12-like molecular integrals have not yet been implemented in many commercial DFT molecular integral packages.

`intception` is one such existing molecular integrals package written in the C programming language by James Womack [114]. It boasts (among other features) highly efficient algorithms for the evaluation of 3-index Coulomb repulsion integrals. The theoretical formalism used in `intception` is unique to `intception`, but is based on various common literature algorithms [114, 115]. `entos` uses `intception` to evaluate the molecular integrals needed in self-consistent Kohn-Sham DFT calculations [42]. To evaluate the UW12 energy and Fock matrix, it was necessary to add the required F12-like integrals to `intception`. The work of adding F12-like 2-index and 3-index integrals was performed by the author of this thesis, and comprises 666 lines of added C and C++ code (see Section 3.1.1). In this chapter, we describe how this was done. Implementing F12-like integrals required re-deriving the `intception` algorithms from scratch, and adding a new library of C files for the required utility functions. The new library can be found in the `unsoldwr` sub-directory of the `intception` source directory, and is entirely the work of the author of this thesis. The library has since been re-used (without modification) by the Manby research group to implement Coulomb-attentuated-methods in `entos` [116, 42].

4.2. Gaussian-Type Geminals

In F12 theory, it is common to simplify the integrals by expressing the Slater-type geminal (STG) function $w^s(r_{12})$ (defined in Eqns. 2.34 and 2.36) approximately as a sum of Gaussian functions of the inter-electron distance r_{12} [104, 94].[1] We thus approximate the STG $w^s(r_{12})$ with a Gaussian-type geminal (GTG)

$$w^s(r_{12}) \approx w^s_{\text{GTG}}(r_{12}) = \sum_{\gamma} c_{s\gamma} e^{-\gamma r_{12}^2},$$

(4.4)

where the coefficients $c_{s\gamma}$ are chosen to minimize the error

$$\Delta^s_{\text{GTG}} = \int_0^{\infty} dr_{12} \left[w^s_{\text{GTG}}(r_{12}) - w^s(r_{12}) \right]^2,$$

(4.5)

Following the work of Ref [104], an even-tempered (logarithmic) sequence of 10 exponents $\{\gamma\}$ was used, with values ranging from 1000 through 0.01. The results of the fitting procedure for a selection of values of r_c are shown in Table 4.1.

Table 4.1.: Coefficients $c_{s\gamma}$ used in the definition of $w^s_{\text{GTG}}(r_{12})$. Note that $c_{1\gamma} = \frac{1}{2}c_{0\gamma}$.

γ	$c_{0\gamma}(r_c = 1.5\,a_0)$	$c_{0\gamma}(r_c = 1.7\,a_0)$	$c_{0\gamma}(r_c = 3.0\,a_0)$
0.010000	0.001362	0.000835	−0.110087
0.035938	−0.046756	−0.085419	−0.447094
0.129155	−0.210732	−0.260011	−0.396460
0.464159	−0.208883	−0.216534	−0.256541
1.668101	−0.130545	−0.135269	−0.131804
5.994843	−0.072601	−0.070814	−0.077794
21.544347	−0.037974	−0.039562	−0.035003
77.426368	−0.022218	−0.021128	−0.024463
278.255940	−0.006996	−0.007673	−0.005627
1000.000000	−0.011640	−0.011382	−0.012164

In practical calculations, the coefficients $c_{s\gamma}$ are first calculated on-the-fly for a given value of

---

[1]Note that in F12 theory the Slater-type geminal is referred to by the symbol f_{12} instead of w_{12}. See Footnote 4 on page 61.

r_c in the

`tools/fit_gtg_to_stg.py`

python module in the `unsoldpaper` repository (see Section 3.1.1). The coefficients $\{c_\gamma\}$ and exponents $\{\gamma\}$ are specified in the `entos` input file and then are passed by entos into the `intception` library when evaluating the three-index $(\alpha\beta|h_{12}|C)$ and two-index $(D|h_{12}|C)$ integrals (where the geminal $h(r_{12}) = w^s_{\text{GTG}}(r_{12})$). In the future, there are plans to modify `entos` to use tabulated exponent and coefficient values instead of specifying them in the `entos` input file. This will enable more convenient routine calculations and will not require users to calculate exponents and coefficients themselves.

The exponents and coefficients are then passed from `entos` into the `intception` library using an object of type `intception::InterElectronPotential`, as shown in Listing 4.1.

Listing 4.1: Computing the modified electron-electron integrals $(\alpha\beta|w_{12}|C)$ in `entos`, with a Gaussian-type geminal function $w(r) = -e^{-r^2}$. Language: C++.

```
const intception::InterElectronPotential Wr(
      arma::vec({  1.0 }), // Exponents $\zeta$
      arma::vec({ -1.0 }), // Coefficients $c_\zeta$
      intception::InterElectronPotential::Type::gaussian
);

  // $ ( \alpha \beta | w(r) |  C ) $.
auto W = integrals::compute_df_integrals(
      ao_basis, // ${ \alpha (r) } $
      df_basis, // ${ C (r) } $
      unsoldw12_schwarz_threshold,
      Wr.c_struct_ptr() // Convert Wr to a C struct for
          ↪ passing to C code
);
```

4.3. Modified Electron-Electron Integrals

Let us now turn our attention to the modified electron-electron integrals $(\alpha\beta|h_{12}|C)$ and $(D|h_{12}|C)$, where α, β, C, D take the form of real contracted Gaussian-type orbitals (GTO)

$$\alpha(\mathbf{r}) = \sum_{\zeta} d_{\zeta} G(\mathbf{r};\ \zeta, l_a, m_a, \mathbf{A}), \tag{4.6}$$

where d_{ζ} are contraction coefficients, $\{\zeta\}$ are Gaussian exponents, A is the location of the center of the GTO, and l_a and m_a are angular-momentum quantum numbers. The real uncontracted GTO functions are given by

$$G(\mathbf{r};\ \zeta, l_a, m_a, \mathbf{A}) = \sum_{\mathbf{a}} D_{\mathbf{a}}^{l_a m_a} g_{\mathbf{a}}(\mathbf{r};\ \zeta, \mathbf{A}), \tag{4.7}$$

where $D_{\mathbf{a}}^{l_a m_a}$ are real spherical transformation coefficients, $\mathbf{a} = \begin{pmatrix} a_x & a_y & a_z \end{pmatrix}$ is a vector of three nonnegative integers that sum to l_a, and where the primitive Cartesian Gaussian (PCG) functions are given by[2]

$$g_{\mathbf{a}}(\mathbf{r};\ \zeta, \mathbf{A}) = (r_x - A_x)^{a_x} \left(r_y - A_y\right)^{a_y} (r_z - A_z)^{a_z} \exp\left[-\zeta\,|\mathbf{r}-\mathbf{A}|^2\right]. \tag{4.8}$$

The GTO integrals defined in Eqns. 4.2 and 4.3 can be found by transforming the PCG integral electron-electron integrals

$$(\mathbf{ab}|h(r)|\mathbf{c}) = \int d\mathbf{r}_1 \int d\mathbf{r}_2\, g_{\mathbf{a}}(\mathbf{r}_1)\, g_{\mathbf{b}}(\mathbf{r}_1)\, h(r_{12})\, g_{\mathbf{c}}(\mathbf{r}_2) \tag{4.9}$$

$$(\mathbf{d}|h(r)|\mathbf{c}) = \int d\mathbf{r}_1 \int d\mathbf{r}_2\, g_{\mathbf{d}}(\mathbf{r}_1)\, h(r_{12})\, g_{\mathbf{c}}(\mathbf{r}_2). \tag{4.10}$$

---

[2]We henceforth omit the ζ and $\mathbf{A}$ arguments to the g_a function.

It is convenient to write both of these in terms of the four-index electron-electron integrals

$$(\mathbf{ab}|h(r)|\mathbf{cd}) = \int d\mathbf{r}_1 \int d\mathbf{r}_2\, g_a(\mathbf{r}_1)\, g_b(\mathbf{r}_1)\, h(r_{12})\, g_c(\mathbf{r}_2)\, g_d(\mathbf{r}_2). \tag{4.11}$$

The three-index repulsion integral $(\mathbf{ab}|w(r)|\mathbf{c})$ can then be obtained by setting $\zeta_d = 0$ and $\mathbf{d} = (0,0,0)$ and the two-index repulsion integral $(\mathbf{a}|w(r)|\mathbf{c})$ by setting $\zeta_d = \zeta_b = 0$ and $\mathbf{a} = \mathbf{d} = (0,0,0)$. We can see this by substituting $\zeta_d = d_x = d_y = d_z = 0$ into the primitive Cartesian Gaussian definition (Eqn 4.8) in which case

$$g_{\mathbf{d}}(\mathbf{r};\ \zeta_d, \mathbf{D}) = 1\ \forall\mathbf{r}. \tag{4.12}$$

To evaluate the integrals, we follow the recurrence-relation method derived by Obara and Saika [115] in 1986. This method boasts several advantages over pre-existing methods: it has a lower prefactor than the McMurchie-Davidson 1978 Hermite Gaussian method [117]; and (unlike the Pople-Hehre 1978 method [118]) it is simple to extend to bases with high angular momentum.

4.3.1. Recurrence Relation

We aim to find a recurrence relation for the four-index electron-electron integrals for arbitrary angular-momentum vectors $\mathbf{a}$, $\mathbf{b}$, $\mathbf{c}$, $\mathbf{d}$. We begin by expressing the geminal as an integral over Gaussian functions

$$h(r) = \int_0^\infty du\, H\left(u^2\right) \exp\left[-r^2 u^2\right], \tag{4.13}$$

where $H\left(u^2\right)$ is some real dimensionless function which we will call the "potential weighting function". In the case of the standard electron-electron integrals, the potential weighting function $H\left(u^2\right) = \frac{2}{\sqrt{\pi}} \forall u$. We have that

$$(\mathbf{ab}|h(r)|\mathbf{cd}) = \int_0^\infty du\, H\left(u^2\right) (\mathbf{ab}|u|\mathbf{cd}), \tag{4.14}$$

where the Gaussian repulsion integral is

$$(\mathbf{ab}|u|\mathbf{cd}) = \int d\mathbf{r}_2\, g_{\mathbf{c}}(\mathbf{r}_2)\, g_{\mathbf{d}}(\mathbf{r}_2)\, \left(\mathbf{a}|\mathbf{0}_{\mathbf{r}_2}|\mathbf{b}\right), \tag{4.15}$$

and the quantity $\left(\mathbf{a}|\mathbf{0}_{\mathbf{r}_2}^{u^2}|\mathbf{b}\right)$ is a three-index overlap integral given by

$$\left(\mathbf{a}|\mathbf{0}_{\mathbf{r}_2}^{u^2}|\mathbf{b}\right) = \int d\mathbf{r}_1\, g_{\mathbf{a}}(\mathbf{r}_1)\, g_{\mathbf{b}}(\mathbf{r}_1) \exp\left[-u^2 r_{12}^2\right]. \tag{4.16}$$

Three-index overlap integrals are defined more generally as

$$(\mathbf{a}|\mathbf{c}|\mathbf{b}) = \int d\mathbf{r}_1\, g_{\mathbf{a}}(\mathbf{r}_1)\, g_{\mathbf{c}}(\mathbf{r}_1)\, g_{\mathbf{b}}(\mathbf{r}_1). \tag{4.17}$$

From Obara and Saika's paper [115] we have the recursion relation for the three-index overlap integrals[3]

$$(\mathbf{a}|\mathbf{c}+\mathbf{1}_i|\mathbf{b}) = \mathbf{CG}_i\,(\mathbf{a}|\mathbf{c}|\mathbf{b}) + \frac{1}{2\left(\zeta+\zeta_c\right)} N_i(\mathbf{a})\,(\mathbf{a}-\mathbf{1}_i|\mathbf{c}|\mathbf{b})$$
$$+ \frac{1}{2\left(\zeta+\zeta_c\right)} N_i(\mathbf{b})\,(\mathbf{a}|\mathbf{c}|\mathbf{b}-\mathbf{1}_i) + \frac{1}{2\left(\zeta+\zeta_c\right)} N_i(\mathbf{c})\,(\mathbf{a}|\mathbf{c}-\mathbf{1}_i|\mathbf{b}), \tag{4.18}$$

---

[3]The derivation that follows is taken from Eqns 29-36 of Ref [115].

where

$$\zeta = \zeta_a + \zeta_b \qquad (4.19)$$

$$\mathbf{P} = \frac{\zeta_a \mathbf{A} + \zeta_b \mathbf{B}}{\zeta_a + \zeta_b} \qquad (4.20)$$

$$\mathbf{CG} = \mathbf{G} - \mathbf{C} \qquad (4.21)$$

$$\mathbf{G} = \frac{\zeta \mathbf{P} + \zeta_c \mathbf{C}}{\zeta + \zeta_c} \qquad (4.22)$$

$$N_i(\mathbf{a}) = a_i. \qquad (4.23)$$

The zero angular momentum integral is

$$(\mathbf{0}_A | \mathbf{0}_C | \mathbf{0}_B) = \left(\frac{\zeta}{\zeta + \zeta_c} \right)^{\frac{3}{2}} (\mathbf{0}_A || \mathbf{0}_B) \exp \left[-\frac{\zeta \zeta_c}{\zeta + \zeta_c} (\mathbf{P} - \mathbf{C})^2 \right], \qquad (4.24)$$

where the two-index overlap integral is

$$(\mathbf{0}_A || \mathbf{0}_B) = \left(\frac{\pi}{\zeta} \right)^{\frac{3}{2}} \exp \left[-\zeta (\mathbf{A} - \mathbf{B})^2 \right]. \qquad (4.25)$$

Two-index overlap integrals are defined more generally as

$$(\mathbf{a} || \mathbf{b}) = \int d\mathbf{r}_1 \, g_{\mathbf{a}}(\mathbf{r}_1) g_{\mathbf{b}}(\mathbf{r}_1). \qquad (4.26)$$

Now, defining

$$\eta = \zeta_c + \zeta_d \qquad (4.27)$$

$$\rho = \frac{\zeta \eta}{\zeta + \eta} \qquad (4.28)$$

$$\mathbf{Q} = \frac{1}{\eta} (\zeta_c \mathbf{C} + \zeta_d \mathbf{D}) \qquad (4.29)$$

and using the recurrance relation for the 3-index overlap integrals (Eqn 4.18) we can write[4]

$$
\begin{aligned}
\left(\mathbf{a}+\mathbf{1}_i|\mathbf{0}_{\mathbf{r}_2}|\mathbf{b}\right) = &\ \mathbf{AP}_i\left(\mathbf{a}|\mathbf{0}_{\mathbf{r}_2}|\mathbf{b}\right) \\
& + \frac{1}{2\zeta}N_i(\mathbf{a})\left(1 - \frac{\rho}{\zeta}\frac{u^2}{\rho+u^2}\right)\left(\mathbf{a}-\mathbf{1}_i|\mathbf{0}_{\mathbf{r}_2}|\mathbf{b}\right) \\
& + \frac{1}{2\zeta}N_i(\mathbf{b})\left(1 - \frac{\rho}{\zeta}\frac{u^2}{\rho+u^2}\right)\left(\mathbf{a}|\mathbf{0}_{\mathbf{r}_2}|\mathbf{b}-\mathbf{1}_i\right) \\
& + \frac{1}{\zeta+\eta}\frac{u^2}{\rho+u^2}\eta\,(\mathbf{r}_2-\mathbf{P})_i\left(\mathbf{a}|\mathbf{0}_{\mathbf{r}_2}|\mathbf{b}\right) \\
& - \frac{1}{\zeta+\eta}\frac{u^2}{\rho+u^2}u^2\left(\mathbf{a}|\mathbf{0}_{\mathbf{r}_2}+\mathbf{1}_i|\mathbf{b}\right)
\end{aligned}
\tag{4.30}
$$

where the following relation has been used (which can also be derived from Eqn 4.18)

$$
\begin{aligned}
\left(\mathbf{a}|\mathbf{0}_{\mathbf{r}_2}+\mathbf{1}_i|\mathbf{b}\right) = &\ -\frac{\zeta}{\zeta+u^2}(\mathbf{r}_2-\mathbf{P})_i\left(\mathbf{a}|\mathbf{0}_{\mathbf{r}_2}|\mathbf{b}\right) \\
& + \frac{1}{2\left(\zeta+u^2\right)}N_i(\mathbf{a})\left(\mathbf{a}-\mathbf{1}_i|\mathbf{0}_{\mathbf{r}_2}|\mathbf{b}\right) \\
& + \frac{1}{2\left(\zeta+u^2\right)}N_i(\mathbf{b})\left(\mathbf{a}|\mathbf{0}_{\mathbf{r}_2}|\mathbf{b}-\mathbf{1}_i\right).
\end{aligned}
\tag{4.31}
$$

The helpful identity

$$
\frac{1}{\zeta+u^2} = \frac{1}{\zeta}\left(1 - \frac{\rho}{\zeta}\frac{u^2}{\rho+u^2}\right) - \frac{1}{\zeta+\eta}\frac{u^2}{\zeta+u^2}\frac{u^2}{\rho+u^2}
\tag{4.32}
$$

has been used also. The primitive $\left(\mathbf{0}_{\mathbf{r}_1}+\mathbf{1}_i\right)$ in Eqn 4.30 is defined as

$$
g_{\mathbf{0}_{\mathbf{r}_1}+\mathbf{1}_i}(\mathbf{r}_2) = (\mathbf{r}_2-\mathbf{r}_1)\exp\left(-u^2 r_{12}^2\right).
\tag{4.33}
$$

Let us turn our attention now to the related quantity $\left(\mathbf{c}|\mathbf{0}_{\mathbf{r}_1}+\mathbf{1}_i|\mathbf{d}\right)$. We can use the 3-index

---

[4]Note that Eqn 4.30 holds for any values of η and ρ, since the integral $\left(\mathbf{a}+\mathbf{1}_i|\mathbf{0}_{\mathbf{r}_2}|\mathbf{b}\right)$ does not depend on $g_{\mathbf{c}}$ and $g_{\mathbf{d}}$.

overlap recurrance relation again (Eqn 4.18) to write

$$\left(\mathbf{c}|\mathbf{0}_{\mathbf{r}_1} + \mathbf{1}_i|\mathbf{d}\right) = -\frac{\eta}{\eta + u^2} \left(\mathbf{r}_1 - \mathbf{Q}\right)_i \left(\mathbf{c}|\mathbf{0}_{\mathbf{r}_1}|\mathbf{d}\right)$$
$$+ \frac{1}{2\left(\eta + u^2\right)} N_i(\mathbf{a}) \left(\mathbf{a} - \mathbf{1}_i|\mathbf{0}_{\mathbf{r}_1}|\mathbf{d}\right)$$
$$+ \frac{1}{2\left(\eta + u^2\right)} N_i(\mathbf{d}) \left(\mathbf{a}|\mathbf{0}_{\mathbf{r}_1}|\mathbf{d} - \mathbf{1}_i\right). \tag{4.34}$$

Rearranging this leads to

$$u^2 \left(\mathbf{c}|\mathbf{0}_{\mathbf{r}_1} + \mathbf{1}_i|\mathbf{d}\right) = -\eta \left(\mathbf{r}_1 - \mathbf{Q}\right)_i \left(\mathbf{c}|\mathbf{0}_{\mathbf{r}_1}|\mathbf{d}\right)$$
$$+ \frac{1}{2} N_i(\mathbf{a}) \left(\mathbf{c} - \mathbf{1}_i|\mathbf{0}_{\mathbf{r}_1}|\mathbf{d}\right)$$
$$+ \frac{1}{2} N_i(\mathbf{d}) \left(\mathbf{c}|\mathbf{0}_{\mathbf{r}_1}|\mathbf{d} - \mathbf{1}_i\right)$$
$$- \eta \left(\mathbf{c}|\mathbf{0}_{\mathbf{r}_1} + \mathbf{1}_i|\mathbf{d}\right). \tag{4.35}$$

Now we can attempt to relate $\left(\mathbf{c}|\mathbf{0}_{\mathbf{r}_1} + \mathbf{1}_i|\mathbf{d}\right)$ and $\left(\mathbf{a}|\mathbf{0}_{\mathbf{r}_2} + \mathbf{1}_i|\mathbf{b}\right)$. From their definitions we see that (note the negative sign)

$$\int d\mathbf{r}_2 \, g_{\mathbf{c}}(\mathbf{r}_2) g_{\mathbf{d}}(\mathbf{r}_2) \left(\mathbf{a}|\mathbf{0}_{\mathbf{r}_2} + \mathbf{1}_i|\mathbf{b}\right) = -\int d\mathbf{r}_1 g_{\mathbf{a}}(\mathbf{r}_1) g_{\mathbf{b}}(\mathbf{r}_1) \left(\mathbf{c}|\mathbf{0}_{\mathbf{r}_1} + \mathbf{1}_i|\mathbf{d}\right). \tag{4.36}$$

Multiplying with u^2, substituting in Eqn 4.35, and using Eqn 4.15 gives

$$\int d\mathbf{r}_2 \, g_{\mathbf{c}}(\mathbf{r}_2) g_{\mathbf{d}}(\mathbf{r}_2) u^2 \left(\mathbf{a}|\mathbf{0}_{\mathbf{r}_2} + \mathbf{1}_i|\mathbf{b}\right) = \int d\mathbf{r}_1 g_{\mathbf{a}}(\mathbf{r}_1) g_{\mathbf{b}}(\mathbf{r}_1) \eta \left(\mathbf{r}_1 - \mathbf{Q}\right)_i \left(\mathbf{c}|\mathbf{0}_{\mathbf{r}_1}|\mathbf{d}\right)$$
$$- \frac{1}{2} N_i(\mathbf{c}) (\mathbf{ab}|u|(\mathbf{c} - \mathbf{1}_i)\mathbf{d})$$
$$- \frac{1}{2} N_i(\mathbf{d}) (\mathbf{ab}|u|\mathbf{c}(\mathbf{d} - \mathbf{1}_i))$$
$$+ \int d\mathbf{r}_1 g_{\mathbf{a}}(\mathbf{r}_1) g_{\mathbf{b}}(\mathbf{r}_1) \eta \left(\mathbf{c}|\mathbf{0}_{\mathbf{r}_1} + \mathbf{1}_i|\mathbf{d}\right) \tag{4.37}$$

and using the definition of $\left(\mathbf{0_{r_1}} + \mathbf{1}_i\right)$ (Eqn 4.33) we recognise that this can be written more simply as

$$\int d\mathbf{r}_2\, g_{\mathbf{c}}(\mathbf{r}_2)\, g_{\mathbf{d}}(\mathbf{r}_2)\, u^2 \left(\mathbf{a}|\mathbf{0_{r_2}} + \mathbf{1}_i|\mathbf{b}\right) = \int d\mathbf{r}_2 \int d\mathbf{r}_1 g_{\mathbf{a}}(\mathbf{r}_1)\, g_{\mathbf{b}}(\mathbf{r}_2)\, g_{\mathbf{c}}(\mathbf{r}_2)\, g_{\mathbf{d}}(\mathbf{r}_2)$$

$$\times \eta\, (\mathbf{r}_1 - \mathbf{Q} + \mathbf{r}_2 - \mathbf{r}_1)_i \exp\left(-u^2 r_{12}^2\right) \tag{4.38}$$

$$-\frac{1}{2} N_i(\mathbf{c})\,(\mathbf{ab}|u|\,(\mathbf{c} - \mathbf{1}_i)\mathbf{d})$$

$$-\frac{1}{2} N_i(\mathbf{d})\,(\mathbf{ab}|u|\mathbf{c}\,(\mathbf{d} - \mathbf{1}_i)) \tag{4.39}$$

$$= \int d\mathbf{r}_2 g_{\mathbf{c}}(\mathbf{r}_2)\, g_{\mathbf{d}}(\mathbf{r}_2)\, \eta\, (\mathbf{r}_2 - \mathbf{Q})_i\, \left(\mathbf{a}|\mathbf{0_{r_2}}|\mathbf{b}\right)$$

$$-\frac{1}{2} N_i(\mathbf{c})\,(\mathbf{ab}|u|\,(\mathbf{c} - \mathbf{1}_i)\mathbf{d})$$

$$-\frac{1}{2} N_i(\mathbf{d})\,(\mathbf{ab}|u|\mathbf{c}\,(\mathbf{d} - \mathbf{1}_i)). \tag{4.40}$$

Putting all this together, we can use Eqn 4.15 to write

$$((\mathbf{a} + \mathbf{1_i})\mathbf{b}|u|\mathbf{cd}) = \int d\mathbf{r}_2\, g_{\mathbf{c}}(\mathbf{r}_2)\, g_{\mathbf{d}}(\mathbf{r}_2)\, \left((\mathbf{a} + \mathbf{1}_i)\,|\mathbf{0_{r_2}}|\mathbf{b}\right) \tag{4.41}$$

and substituting in Eqn 4.30 for $\left((\mathbf{a} + \mathbf{1}_i)\,|\mathbf{0_{r_2}}|\mathbf{b}\right)$ gives

$$((\mathbf{a} + \mathbf{1_i})\mathbf{b}|u|\mathbf{cd}) = \mathbf{AP}_i\,(\mathbf{ab}|u|\mathbf{cd})$$

$$+ \frac{1}{2\zeta} N_i(\mathbf{a}) \left(1 - \frac{\rho}{\zeta}\frac{u^2}{\rho + u^2}\right)((\mathbf{a} - \mathbf{1}_i)\mathbf{b}|u|\mathbf{cd})$$

$$+ \frac{1}{2\zeta} N_i(\mathbf{b}) \left(1 - \frac{\rho}{\zeta}\frac{u^2}{\rho + u^2}\right)(\mathbf{a}\,(\mathbf{b} - \mathbf{1}_i)\,|u|\mathbf{cd})$$

$$+ \frac{1}{\zeta + \eta}\frac{u^2}{\rho + u^2} \int d\mathbf{r}_2 g_{\mathbf{c}}(\mathbf{r}_2)\, g_{\mathbf{d}}(\mathbf{r}_2)\, \eta\, (\mathbf{r}_2 - \mathbf{P})_i\, \left(\mathbf{a}|\mathbf{0_{r_2}}|\mathbf{b}\right)$$

$$- \frac{1}{\zeta + \eta}\frac{u^2}{\rho + u^2} \int d\mathbf{r}_2 g_{\mathbf{c}}(\mathbf{r}_2)\, g_{\mathbf{d}}(\mathbf{r}_2)\, u^2 \left(\mathbf{a}|\mathbf{0_{r_2}} + \mathbf{1}_i|\mathbf{b}\right). \tag{4.42}$$

Substituting in Eqn 4.40 for the integral involving $(\mathbf{a}|\mathbf{0_{r_2}} + \mathbf{1}_i|\mathbf{b})$ gives

$$
\begin{aligned}
((\mathbf{a} + \mathbf{1_i})\mathbf{b}|u|\mathbf{cd}) = {} & \mathbf{AP}_i (\mathbf{ab}|u|\mathbf{cd}) \\
& + \frac{1}{\zeta + \eta} \frac{u^2}{\rho + u^2} \int d\mathbf{r}_2 g_{\mathbf{c}} (\mathbf{r}_2) g_{\mathbf{d}} (\mathbf{r}_2) \eta (\mathbf{r}_2 - \mathbf{P})_i (\mathbf{a}|\mathbf{0_{r_2}}|\mathbf{b}) \\
& - \frac{1}{\zeta + \eta} \frac{u^2}{\rho + u^2} \int d\mathbf{r}_2 g_{\mathbf{c}} (\mathbf{r}_2) g_{\mathbf{d}} (\mathbf{r}_2) \eta (\mathbf{r}_2 - \mathbf{Q})_i (\mathbf{a}|\mathbf{0_{r_2}}|\mathbf{b}) \\
& + \frac{1}{2\zeta} N_i (\mathbf{a}) \left(1 - \frac{\rho}{\zeta} \frac{u^2}{\rho + u^2} \right) ((\mathbf{a} - \mathbf{1}_i)\mathbf{b}|u|\mathbf{cd}) \\
& + \frac{1}{2\zeta} N_i (\mathbf{b}) \left(1 - \frac{\rho}{\zeta} \frac{u^2}{\rho + u^2} \right) (\mathbf{a}(\mathbf{b} - \mathbf{1}_i)|u|\mathbf{cd}) \\
& + \frac{1}{2} N_i (\mathbf{c}) (\mathbf{ab}|u|(\mathbf{c} - \mathbf{1}_i)\mathbf{d}) \\
& + \frac{1}{2} N_i (\mathbf{d}) (\mathbf{ab}|u|\mathbf{c}(\mathbf{d} - \mathbf{1}_i)).
\end{aligned}
\tag{4.43}
$$

Now recognising that the vector

$$
(\mathbf{r}_2 - \mathbf{P}) - (\mathbf{r}_2 - \mathbf{Q}) = \mathbf{Q} - \mathbf{P} = \mathbf{PQ}
\tag{4.44}
$$

we see that Eqn 4.43 simplifies to

$$
\begin{aligned}
((\mathbf{a} + \mathbf{1}_i)\mathbf{b}|u|\mathbf{cd}) = {} & \mathbf{AP}_i (\mathbf{ab}|u|\mathbf{cd}) + \frac{u^2}{\rho + u^2} \frac{\eta}{\zeta + \eta} \mathbf{PQ}_i (\mathbf{ab}|u|\mathbf{cd}) \\
& + \frac{1}{2\zeta} N_i (\mathbf{a}) \left(1 - \frac{\rho}{\zeta} \frac{u^2}{\rho + u^2} \right) ((\mathbf{a} - \mathbf{1}_i)\mathbf{b}|u|\mathbf{cd}) \\
& + \frac{1}{2\zeta} N_i (\mathbf{b}) \left(1 - \frac{\rho}{\zeta} \frac{u^2}{\rho + u^2} \right) (\mathbf{a}(\mathbf{b} - \mathbf{1}_i)|u|\mathbf{cd}) \\
& + \frac{1}{2(\zeta + \eta)} N_i (\mathbf{c}) \frac{u^2}{(\rho + u^2)} (\mathbf{ab}|u|(\mathbf{c} - \mathbf{1}_i)\mathbf{d}) \\
& + \frac{1}{2(\zeta + \eta)} N_i (\mathbf{d}) \frac{u^2}{(\rho + u^2)} (\mathbf{ab}|u|\mathbf{c}(\mathbf{d} - \mathbf{1}_i))
\end{aligned}
\tag{4.45}
$$

which is our final expression for the recurrence relation for the four-index electron-electron

integrals. As a final remark, note that Obara and Saika choose to introduce the vector $\mathbf{W}$ as follows [115]

$$\mathbf{W} = \frac{\zeta \mathbf{P} + \eta \mathbf{Q}}{\zeta + \eta} \implies \mathbf{PW} = \mathbf{W} - \mathbf{P} = \frac{\eta}{\zeta + \eta}(\mathbf{Q} - \mathbf{P}) = \frac{\eta}{\zeta + \eta}\mathbf{PQ} \tag{4.46}$$

which makes their final expression look slightly different to that shown in Eqn 4.45.

4.3.2. Auxiliary Index

The zero angular momentum integrals are (using Eqn 4.18)

$$\left(\mathbf{0}_A|\mathbf{0}_{\mathbf{r}_2}|\mathbf{0}_B\right) = \left(\frac{\zeta}{\zeta + u^2}\right)^{\frac{3}{2}} \left(\mathbf{0}_A||\mathbf{0}_B\right)\exp\left[-\frac{\zeta u^2}{\zeta + u^2}(\mathbf{P} - \mathbf{r}_2)^2\right] \tag{4.47}$$

and using Eqn 4.15 yields

$$
\begin{aligned}
\left(\mathbf{0}_A\mathbf{0}_B|u|\mathbf{0}_C\mathbf{0}_D\right) &= \left(\frac{\zeta}{\zeta + u^2}\right)^{\frac{3}{2}} \left(\mathbf{0}_A||\mathbf{0}_B\right)\int d\mathbf{r}_2\, g_c(\mathbf{r}_2)\, g_d(\mathbf{r}_2)\exp\left[-\frac{\zeta u^2}{\zeta + u^2}(\mathbf{P} - \mathbf{r}_2)^2\right] \\
&= \left(\frac{\rho}{\rho + u^2}\right)^{\frac{3}{2}} \left(\mathbf{0}_A||\mathbf{0}_B\right)\left(\mathbf{0}_C||\mathbf{0}_D\right)\exp\left[-\frac{\rho u^2}{\rho + u^2}(\mathbf{P} - \mathbf{Q})^2\right].
\end{aligned} \tag{4.48}
$$

Now we can introduce the "auxiliary integral" $(\mathbf{ab}|h(r)|\mathbf{cd})^{(m)}$ with "auxiliary index" m

$$(\mathbf{ab}|h(r)|\mathbf{cd})^{(m)} := \int_0^\infty du\, H\left(u^2\right)\left[\frac{u^2}{(\rho + u^2)}\right]^m (\mathbf{ab}|u|\mathbf{cd}).$$

By multiplying Eqn 4.45 with $H\left(u^2\right)\left[\frac{u^2}{(\rho + u^2)}\right]^m$ and integrating du we obtain the recurrence

relation

$$
\begin{aligned}
((\mathbf{a}+\mathbf{1}_i)\mathbf{b}|h(r)|\mathbf{cd})^{(m)} =& \mathbf{AP}_i (\mathbf{ab}|h(r)|\mathbf{cd})^{(m)} + \frac{\eta}{\zeta+\eta}\mathbf{PQ}_i (\mathbf{ab}|h(r)|\mathbf{cd})^{(m+1)} \\
&+ \frac{1}{2\zeta}N_i(\mathbf{a})\left(((\mathbf{a}-\mathbf{1}_i)\mathbf{b}|h(r)|\mathbf{cd})^{(m)} - \frac{\rho}{\zeta}((\mathbf{a}-\mathbf{1}_i)\mathbf{b}|h(r)|\mathbf{cd})^{(m+1)}\right) \\
&+ \frac{1}{2\zeta}N_i(\mathbf{b})\left((\mathbf{a}(\mathbf{b}-\mathbf{1}_i)|h(r)|\mathbf{cd})^{(m)} - \frac{\rho}{\zeta}(\mathbf{a}(\mathbf{b}-\mathbf{1}_i)|h(r)|\mathbf{cd})^{(m+1)}\right) \\
&+ \frac{1}{2(\zeta+\eta)}N_i(\mathbf{c})(\mathbf{ab}|h(r)|(\mathbf{c}-\mathbf{1}_i)\mathbf{d})^{(m+1)} \\
&+ \frac{1}{2(\zeta+\eta)}N_i(\mathbf{d})(\mathbf{ab}|h(r)|\mathbf{c}(\mathbf{d}-\mathbf{1}_i))^{(m+1)}.
\end{aligned}
\tag{4.49}
$$

This is Eqn 39 in Obara and Saika's paper [115]. We see that the factors of $u^2/(\rho+u^2)$ have been absorbed into the integrals.

The zero-angular momentum integral is (from multiplying Eqn 4.48 by $H(u^2)\left[u^2/(\rho+u^2)\right]^m$ and integrating du)

$$
\begin{aligned}
(\mathbf{0}_A\mathbf{0}_B|h(r)|\mathbf{0}_C\mathbf{0}_D)^{(m)} =& (\mathbf{0}_A||\mathbf{0}_B)(\mathbf{0}_C||\mathbf{0}_D) \\
&\times \int_0^\infty du\, H(u^2)\left[\frac{u^2}{(\rho+u^2)}\right]^m \left(\frac{\rho}{\rho+u^2}\right)^{\frac{3}{2}} \exp\left[-\frac{\rho u^2}{\rho+u^2}(\mathbf{P}-\mathbf{Q})^2\right].
\end{aligned}
\tag{4.50}
$$

Now, making the substitution

$$
t^2 = \frac{u^2}{\rho+u^2},
\tag{4.51}
$$

we see that

$$
\begin{aligned}
&(\mathbf{0}_A\mathbf{0}_B|h(r)|\mathbf{0}_C\mathbf{0}_D)^{(m)} \\
&\qquad = (\mathbf{0}_A||\mathbf{0}_B)(\mathbf{0}_C||\mathbf{0}_D)\rho^{\frac{1}{2}} \int_0^1 dt\, H\left(\frac{\rho t^2}{1-t^2}\right) t^{2m} \exp\left[-\rho t^2 (\mathbf{P}-\mathbf{Q})^2\right].
\end{aligned}
\tag{4.52}
$$

This is Eqn 40 in Obara and Saika's paper[115]. By recursively applying Eqn 4.49 we can evaluate $(\mathbf{ab}|h(r)|\mathbf{cd})^{(m=0)} = (\mathbf{ab}|h(r)|\mathbf{cd})$ starting from $(\mathbf{0}_A\mathbf{0}_B|h(r)|\mathbf{0}_C\mathbf{0}_D)^{(m=l_a+l_b+l_c+l_d)}$

Let us consider the case of the standard electron-electron repulsion integrals. If we set $h(r_{12}) = r_{12}^{-1}$, then the potential weighting function is

$$H\left(u^2\right) = \frac{2}{\sqrt{\pi}} \,\forall u. \tag{4.53}$$

The integral in Eqn 4.50 is

$$\int_0^\infty du\, H\left(u^2\right) \left[\frac{u^2}{(\rho+u^2)}\right]^m \left(\frac{\rho}{\rho+u^2}\right)^{\frac{3}{2}} \exp\left[-\frac{\rho u^2}{\rho+u^2}(\mathbf{P}-\mathbf{Q})^2\right]$$
$$= \frac{2}{\sqrt{\pi}}\rho^{\frac{1}{2}} \underbrace{\int_0^1 dt\, t^{2m} \exp\left[-\rho t^2(\mathbf{P}-\mathbf{Q})^2\right]}_{=:F_m\left(\rho(\mathbf{P}-\mathbf{Q})^2\right)}. \tag{4.54}$$

We refer to F_m as the "standard Auxiliary Boys Function".

4.3.2.1. Aside - Comparison to Related Work

When comparing the present analysis with other work, it is important to note that some authors define the auxiliary integrals $(\mathbf{a}|h(r)|\mathbf{c})^{(m)}$ as [119]

$$(\mathbf{a}|h(r)|\mathbf{c})^{(m)} = \int_0^\infty du\, H\left(u^2\right) \left(\frac{u^2-\gamma}{u^2-\gamma+\rho}\right)^m (\mathbf{a}|u|\mathbf{c}) \tag{4.55}$$

whereas in the present work they are defined as

$$(\mathbf{a}|h(r)|\mathbf{c})^{(m)} = \int_0^\infty du\, H\left(u^2\right) \left(\frac{u^2}{u^2+\rho}\right)^m (\mathbf{a}|u|\mathbf{c}). \tag{4.56}$$

The recurrence relations and zero-angular-momentum expressions are thus slightly different, but the results for $m = 0$ are of course the same.

The choice of formalism is significant since it affects the ease with which the integrals can be implemented in molecular integral codes. In the formalism of Eqn 4.55, changing the geminal function $h(r_{12})$ requires modification to both the recurrance-relation routines (such as Eqn 4.49) and the routines for evaluating the zero-angular momentum integrals $(\mathbf{0}_A\mathbf{0}_B|h(r)|\mathbf{0}_C\mathbf{0}_D)^{(m)}$. However, in the formalism of Eqn 4.56, the recurrance-relations do not depend on the choice of geminal function, and only modification of the zero-angular momentum integrals is necessary. We thus choose the formalism of Eqn 4.56 in the present work. In Section 4.3.3 we describe how the zero-angular momentum integrals were implemented.

4.3.3. Modified Electron-Electron Integrals for Gaussian-Type Geminals

Let us consider the case where $h(r_{12}) = w_{\mathrm{GTG}}(r_{12})$ (defined in Eqn 4.4).[5] The potential weighting function $H\left(u^2\right)$ becomes a sum of delta functions

$$H\left(u^2\right) = \sum_{\gamma} c_{\gamma} \delta\left(u - \sqrt{\gamma}\right). \tag{4.57}$$

The integral in Eqn 4.50 is now

$$\int_0^{\infty} du\, H\left(u^2\right) \left[\frac{u^2}{(\rho + u^2)}\right]^m \left(\frac{\rho}{\rho + u^2}\right)^{\frac{3}{2}} \exp\left[-\frac{u^2}{\rho + u^2}\rho(\mathbf{P} - \mathbf{Q})^2\right]$$
$$= \frac{2}{\sqrt{\pi}}\rho^{\frac{1}{2}} \underbrace{\frac{\sqrt{\pi}}{2}\frac{1}{\rho^{\frac{1}{2}}}\sum_{\gamma} c_{\gamma} \left(\frac{\gamma}{\rho + \gamma}\right)^m \left(\frac{\rho}{\rho + \gamma}\right)^{\frac{3}{2}} \exp\left[-\frac{\rho\gamma}{\rho + \gamma}(\mathbf{P} - \mathbf{Q})^2\right]}_{\tilde{F}_m\left(\rho,\, (\mathbf{P}-\mathbf{Q})^2\right)}, \tag{4.58}$$

---

[5]Henceforth we omit the spin script s on w_{GTG}.

where $\tilde{F}_m\left(\rho,\,(\mathbf{P}-\mathbf{Q})^2\right)$ is an "effective Boys function". Note that $\tilde{F}_m$ depends on both ρ and $(\mathbf{P}-\mathbf{Q})^2$, as opposed to just their product. Substituting into Eqn 4.50, the zero-angular-momentum integral is given by

$$(\mathbf{0}_A\mathbf{0}_B|h(r)|\mathbf{0}_C\mathbf{0}_D)^{(m)} = (\mathbf{0}_A||\mathbf{0}_B)(\mathbf{0}_C||\mathbf{0}_D)\frac{2}{\sqrt{\pi}}\rho^{\frac{1}{2}}\tilde{F}_m\left(\rho,\,(\mathbf{P}-\mathbf{Q})^2\right). \tag{4.59}$$

By choosing $\tilde{F}_m$, it is possible to express the zero-angular-momentum integrals for any geminal $h(r_{12})$ in the form of Eqn 4.59.

Eqn 4.58 was implemented in the

`intception/unsoldwr/boys_function_wr.c`

file in the `entos` source directory. The information on the exponents $\{\gamma\}$ and coefficients $\{c_\gamma\}$ is passed in using an object of type `InterElectronPotential`, as shown in Listing 4.1 on page 90.

4.3.3.1. Limit Where $w_{\mathbf{GTG}}(r_{12})$ is Constant

It is interesting to note the limiting cases of Eqn 4.58. In the case where $w(r) = w_0\,\forall r$, $c = w_0$, $\gamma = 0$,

$$\tilde{F}_m\left(\rho,\,(\mathbf{P}-\mathbf{Q})^2\right) = \frac{\sqrt{\pi}}{2}\frac{1}{\rho^{\frac{1}{2}}}\sum_\gamma c_\gamma\left(\frac{\gamma}{\rho+\gamma}\right)^m\left(\frac{\rho}{\rho+\gamma}\right)^{\frac{3}{2}}\exp\left[-\frac{\rho\gamma}{\rho+\gamma}(\mathbf{P}-\mathbf{Q})^2\right] \tag{4.60}$$

$$= \frac{\sqrt{\pi}}{2}\frac{1}{\rho^{\frac{1}{2}}}w_0\delta_{m0}, \tag{4.61}$$

and hence

$$\int_0^\infty du\,H\left(u^2\right)\left[\frac{u^2}{(\rho+u^2)}\right]^m\left(\frac{\rho}{\rho+u^2}\right)^{\frac{3}{2}}\exp\left[-\frac{\rho u^2}{\rho+u^2}(\mathbf{P}-\mathbf{Q})^2\right] = w_0\delta_{m0}. \tag{4.62}$$

The zero-angular-momentum integral is then

$$(\mathbf{0}_A\mathbf{0}_B|w(r)|\mathbf{0}_C\mathbf{0}_D)^{(m)} = (\mathbf{0}_A||\mathbf{0}_B)(\mathbf{0}_C||\mathbf{0}_D)\,w_0\delta_{m0}, \tag{4.63}$$

and the four-index integral factorizes into two overlap integrals. This is expected, since a geminal $h(r_{12})$ that is constant everywhere implies no coupling between the electron positions.

4.3.3.2. Limit Where $w_{\mathsf{GTG}}(r_{12}) = \delta^3(r)$

In the case where $w(r) = \delta^3(r)$, $c = (\gamma/\pi)^{\frac{3}{2}}$, $\gamma/\rho \to \infty$,

$$\tilde{F}_m\left(\rho,\,(\mathbf{P}-\mathbf{Q})^2\right) = \frac{\sqrt{\pi}}{2}\frac{1}{\rho^{\frac{1}{2}}}(\gamma/\pi)^{\frac{3}{2}}\left(\frac{\gamma}{\rho+\gamma}\right)^m\left(\frac{\rho}{\rho+\gamma}\right)^{\frac{3}{2}}\exp\left[-\frac{\rho\gamma}{\rho+\gamma}(\mathbf{P}-\mathbf{Q})^2\right] \tag{4.64}$$

$$\to \frac{\sqrt{\pi}}{2}\frac{1}{\rho^{\frac{1}{2}}}\left(\frac{1}{\pi}\right)^{\frac{3}{2}}(\rho)^{\frac{3}{2}}\exp\left[-\rho(\mathbf{P}-\mathbf{Q})^2\right] \text{ (as } \gamma/\rho \to \infty) \tag{4.65}$$

$$= \frac{\rho}{2\pi}\exp\left[-\rho(\mathbf{P}-\mathbf{Q})^2\right]. \tag{4.66}$$

The zero-angular-momentum integral is therefore

$$(\mathbf{0}_A\mathbf{0}_B|w(r)|\mathbf{0}_C\mathbf{0}_D)^{(m)} = (\mathbf{0}_A||\mathbf{0}_B)(\mathbf{0}_C||\mathbf{0}_D)\left(\frac{\rho}{\pi}\right)^{\frac{3}{2}}\exp\left[-\rho(\mathbf{P}-\mathbf{Q})^2\right] \tag{4.67}$$

$$= (\mathbf{0}_A|\mathbf{0}_B|\mathbf{0}_C|\mathbf{0}_D), \tag{4.68}$$

where $(\mathbf{0}_A|\mathbf{0}_B|\mathbf{0}_C|\mathbf{0}_D)$ is the four-index overlap integral defined by

$$(\mathbf{a}|\mathbf{b}|\mathbf{c}|\mathbf{d}) = \int d\mathbf{r}_1\, g_{\mathbf{a}}(\mathbf{r}_1)g_{\mathbf{b}}(\mathbf{r}_1)g_{\mathbf{c}}(\mathbf{r}_1)g_{\mathbf{d}}(\mathbf{r}_1). \tag{4.69}$$

This is expected, since a delta-function geminal $h(r_{12})$ implies that the integral is only nonzero when the electrons are at the same position in space.

4.3.4. Modified Electron-Electron Integrals for Gaussian-Type Geminals Multiplied by r_{12}^{-1}

We now aim to calculate the integral $(\mathbf{0}_A\mathbf{0}_B|h(r)|\mathbf{0}_C\mathbf{0}_D)^{(m)}$ where

$$h(r_{12}) = w_{\text{GTG}}(r_{12})\,r_{12}^{-1}. \tag{4.70}$$

We need to find the potential weighting function $H\left(u^2\right)$ such that

$$\int_0^\infty du\, H\left(u^2\right) \exp\left[-u^2 r^2\right] = h(r) \tag{4.71}$$

$$= \sum_\gamma c_\gamma \exp\left[-\gamma r^2\right] r^{-1} \tag{4.72}$$

$$= \sum_\gamma c_\gamma \exp\left[-\gamma r^2\right]\left(\int_0^\infty ds\, \frac{2}{\sqrt{\pi}} \exp\left[-s^2 r^2\right]\right) \tag{4.73}$$

$$= \frac{2}{\sqrt{\pi}} \sum_\gamma c_\gamma \int_0^\infty ds\, \exp\left[-\left(\gamma + s^2\right) r^2\right]. \tag{4.74}$$

Making the substitution

$$u^2 = \gamma + s^2, \tag{4.75}$$

Eqn 4.74 becomes

$$\int_0^\infty du\, H\left(u^2\right) \exp\left[-u^2 r^2\right]$$

$$= \frac{2}{\sqrt{\pi}} \sum_\gamma c_\gamma \int_{\sqrt{\gamma}}^\infty \left(u\, du\left(u^2 - \gamma\right)^{-\frac{1}{2}}\right) \exp\left[-u^2 r^2\right], \tag{4.76}$$

and we see immediately that

$$H\left(u^2\right) = \sum_{\gamma} c_{\gamma} \frac{2}{\sqrt{\pi}} u \, \Theta\left(u^2 - \gamma\right)\left(u^2 - \gamma\right)^{-\frac{1}{2}} \tag{4.77}$$

$$= \sum_{\gamma} c_{\gamma} \frac{2}{\sqrt{\pi}} \Theta\left(u^2 - \gamma\right) \frac{u}{\left(u^2 - \gamma\right)^{\frac{1}{2}}}, \tag{4.78}$$

where $\Theta(x)$ is the Heaviside step function

$$\Theta(x) = \begin{cases} 1 & x > 0 \\ \frac{1}{2} & x = 0 \\ 0 & x < 0 \end{cases} . \tag{4.79}$$

Now we substitute the potential weight function $H\left(u^2\right)$ into the integral in Eqn 4.50. Defining t' such that

$$\frac{u^2}{\rho + u^2} = \frac{\rho}{\rho + \gamma}\left(t'\right)^2 + \frac{\gamma}{\rho + \gamma},$$

the integral in Eqn 4.50 becomes

$$\int_0^\infty du \, H\left(u^2\right)\left[\frac{u^2}{\left(\rho + u^2\right)}\right]^m \left(\frac{\rho}{\rho + u^2}\right)^{\frac{3}{2}} \exp\left[-\frac{u^2}{\rho + u^2}\rho(\mathbf{P} - \mathbf{Q})^2\right]$$

$$= \frac{2}{\sqrt{\pi}}\rho^{\frac{1}{2}}\sum_{\gamma} c_{\gamma} \exp\left[-\frac{\rho\gamma}{\rho + \gamma}(\mathbf{P} - \mathbf{Q})^2\right]\frac{\rho}{\rho + \gamma}\underbrace{\sum_{n=0}^m \binom{m}{n}\frac{\rho^n\gamma^{m-n}}{(\rho + \gamma)^m} F_n\left(\frac{\rho^2}{\rho + \gamma}(\mathbf{P} - \mathbf{Q})^2\right)}_{\Upsilon_{mn}^{\gamma}}, \tag{4.80}$$

$$\underbrace{\phantom{= \frac{2}{\sqrt{\pi}}\rho^{\frac{1}{2}}\sum_{\gamma} c_{\gamma} \exp\left[-\frac{\rho\gamma}{\rho + \gamma}(\mathbf{P} - \mathbf{Q})^2\right]\frac{\rho}{\rho + \gamma}\sum_{n=0}^m \binom{m}{n}\frac{\rho^n\gamma^{m-n}}{(\rho + \gamma)^m} F_n\left(\frac{\rho^2}{\rho + \gamma}(\mathbf{P} - \mathbf{Q})^2\right)}}_{\tilde{F}_m\left(\rho,(\mathbf{P}-\mathbf{Q})^2\right)}$$

where again $\tilde{F}_m\left(\rho, (\mathbf{P} - \mathbf{Q})^2\right)$ is an "effective Boys function". We see that Υ^{γ} is a lower-

triangular matrix ($n \leq m$) that mixes the standard auxiliary Boys functions F_n (see Eqn 4.54).

Eqn 4.80 was implemented in the

`intception/unsoldwr/boys_function_wr.c`

file in the `entos` source directory. The information on the exponents $\{\gamma\}$ and coefficients $\{c_\gamma\}$

is passed in using an object of type `InterElectronPotential`, as shown in Listing 4.2.

Listing 4.2: Computing the modified electron-electron integrals $(\alpha\beta|w_{12}r_{12}^{-1}|C)$ in `entos`, with a Gaussian-type geminal function $w(r) = -e^{-r^2}$. Language: C++.

```cpp
const intception::InterElectronPotential Wr_invr(
    {  1.0 }, // Exponents $\zeta$
    { -1.0 }, // Coefficients $c_\zeta$
    intception::InterElectronPotential::Type::
        ↪ gaussiantimesinvr
);

  // $ ( \alpha \beta | w(r) r^{-1} |  C ) $.
auto W = integrals::compute_df_integrals(
    ao_basis, // ${ \alpha (r) } $
    df_basis, // ${ C (r) } $
    schwarz_threshold,
    Wr_invr.c_struct_ptr() // Convert Wr_invr to a C struct
        ↪ for passing to C code
);
```

4.3.4.1. Aside - Alternative Notation Involving Derivatives

Note that the standard Boys function can also be written

$$F_m(x) = \int_0^1 dt\, t^{2m} \exp\left[-t^2 x\right] \tag{4.81}$$

$$= \left(-\frac{d}{dx}\right)^m F_0(x) \tag{4.82}$$

$$F_m(ax) = \left(\frac{1}{a}\right)^m \left(-\frac{d}{dx}\right)^m F_0(ax), \tag{4.83}$$

and thus the summation over n in Eqn 4.80 can be expressed as

$$\sum_{n=0}^m \binom{m}{n} T^{m-n}(1-T)^{n+1} F_n((1-T)x) = (1-T)\left[T - \frac{d}{dx}\right]^m F_0((1-T)x), \tag{4.84}$$

where

$$T = \frac{\gamma}{\rho + \gamma}. \tag{4.85}$$

4.3.4.2. Limit Where $w_{\text{GTG}}(r_{12})$ is Constant

In the same way as for the $h(r_{12}) = w_{\text{GTG}}(r_{12})$ integrals, we can consider limiting cases of Eqn 4.80. In the case where $w(r) = w_0 \,\forall r$, $c = w_0$, $\gamma = 0$,

$$\tilde{F}_m\left(\rho,\, (\mathbf{P} - \mathbf{Q})^2\right) = w_0 F_m\left(\rho(\mathbf{P} - \mathbf{Q})^2\right), \tag{4.86}$$

and the effective Boys function reduces to the standard Boys function as expected. This is expected, since the geminal function is merely a constant multiplied by the standard electron-electron repulsion geminal r_{12}.

4.3.4.3. Limit Where $w_{\mathbf{GTG}}(r_{12}) = \delta^3(r)$

In the case where $w_{\mathrm{GTG}}(r_{12}) = \delta^3(r_{12})$, $c = (\gamma/\pi)^{\frac{3}{2}}$, $\gamma/\rho \to \infty$,

$$\tilde{F}_m\left(\rho,\, (\mathbf{P}-\mathbf{Q})^2\right) \sim \left(\frac{1}{\pi}\right)^{\frac{3}{2}} \exp\left[-\rho(\mathbf{P}-\mathbf{Q})^2\right] \rho^{\frac{3}{2}} \left(\frac{\gamma}{\rho}\right)^{\frac{1}{2}}, \tag{4.87}$$

$$\to \infty \text{ as } \frac{\gamma}{\rho} \to \infty, \tag{4.88}$$

and the effective Boys function $\tilde{F}_m$ diverges to $+\infty$. This is expected due to behavior of the geminal function $\delta^3(r_{12})r_{12}^{-1}$ as $r_{12} \to 0$.

4.3.5. Modified Electron-Electron Integrals for Coulomb-Attenuated Geminals

We now evaluate electron-electron integrals where $h(r_{12}) = r_{12}^{-1}\mathrm{erf}(\mu r_{12})$, with μ a real screening parameter with dimensions of inverse length. These integrals were not used in the UW12 methods presented in this thesis, but the code presented here has since been used by the Manby research group to implement Coulomb-attentuated-methods (CAM) in `entos` [116, 42]. The potential weighting function is

$$H\left(u^2\right) = \frac{2}{\sqrt{\pi}}\Theta\left(\mu^2 - u^2\right). \tag{4.89}$$

Using the substitutions

$$t^2 = \frac{u^2}{\left(\rho + u^2\right)} \tag{4.90}$$

$$v^2 = \frac{\mu^2}{\left(\rho + \mu^2\right)}t^2, \tag{4.91}$$

the integral in Eqn 4.50 becomes

$$\int_0^\mu du\, H\left(u^2\right) \left[\frac{u^2}{(\rho+u^2)}\right]^m \left(\frac{\rho}{\rho+u^2}\right)^{\frac{3}{2}} \exp\left[-\frac{\rho u^2}{\rho+u^2}(\mathbf{P}-\mathbf{Q})^2\right]$$

$$= \frac{2}{\sqrt{\pi}}\rho^{\frac{1}{2}} \int_0^{\sqrt{\frac{\mu^2}{(\rho+\mu^2)}}} dt\, t^{2m} \exp\left[-\rho t^2(\mathbf{P}-\mathbf{Q})^2\right] \tag{4.92}$$

$$= \frac{2}{\sqrt{\pi}}\rho^{\frac{1}{2}} \left(\frac{\mu^2}{\rho+\mu^2}\right)^{m+\frac{1}{2}} \int_0^1 dv\, v^{2m} \exp\left[-\left(\frac{\rho\mu^2}{\rho+\mu^2}\right)v^2(\mathbf{P}-\mathbf{Q})^2\right] \tag{4.93}$$

$$= \frac{2}{\sqrt{\pi}}\rho^{\frac{1}{2}} \underbrace{\left(\frac{\mu^2}{\rho+\mu^2}\right)^{m+\frac{1}{2}} F_m\left(\frac{\rho\mu^2}{\rho+\mu^2}(\mathbf{P}-\mathbf{Q})^2\right)}_{\tilde{F}_m\left(\rho,\,(\mathbf{P}-\mathbf{Q})^2\right)}, \tag{4.94}$$

where again $\tilde{F}_m\left(\rho,\,(\mathbf{P}-\mathbf{Q})^2\right)$ is an "effective Boys function" and F_n is the standard auxiliary Boys function (see Eqn 4.54).

Eqn 4.94 was implemented in the

`intception/unsoldwr/boys_function_wr.c`

file in the `entos` source directory. The information on the exponents $\{\gamma\}$ and coefficients $\{c_\gamma\}$ is passed in using an object of type `InterElectronPotential`, as shown in Listing 4.3.

Listing 4.3: Computing the modified electron-electron integrals $(\alpha\beta|(A + B\,\mathrm{erf}(\mu r_{12}))r_{12}^{-1}|C)$ in `entos`. *A* and *B* are real coefficients (the CAM coefficients). Language: C++.

```
const intception::InterElectronPotential erfr_rinv(
     { 0, 1/mu }, // Length scale of screening
     { A, B }, // CAM coefficients
     intception::InterElectronPotential::Type::erftimesinvr
);
integrals::compute_df_integrals(
     ao_basis, // ${ \alpha (r) } $
     df_basis, // ${ C (r) } $
     schwarz_threshold,
     erfr_rinv.c_struct_ptr() // Convert erfr_rinv to a C
         ↪ struct for passing to C code
```

```
11  );
```

4.3.6. Modifications to Intception for Electron-Electron Integrals

Code for evaluating the effective Boys function for the inter-electron potentials in Eqns 4.58, 4.80, and 4.94 was written by the author of this thesis, and can be found in the `unsoldwr` subdirectory of the `intception` source code directory, which is contained in the `entos` repository. The 3-index electron-electron code in the

`intception_integral_coulomb_3idx_hrr_abc_m.c`

file intception source directory was also modified to allow the passing of the inter-electron potential information. The signature of the low-level 3-index electron-electron integral $(\alpha\beta|h_{12}|C)$ function `intception_integral_coulomb_3idx_hrr_abc_m_main` thus becomes[6]

```
void intception_integral_coulomb_3idx_hrr_abc_m_main(

    /* Information about basis function \alpha */
    const double * xa,
    const double cA[3],
    const int la,
    const int na,
    const int iskipa,
    const int na_prim,
    const int na_cont,
    const int iskipa_cont,
```

---

[6]Note that the code for the 2-index electron-electron integrals $(D|h_{12}|C)$ (defined in Eqn 4.3) was also modified in a similar way.

```
const double * contract_array_a,

const double * sph_trans_array_a,


/* Information about basis function \beta */

const double * xb,

const double cB[3],

const int lb,

const int nb,

const int iskipb,

const int nb_prim,

const int nb_cont,

const int iskipb_cont,

const double * contract_array_b,

const double * sph_trans_array_b,


/* Information about basis function C */

const double * xc,

const double cC[3],

const int lc,

const int nc,

const int iskipc,

const int nc_prim,

const int nc_cont,

const int iskipc_cont,

const double * contract_array_c,
```

```
    const double * sph_trans_array_c,


    /* Information about the inter-electron potential h(r_{12}) */
    const struct intception_InterElecPot* Wr,


    /*
    double * work_array,

    double * output_array

  );
```

The added parameter `Wr` is shown in bold, and is a pointer to a struct containing

- An enum specifying the type of inter-electron potential:

    - `intception_InterElecPotType_gaussian`: An inter-electron potential of the form $h(r_{12}) = \sum_\gamma c_\gamma e^{-\gamma r_{12}^2}$ (see Section 4.3.3)

    - `intception_InterElecPotType_gaussiantimesinvr`: An inter-electron potential of the form $h(r_{12}) = \sum_\gamma r_{12}^{-1} c_\gamma e^{-\gamma r_{12}^2}$ (see Section 4.3.4)

    - `intception_InterElecPotType_erftimesinvr`: An inter-electron potential of the form $h(r_{12}) = \sum_\mu c_\mu r_{12}^{-1} \mathrm{erf}(\mu r_{12})$ (see Section 4.3.5)

- The exponents $\{\gamma\}$ (or $\{\mu\}$ in the case of an `erftimesinvr` potential)

- The coefficients $\{c_\gamma\}$ (or $\{\mu\}$ in the case of an `erftimesinvr` potential).

If the pointer `Wr` is `null`, then it is assumed that $h(r_{12}) = r_{12}^{-1}$ (as in the case of the standard electron-electron repulsion integrals). The signature of the Boys function is also modified and changes from

```
    void intception_wr_boys(
```

```
        double * f,

        const int ifskip,

        const int nmin,

        const int nmax,

        const double x

    );
```

to

```
    void intception_wr_boys(

        double * f,

        const int ifskip,

        const int nmin,

        const int nmax,

        const double rho,

        const double R2,

        const struct intception_InterElecPot* Wr

    );
```

where the parameter x is the quantity $\rho \ (\mathbf{P} - \mathbf{Q})^2$ in Eqn 4.54. In defining the effective Boys function, x has been replaced by two separate parameters rho (ρ) and R2 ($(\mathbf{P} - \mathbf{Q})^2$) (see Eqns 4.58, 4.80, and 4.94).

4.4. Modified Electron-Nuclear Integrals

We now turn our attention to the modified electron-nuclear integrals $(\mathbf{r}_\lambda | h_{12} | \alpha \beta)$ (defined in Eqn 4.1), where α and β are GTOs and $\mathbf{r}_\lambda$ is a grid-point. For the case where $h_{12} = r_{12}^{-1}$, these are

clearly equivalent to the standard electron-nuclear integrals, which are already implemented in all electronic structure programs. For the case where $h(r_{12}) = w_{\text{GTG}}(r_{12})$, the modified electron-nuclear integrals can be expressed in terms of the three-index overlap integrals defined in Eqn 4.16 using the formula

$$(\mathbf{r}_\lambda|w_{\text{GTG}}(r_{12})|\alpha\beta) = \sum_\gamma c_\gamma \left(\alpha|\mathbf{0}_{r_\lambda}^\gamma|\beta\right).$$

The three-index overlap integrals were already implemented (by James Womack [114]) in the `overlap_3idx()` function in the
`src/integrals/intception_wrapper.cpp`
file in the `entos` source directory, which calls the
`intception_integral_overlap_3idx_hrr_abc.c`
file in the `intception` source directory.

4.5. Chapter Summary

In this chapter, we described how the `intception` molecular integral package was modified to compute the integrals needed for UW12 (see Section 3.2). The `intception` integral routines are called by the electronic structure code `entos`. Note that there is great scope for improvements in the efficiency in the implementation presented in this thesis, some of which are discussed in Sections 3.4 and 3.5. In Chapters 5 and 6, we apply the `entos` implementation of UW12 to various test sets of small molecules. As a final remark, note that the implementation of UW12 outlined in Section does not require any of the complex integral types described in this chapter.

5. Including UW12 in Hybrid Functionals

5.1. Chapter Aims

In Chapter 1, we saw that conventional global hybrid (rung-4) functionals suffer from a trade-off between barrier-height accuracy (which requires an exact exchange fraction $a_{\mathrm{x}}^{\mathrm{HF}}$ of ~ 0.5) and atomization energy accuracy (which requires an exact exchange fraction of ~ 0.2). We reviewed some attempts in the literature to solve this problem, including adding in fractions of MP2 to make double-hybrid functionals. In Chapter 2, we introduced UW12, a correlation model that bears some resemblance to MP2 but which depends only on occupied Kohn-Sham orbitals.

In this chapter, we replace the $E_{\mathrm{c}}^{\mathrm{PT2}}$ term in some existing double-hybrid (rung-5) functionals with $E_{\mathrm{c}}^{\mathrm{UW12}}$. In this way we hope to find a rung-4 method (one that depends only on occupied Kohn-Sham orbitals) that can correctly estimate both atomization energies and barrier heights, but which has a small number of empirical parameters.

5.2. The XCH-BLYP-UW12 Functional

By replacing $E_{\mathrm{c}}^{\mathrm{PT2}}$ with $E_{\mathrm{c}}^{\mathrm{UW12}}$, can we make a hybrid (rung-4) functional with the same accuracy as the double-hybrid (rung-5) functional B2-PLYP (defined in Eqn 1.100)? Recall

that B2-PLYP has the empirical parameters $a_x^{HF}, a_c^{LYP} = 0.53, 0.73$. In this work, we make a slight simplification by setting $a_x^{HF}, a_c^{LYP} = \frac{1}{2}, \frac{3}{4}$, although we make no physical justification for this choice.[1] Our aim in this chapter is to make small perturbations to DFT in order to reproduce the successes of B2-PLYP at simultaneously modelling both barrier-heights and atomization energies. As such, the fraction of UW12 that we add ($a_c^{UW12} = 0.25$) is relatively small compared to that used in Chapter 6. We thus define the XCH-BLYP-UW12 functional

$$E_{xc}^{XCH\text{-}BLYP\text{-}UW12} = \tfrac{1}{2} E_x^{B88} + \tfrac{1}{2} E_x^{HF} + \tfrac{3}{4} E_c^{LYP} + \tfrac{1}{4} E_c^{UW12(r_c)} \tag{5.1}$$

where we use the definition of $E_c^{UW12(r_c)}$ in Eqn 2.34. The XCH-BLYP-UW12 functional contains a single adjustable parameter r_c, which represents the length scale for the correlation hole. An inspection of Eqn 2.34 reveals that changing r_c serves the additional purpose of scaling the UW12 correlation energy. We use the prefix XCH (exchange-and-correlation-hybrid) because the functional contains non-local correlation as well as non-local exchange. Conventional hybrids such as B3LYP contain non-local exchange but only local correlation.

5.3. Computational Details

The UW12 correlation energy expression and the XCH-BLYP-UW12 functional were implemented in the electronic structure program `entos` [42], using the algorithms outlined in Chapter 3. An example input file is shown in Listing 5.1.

---

[1]Note that various authors have attempted to make theoretical justification for the values of the parameters in double-hybrid functionals [50, 120], and some have proposed double-hybrids with no empirical parameters [121, 122]. However, in this thesis we are concerned with finding new ingredients for hybrid density functional theory, rather than the parameters used to mix these ingredients together. Hence we will attempt to choose values for the parameters that match the double-hybrid literature as far as possible.

Listing 5.1: An example input file for an `entos` calculation on the Si atom. Two calculations are performed: The first makes an initial guess for the Kohn-Sham orbitals using the LDA functional. The second runs a fully self-consistent XCH-BLYP-UW12 calculation using the initial guess orbitals from the LDA calculation.

```
1   ! Si_atom_XCH_BLYP_UW12.in
2   ! For use with the 'UW12_double_hybrid_paper' branch of entos.
3   ! Modified from a similar input file
4   ! with MD5 hash f152fde91265c6999128023da7d1e988.
5
6   print(msg='LDA calculation to determine initial guess orbitals
        ↪ .')
7   print(msg='Converges to total energy of -288.211841480 Hartree
        ↪ .')
8   dft(
9       structure ( formula='Si' )
10      charge = 0
11      multiplicity = 3
12      basis  = 'aug-cc-pVTZ-merged' ! aug-cc-pV(T+d)Z
13      density_fitting = true
14      df_basis = 'Def2-SVP-JKFIT'
15      mom = true
16
17      xc = 'LDA'
18  )
19
20  print(msg='Self-consistent XCH-BLYP-UW12 calculation.')
21  print(msg='Converges to total energy of -289.438566948 Hartree
        ↪ ')
22  dft(
23      structure ( formula='Si' )
24      charge = 0
25      multiplicity = 3
26      basis  = 'aug-cc-pVTZ-merged' ! aug-cc-pV(T+d)Z
27      density_fitting = true
28      df_basis = 'Def2-SVP-JKFIT'
29      mom = true
30
31      ! Use the LDA orbitals as an initial guess
```

```
32      guess  =  'use_loaded_mos'
33
34      ! Hybrid mixing parameters
35      xc = '0.5 B88 0.75 LYP'
36      exchange_factor = 0.5
37      unsoldw12_factor = 0.25
38
39      ! Use the Gaussian-type geminal (GTG) approximation to the
40      ! Slater-type geminal (STG) function with $ r_c = 1.7 a_0
           ↪ $.
41      unsoldw12_coeffs = [
42         0.000835,
43        -0.085419,
44        -0.260011,
45        -0.216534,
46        -0.135269,
47        -0.070814,
48        -0.039562,
49        -0.021128,
50        -0.007673,
51        -0.011382
52      ]
53      unsoldw12_exponents = [
54         0.010000,
55         0.035938,
56         0.129155,
57         0.464159,
58         1.668101,
59         5.994843,
60         21.544347,
61         77.426368,
62         278.255940,
63         1000.000000
64      ]
65      unsoldw12_scale_samespin = 0.5
66
67
68      ! Uncomment the following lines to disable self-consistent
69      ! orbital optimization:
70      !max_iter = 0
71      !no_fail = true
72 )
```

We use the Dunning aug-cc-pV(X+d)Z basis-sets for the calculations presented in this chapter [20, 21, 22, 23, 123]. Energies of singlet molecules and atoms were calculated with the spin-restricted Kohn-Sham formalism, and energies of other molecules and atoms were calculated with the spin-unrestricted formalism. For `entos` calculations, the Def2-SVP-JKFIT density-fitting basis-set was used [124, 82].

5.4. Atomization Energies and Barrier-Heights
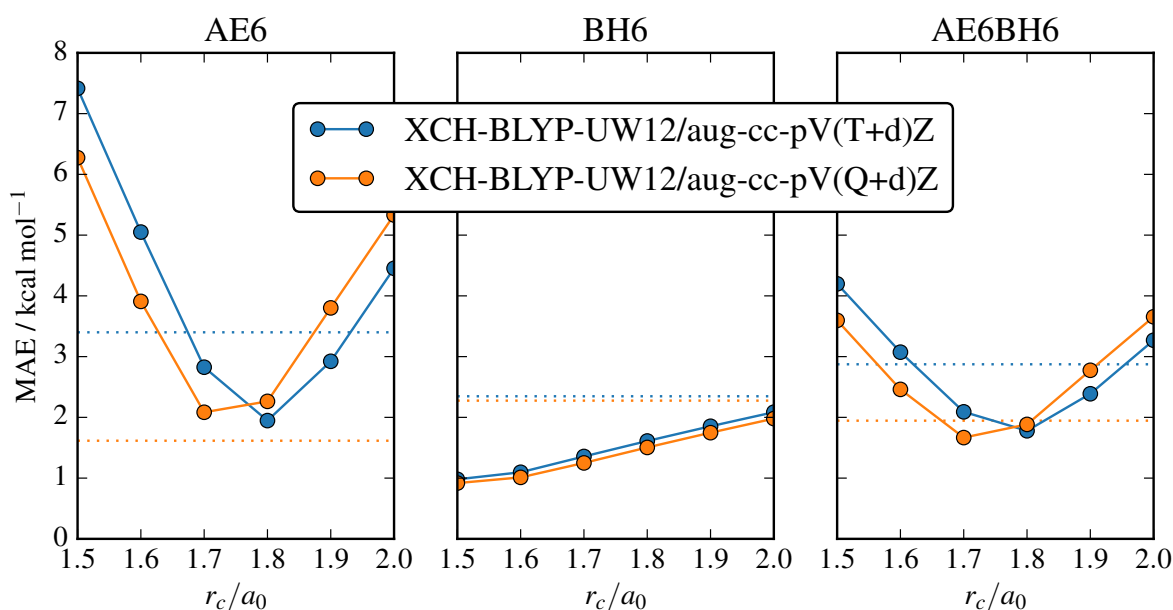
Figure 5.1.: Mean absolute errors (MAE) for the AE6 (far left), BH6 (center), and combined AE6+BH6 (far right) test sets [125] as functions of the parameter r_c for the single-parameter UW12 hybrid functional XCH-BLYP-UW12. In this plot, the XCH-BLYP-UW12 results use B3LYP orbitals rather than using full self-consistency. The horizontal dotted lines show the MAE for the existing two-parameter double-hybrid functional B2-PLYP [33]. Figure reproduced with permission from the Journal of Chemical Theory and Computation [1]. Copyright 2018 American Chemical Society. .

We wish to find a method that can correctly estimate both atomization energies and barrier-heights. Following the procedure of Ref [50], we optimize the value of the single parameter r_c in XCH-BLYP-UW12 on the AE6 (atomization energies) and BH6 (barrier-heights) test sets[125]. All the calculations for the AE6 and BH6 sets were performed at the geometries optimized by quadratic configuration interaction with single and double excitations with the modified Gaussian-3 basis-set (QCISD/MG3).[2] Reference values (with zero-point energies removed) were taken from Tables 1 and 2 of Ref [125]. Mean absolute errors are plotted in Fig 5.1, where it can be seen that $r_c = 1.7\,a_0$ (where a_0 is the Bohr radius) is around the optimum length scale for $w(r_{12})$ for both the AE6 set and the combined AE6+BH6 set, if an aug-cc-pV(Q+d)Z basis is used.

In Fig 5.2 we plot the signed errors for individual atomization energies in the AE6 set. We observe that the gap between the orange and blue lines is smaller for XCH-BLYP-UW12 than for the existing double-hybrid functionals B2-PLYP and DSD-PBEB95-D3BJ. Hence XCH-BLYP-UW12 converges more rapidly with respect to basis-set than double-hybrid functionals. The slow basis-set convergence of the double-hybrids is due to the double-sum over unoccupied orbitals that is present in the E_c^{PT2} term. Some authors have applied the explicitly-correlated MP2-F12 method to double-hybrids in order to improve the basis-set convergence [126], and the resulting theory resembles UW12 hybrid DFT (see Section 2.2.2). As a final remark on basis-set convergence, it should be noted that the parameters in B2-PLYP were optimized using a quadruple-ζ basis-set. Chan and Radom[127] have investigated re-optimizing the parameters in B2-PLYP to obtain accurate results in triple-ζ basis-sets, but we do not use their parameters here. It will be interesting in the future to investigate whether triple-ζ basis-sets (as opposed to quadruple-ζ basis-sets) can be used with UW12 hybrids across all systems.

In Fig 5.4b we compare XCH-BLYP-UW12 (with the length-scale $r_c = 1.7\,a_0$ with existing

---

[2]QCISD/MG3 geometries for AE6 and BH6 compounds were taken from the Minnesota Database Collection at `https://comp.chem.umn.edu/db/`.

hybrid and double-hybrid functionals on larger benchmark sets of atomization energies and reaction barrier heights. The atomization-energy set referred to here as G2-1-AE-noLiBeNa contains the 49 molecules of Ref [128] (G2-1 set except for the six molecules containing Li, Be, and Na), with MP2(full)/6-31G* geometries.[3] Reference values were taken from Table 2 of Ref [128]. The barrier-height set DBH24/08 used QCISD/MG3 geometries.[4] Reference values were taken from Table 1 of Ref [129]. The aug-cc-pV(Q+d)Z basis-set was used for all calculations. The zero-point energies are removed in the reference values in all cases. For comparison, we also include results from older (pre-B3LYP) DFT methods in Fig 5.4a. As expected (see Section 1.12), we see that B-HH-LYP performs better than B3LYP for barrier heights, but worse for atomization energies.

Fig 5.4b shows that the (proof-of-concept) XCH-BLYP-UW12 functional has better accuracy than B2-PLYP for reaction barrier-heights. XCH-BLYP-UW12 does not perform as well as B3LYP and B2-PLYP on the G2-1 atomization energy set, although note that this set was one of those used to fit the three parameters in B3LYP [35, 46]. Note also that all of the molecules in the G2-1 atomization energy set are also in the G2/97 heats of formation set, which was used to fit the two parameters in B2-PLYP [33]. The performance demonstrated here for XCH-BLYP-UW12 is achieved with a single varied parameter, r_c, optimized over a set (AE6) of six atomization energies. It appears that barrier height estimation requires a lower value of r_c than atomization energy. The reason for this is unknown, and is an interesting avenue for future research. In particular, it will be interesting to see whether using the frozen-core approximation (*i.e.* neglecting the core-electron-valence-electron and core-electron-core-electron UW12 correlation terms) has an effect on the fitting parameters.

Density-corrected (HF-DFT) B3LYP [75] — where the DFT energy is calculated using Hartree-

---

[3]MP2(full)/6-31G* geometries were obtained from the Argonne National Laboratory website http://www.cse.anl.gov/OldCHMwebsiteContent/compmat/g2geoma.htm

[4]QCISD/MG3 geometries for DBH24/08 compounds were taken from the Minnesota Database Collection at http://comp.chem.umn.edu/db/.

Fock molecular orbitals[5] — performs better than B3LYP for barrier-heights, but XCH-BLYP-UW12 performs better still. Fig 5.3 shows that the systematic under-estimation of the transition state energy by standard B3LYP (upper-left panel) is density-driven, since it is all but eliminated when using density-corrected B3LYP. This is particularly true for the transition states involving breaking or forming of an O-H bond (the first 4 data points in Fig 5.3). Fig 5.3 also shows that the remaining error in barrier-height accuracy for XCH-BLYP-UW12 and B2-PLYP is evenly distributed across the barrier height set, with barrier heights being under-estimated by 1-2 kcal mol^{-1}.

We thus conclude that XCH-BLYP-UW12 helps to reduce both the density-driven and energy-driven errors in B3LYP barrier heights (see Section 1.15). XCH-BLYP-UW12 predicts barrier heights with an accuracy comparable to that of the modern DSD-PBEB95-D3BJ double-hybrid. Note that the DBH24 barrier height set was one of the sets used to fit the 6 adjustable parameters in DSD-PBEB95-D3BJ. We return to barrier-height and atomization-energy estimation in Section 6.4.

---

[5]In density-corrected DFT, it is hoped — for systems prone to delocalization error — that the HF density ρ_{HF} is a closer match to the true density ρ than is the DFT density ρ_{B3LYP}. Although this is true in many cases, it should be noted that the HF density is itself an approximation to the true density [13].
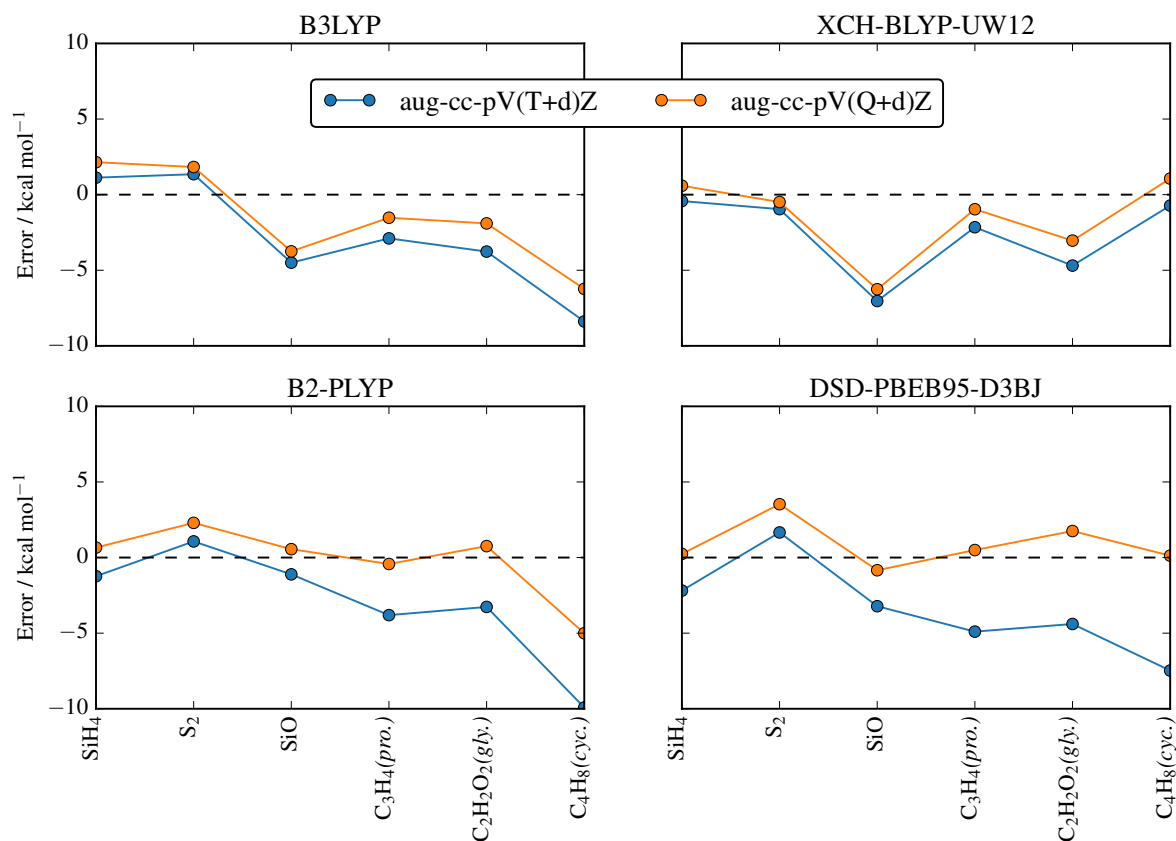
Figure 5.2.: Atomization energy errors for individual molecules in the AE6 test set for the existing hybrid (rung-4a) functional B3LYP [35], the existing double-hybrid (rung-5) functionals B2-PLYP [33] and DSD-PBEB95-D3BJ [34], and the new UW12 hybrid (rung-4b) functional XCH-BLYP-UW12. The abbreviations *(pro.)*, *(gly.)*, and *(cyc.)* refer to the isomers propyne, glyoxal, and cyclobutane respectively. For the rung-4 functionals, the orbitals are self-consistently optimized using the full energy expression. For the rung-5 functionals, the orbitals are optimized using a truncated version of the energy expression that does not include the $E_{\text{c}}^{\text{PT2}}$ term. Figure reproduced with permission from the Journal of Chemical Theory and Computation [1]. Copyright 2018 American Chemical Society. .
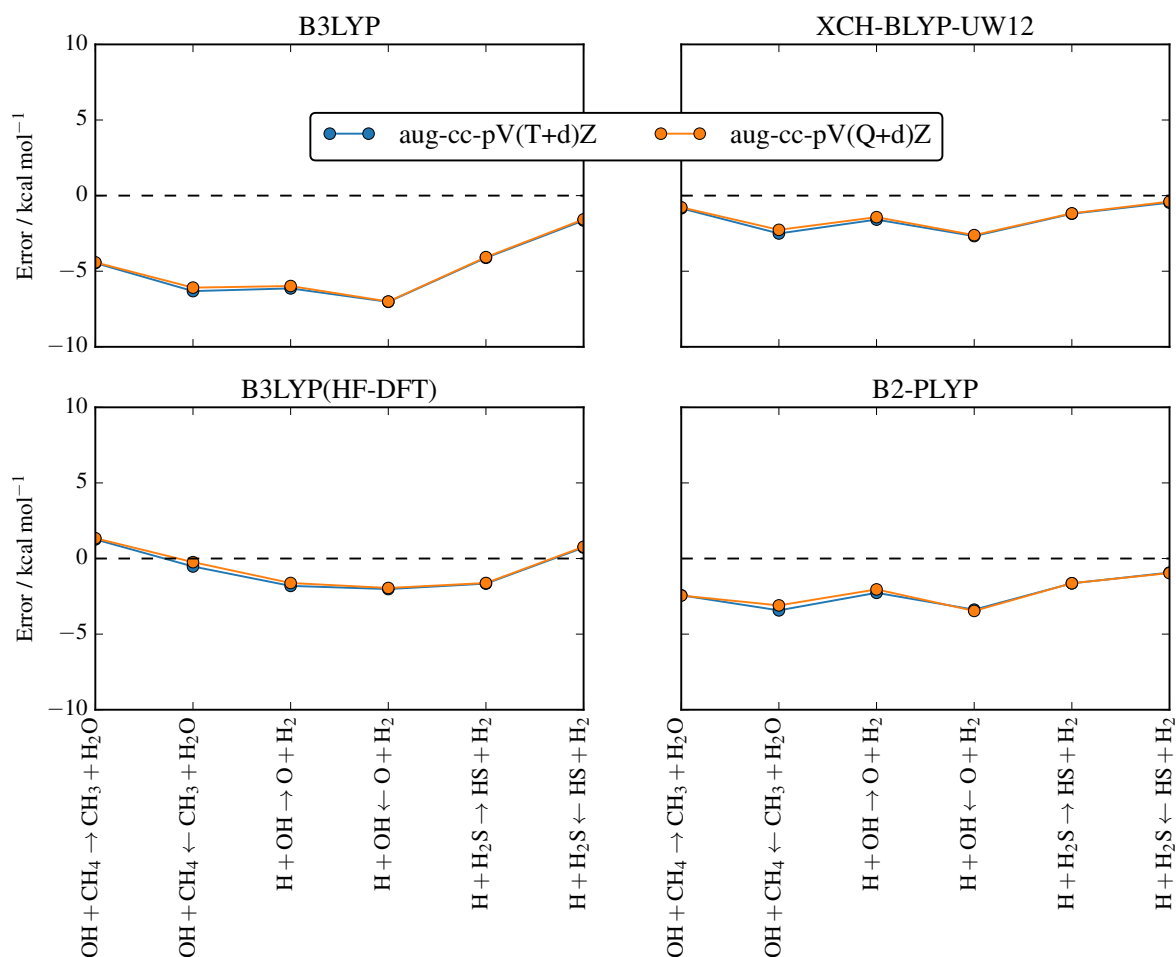
Figure 5.3.: Reaction energy errors for individual reactions in the BH6 test set for the existing hybrid (rung-4a) functional B3LYP [35], the existing double-hybrid (rung-5) functional B2-PLYP [33], and the new UW12 hybrid (rung-4b) functional XCH-BLYP-UW12. HF-DFT values for B3LYP (where the B3LYP energy is evaluated using Hartree-Fock orbitals) are also shown. For the rung-4 functionals, the orbitals are self-consistently optimized using the full energy expression. For B2-PLYP, the orbitals are optimized using a truncated version of the energy expression that does not include the E_c^{PT2} term.
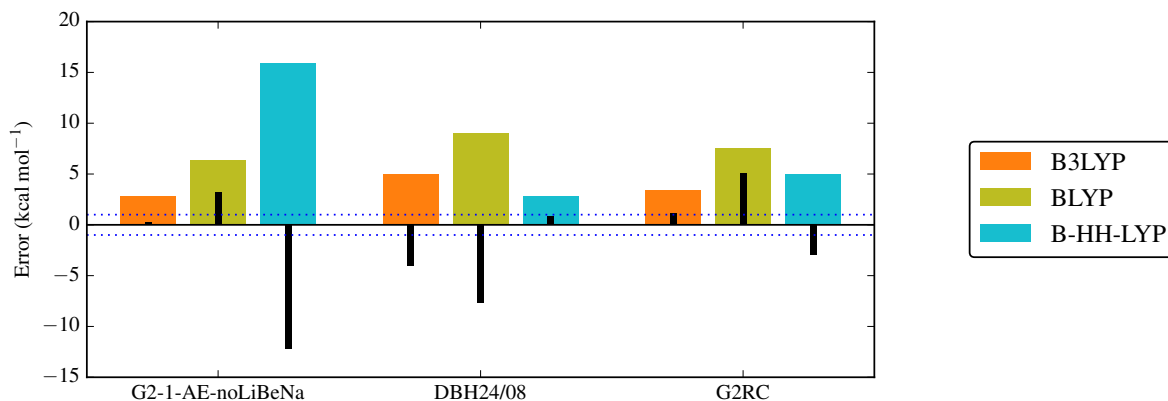
(a) DFT methods invented before B3LYP.
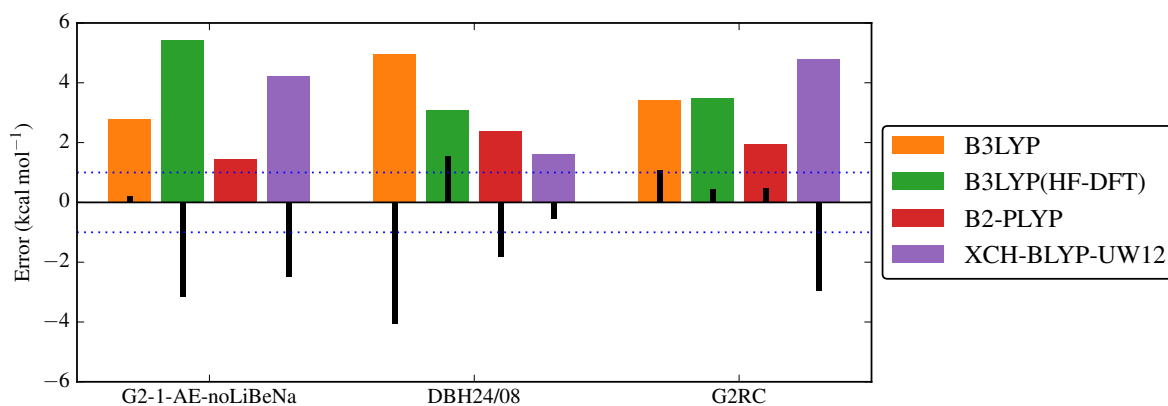
(b) DFT methods invented since B3LYP.

Figure 5.4.: Root-mean-square errors (RMSE, colored bars) and mean-errors (ME, black bars) for the larger test sets of atomization energies (G2-1-AE-noLiBeNa), reaction barrier-heights (DBH24/08), and reaction energies (G2RC). HF-DFT refers to the use of density-corrected DFT (see text). Chemical accuracy (± 1 kcal mol^{-1}) is shown with horizontal dotted lines. For comparison, the RMSE for the more recent double-hybrid DSD-PBEB95-D3BJ for the DBH24/08 set is 1.07 kcal mol^{-1} (taken from Ref [34]), and for the G2RC set is 2.33 kcal mol^{-1} (taken from Ref [7]). For B3LYP and XCH-BLYP-UW12 (but not B3LYP(HF-DFT)), the orbitals are self-consistently optimized using the full energy expression. For B2PLYP, the orbitals are optimized using a truncated version of the energy expression that does not include the $E_{\text{c}}^{\text{PT2}}$ term. Figure reproduced with permission from the Journal of Chemical Theory and Computation [1]. Copyright 2018 American Chemical Society. .

127

5.5. Reaction Energies

Results for the XCH-BLYP-UW12 functional for the G2RC [7] reaction energy test set are also plotted in Fig 5.4b. Note that all the compounds in the G2RC set are also in the G2-1 and G2/97 sets. MP2(full)/6-31G(d) geometries and reference values (with single-point energies removed) are taken from the GMTKN55 database collection at `http://www.chemie.uni-bonn.de/pctc/mulliken-center/software/GMTKN/gmtkn55/`. As with the G2-1 atomization energies, we observe that XCH-BLYP-UW12 performs with slightly worse accuracy than B3LYP (although it should be noted that B3LYP was parameterised using all of the molecules in this set, whereas XCH-BLYP-UW12 was not). We return to the problem of reaction energies in Section 6.4.2.

5.6. Chapter Summary

We have suggested a one-parameter hybrid ("rung-4b") functional XCH-BLYP-UW12 containing the UW12 correlation model, and this new functional estimates reaction barrier-heights with the same level of accuracy as modern double-hybrid (rung-5) functionals containing six parameters. UW12 hybrids show a faster convergence with respect to basis-set than double-hybrid functionals, due to the removal of the summation over unoccupied orbitals (see Section 2.2.1). It is surprising that the results of using E_c^{UW12} (defined in Eqn 2.4) match those of using E_c^{PT2} (defined in Eqn 1.97) so closely, given that the two energy expressions are so different in form. In particular, the E_c^{UW12} expression contains no information about the energies of the occupied and unoccupied orbitals.

Our aim in this chapter was to produce a B3LYP-like hybrid functional, and so we chose to test the functional on the sets that were used to parameterise B3LYP. We succeeded in

demonstrating that our XCH-BLYP-UW12 hybrid functional shared some of the desirable properties of the B2-PLYP double-hybrid functional. In Chapter 6, we further develop the UW12 hybrid functional approach, and aim to emulate the success of more modern double-hybrid functionals (such as DSD-BLYP). In recent years the W4-08 atomization energy set [18] has largely replaced the G2-1 atomization energy set, due to its broader range of molecules [130]. In Chapter 6 we use it in preference to the G2-1 set. Geometries and reference values (with zero-point energies removed) are taken from the Mulliken Center website `http://www.chemie.uni-bonn.de/pctc/mulliken-center/software/GMTKN/gmtkn24`.

Recent work suggests that atomization energies are not necessarily indicative of the performance for reaction energies, and so modern benchmarking sets include both reaction energy test sets and atomization energy test sets [52, 19, 131, 7]. The GMTKN30 and GMTKN55 super-sets are today regarded as among the most comprehensive sets for benchmarking general-purpose DFT functionals, including both a range of properties and a range of molecules [52, 7]. The sets also feature highly-accurate reference data from both theory and experiment. These reference data are freely available, and the energetic properties have had their zero-point energies removed to simplify the comparisons. The GMTKN30 and GMTKN55 super-sets are thus are a clear choice for fitting and benchmarking the ground-state properties of new general-purpose functionals.

Our aim is to rapidly prototype new functionals containing the UW12 model. In Chapter 6, we choose two of the sets from GMTKN30 (W4/08 and DBH24/08) and use them to fit the parameters in our hybrid functionals. In this way, we emulate the work of Kozuch *et al.* in fitting their DSD and DOD double-hybrid functionals [34]. Note that Kozuch *et al.* use additional training sets (referred to in Ref [34] as Grubbs, S22, Pd, and MB) in their fitting procedure. A future student may wish to extend the UW12 method (using range-separation and empirical dispersion corrections) so that the UW12 hybrids can accurately model these

sets too.

6. Improving UW12 Hybrid Functionals

6.1. Chapter Aims

In Chapter 5, we suggested a new hybrid (rung-4b) functional XCH-BLYP-UW12 containing the UW12 correlation model. XCH-BLYP-UW12 estimates barrier heights to the same level of accuracy as modern double-hybrid (rung-5) functionals, and estimates atomization energies to the same level of accuracy as the popular hybrid (rung-4) functional B3LYP. XCH-BLYP-UW12 contains a higher fraction ($a_x^{HF} = 0.5$) of exact exchange than B3LYP ($a_x^{HF} = 0.2$). However, modern double-hybrid (rung-5) functionals such as DSD-PBEB95 contain an even higher fraction of exact exchange ($a_x^{HF} \sim 0.75$), which gives them other advantages over conventional global single-hybrids. One such advantage is the reduction of the (de)localization error that is present in DFT functionals. In this chapter, we suggest additional hybrid (rung-4) functionals containing UW12 that give accurate atomization energies, barrier heights, and have minimal (de)localization error (see Section 1.17).

6.2. The rBLYP-osUW12 Functional

Our aim is to construct UW12 functionals that have a high fraction of exact exchange a_x^{HF} (between 0.50 and 0.75) and are still as accurate for atomization energies as popular hybrid

(rung-4) functionals such as B3LYP. We wish to keep the number of adjustable parameters low [13]. We begin by making the fraction of exact exchange a_x^HF into an adjustable parameter. We then relax two of the constraints present in the XCH-BLYP-UW12 functional (see Section 5.2) namely the constraint that $a_\mathrm{c}^\mathrm{LYP} + a_\mathrm{c}^\mathrm{UW12} = 1$, and the constraint that $a_\mathrm{c}^\mathrm{UW12} = \left(a_\mathrm{x}^\mathrm{HF}\right)^2$. Since many developers of double-hybrid functionals [132, 48, 34, 81, 52] have found that one can describe atomization energies accurately using only the opposite-spin component of MP2, in this chapter we only include the opposite-spin ($s = 0$) component of UW12 (see Eqn). We thus define the four-parameter rBLYP-osUW12 functional

$$E_\mathrm{xc}^\mathrm{rBLYP\text{-}osUW12} = \left(1 - a_\mathrm{x}^\mathrm{HF}\right) E_\mathrm{x}^\mathrm{B88} + a_\mathrm{x}^\mathrm{HF} E_\mathrm{x}^\mathrm{HF} + a_\mathrm{c}^\mathrm{LYP} E_\mathrm{c}^\mathrm{LYP} + a_\mathrm{c}^\mathrm{UW12} E_{\mathrm{c}, s=0}^{\mathrm{UW12}(r_\mathrm{c})}. \qquad (6.1)$$

rBLYP-osUW12 resembles the DOD-BLYP double-hybrid functional (defined in Eqn 1.103), but with MP2 correlation replaced with UW12 correlation. The "os" refers to the use of only the opposite-spin ($s = 0$) component of UW12. Note that the functionals introduced in this chapter do not have the unnecessary "XCH" prefix. We used the "XCH" prefix in our first paper [1] to emphasize the similarities between our work and the 1DH-BLYP class of functionals, but have since made the decision to remove it for simplicity. The "r" prefix refers to the fact that the fraction of exact exchange is relaxed (allowed to vary freely). In Section 6.4, we remove the a_x^HF parameter and define the BLYP-osUW12 functional.

6.2.1. Double-counting

Note that allowing $a_\mathrm{c}^\mathrm{LYP} + a_\mathrm{c}^\mathrm{UW12}$ to be greater than unity means that some correlation effects could be counted twice in the final energy expression. In opposite-spin-only functionals (such as rBLYP-osUW12 and DOD-BLYP) this is partly offset by exclusion of the same-spin ($s = 0$) correlation term. The relationship between the same-spin and opposite-spin terms is difficult

to estimate, and would be an interesting avenue for future research. It would also be interesting to investigate which values of a_c^{UW12} and a_c^{LYP} make rBLYP-osUW12 exact for a series of model systems.[1]

6.3. Computational Details

For comparison with double-hybrid functional literature[34, 7], we used quadruple-zeta basis sets for the calculations presented in this chapter. However, note that UW12 hybrid functionals have a faster basis-set convergence than double-hybrid functionals (as shown in Chapter 5), and so a triple-zeta basis may be sufficient. The basis sets used for the various test sets mentioned in the remainder of this chapter were

- aug′-pc3+d [133, 134, 135, 136, 137] for W4/08 (with diffuse functions for non-hydrogen atoms and a high-exponent d function) — Following Ref [34].

- aug′-pc3 for DBH24/08 (with diffuse functions for non-hydrogen atoms) — Following Ref [34].

- Def2-QZVP [138, 124] for SIE4x4 — Following Ref [7].

- aug-cc-pV(Q+d)Z for Δ_{frac} — Following our previous work in Chapter 5.

6.4. Atomization Energies, Barrier Heights, and Reaction Energies

Following the work of Kozuch *et al.* [34], we chose the values of the four parameters (a_x^{HF}, a_c^{LYP}, a_c^{UW12}, r_c) in rBLYP-osUW12 to minimize the sum of the mean-square-errors of two training sets: the W4/08 set of atomization energies, and the DBH24/08 set of reaction barrier heights (see Section 5.4).

The results of the fitting procedure are shown in Table 6.1, along with the RMSEs for the training sets (W4/08 and DBH24/08). We see that the value of $a_x^{HF} = 0.57$ in rBLYP-osUW12 is still not as high as that used in modern double-hybrid functionals such as DSD-BLYP (which has $a_x^{HF} = 0.75$). If we instead fix the value of exact exchange factor to be $a_x^{HF} = 3/4$, and re-optimize the values of the other three parameters, we obtain the BLYP-osUW12 functional.

$$E_{xc}^{\text{BLYP-osUW12}} = \frac{1}{4} E_x^{B88} + \frac{3}{4} E_x^{HF} + a_c^{LYP} E_c^{LYP} + a_c^{UW12} E_{c,s=0}^{UW12,r_c}. \tag{6.2}$$

Note that there is no physical justification for the choice of $a_x^{HF} = 3/4$ in BLYP-osUW12. The value is merely chosen to match various common double-hybrid functionals. xDH-PBE0, XYG3, PBE0-2, XYGJ-OS, DSD-BLYP, DOD-BLYP have a_x^{HF} values of 0.83, 0.80, 0.79, 0.77, 0.75, 0.65 respectively (each value quoted to two significant figures) [139, 57, 122, 81, 34]. However, what is interesting to note is that rBLYP-osUW12 and BLYP-osUW12 both perform as well as B3LYP for atomization energies, despite having widely different values of a_x^{HF}. Thus we have demonstrated that the accuracy of UW12 functionals for the thermochemical properties of simple molecules is not sensitive to the value of a_x^{HF}, provided the other parameters are

---

[1] As we saw in Section 1.12, most conventional hybrid (but not double-hybrid) functionals are constrained such that they give the exact correlation energy for a series of Jellium (uniform electron gas) systems with different densities ρ. [32, 35]

re-optimized: The small amount of added UW12 correlation appears to "cure" some of the spurious effects of the Hartree-Fock exchange that plague conventional global hybrid (rung-4) functionals such as B-HH-LYP [45, 34].[2] A similar phenomenon is noticed with the MP2 term in double-hybrid (rung-5) functionals [34]. The performance for barrier heights of the UW12 functionals is comparable to the performance for the double-hybrids. It will be interesting in the future to investigate which parts of the UW12 and MP2 energy expressions are responsible for the curing of the exchange problems. In the remainder of this chapter, we exploit the new freedom in choosing a_x^{HF} that UW12 brings to reduce the (de)localization error that is present in DFT functionals.

6.4.1. Parameter Optimization Algorithms

The a_x^{HF}, a_c^{LYP}, a_c^{UW12} parameters in rBLYP-osUW12, and the a_c^{LYP}, a_c^{UW12} parameters in BLYP-osUW12 were optimized using a linear least-squares fitting procedure to minimize the mean-square-errors of the W4/08 and DBH24/08 test sets. The objective function Δ_{MSE}^{tot} was defined as the sum of the mean-square-error of the two training sets, such that $\Delta_{MSE}^{tot} = \Delta_{MSE}^{W4/08} + \Delta_{MSE}^{DBH24/08}$. The mean-square-error (MSE) over a test set is defined as

$$\Delta_{MSE} = \frac{\sum_{i=1}^{N} \left(E_i - E_i^{ref} \right)^2}{N} \tag{6.3}$$

where $\{E_i\}$ are the quantities of interest (barrier heights, atomization energies, etc.) and $\{E_i^{ref}\}$ are the reference values. N is the number of reference values in the test set. The root-mean-square-error (RMSE) is then defined as the square-root of the MSE. As we discuss in Section 6.4.3, our method differs from that of many modern authors since we chose not

---

[2]For comparison, the literature quotes the RMSE of B-HH-LYP over the W4/08 set as 23.95 kcal mol^{-1} [52]: far worse than any method in Table 6.1.

to optimize the *orbitals* during the parameter optimization. This decision was made for performance reasons, but has the added advantage that our parameter optimization is guaranteed not to have multiple minima.[3] The r_c parameter is optimized manually, and so may have multiple minima. Hence the error plots are inspected to ensure that the r_c value chosen is indeed the global minimum (see Section 6.4.2). The optimization procedure is thus:

1. For each value of r_c in a series (see Section 6.4.2), optimize a_x^{HF}, a_c^{LYP}, a_c^{UW12} to minimize the RMSE over the test set using a least-squares fitting package.[4]

2. Plot the RMSE for each value of r_c.

3. Choose the global minimum value of r_c.

6.4.2. Choice of Correlation Length Scale Parameter r_c

We now come to the choice of geminal length scale r_c that is present in the UW12 energy expression. In our previous work (see Chapter 5) we found that the value of r_c that led to the most accurate description of atomization energies was $r_c = 1.7\, a_0$, which is similar to the value of $1.0\, a_0$ used in F12 methods [140]. Now that we have made a_c^{UW12} into an adjustable parameter in its own right, we are free to experiment with a range of length scales r_c.[5] Tew and Klopper demonstrated excellent accuracy for the energy of the Helium atom when using the Hyleraas method and a geminal of the form of Eqn 2.34, and with a value of r_c of any value larger than $0.5\, a_0$ [105]. We chose to test r_c values in the range $a_0 \leq r_c \leq 4a_0$. From Fig 6.1 we see that the optimum r_c for the W4/08 set is around $3.0\, a_0$, whereas for the G2RC set it is

---

[3]The a_x^{HF}, a_c^{LYP}, a_c^{UW12} minimization is guaranteed to have a single minimum since the objective function Δ_{MSE} is quadratic in a_x^{HF}, a_c^{LYP}, a_c^{UW12}. The square-root of Δ_{MSE} can thus be viewed as a Frobenius norm.

[4]The `statsmodels` python package was used for this. See the `tools/DOUfunctionals.py` file in the `unsoldpaper` repository.

[5]In XCH-BLYP-UW12, the length scale parameter r_c affected both the length-scale of the correlation hole and also its depth, due to prefactor of r_c in the definition of the geminal function $w(r_{12})$ (Eqn 2.34). Here the depth and width of the hole are determined by separate adjustable parameters (a_c^{UW12} and r_c respectively).

around 1.7 a_0 (as in our previous work in Chapter 5 on page 117). Atomization energies in the W4/08 set thus need a larger UW12 correlation hole correction in order to cure the errors that arise from using a large fraction of Hartree-Fock exchange. We speculate that the larger value of r_c that is needed for the W4/08 set is due to the more diverse range of molecules in this set than in the AE6 and G2 sets. The DBH24/08 set has a minimum at an even higher value of r_c, which may reflect correlation effects in the more diffuse transition states. The SIE4x4 set has an excellent RMSE for all the values of r_c tested (see discussion in Section 6.5).

Note that although F12 methods seem to be relatively insensitive to the choice of geminal $f(r_{12})$ [105, 95], there is no similar guarantee for the UW12 geminal $w(r_{12})$, since $w(r_{12})$ and $f(r_{12})$ have different purposes: The F12 geminal $f(r_{12})$ is there to approximate the parts of the correlation hole that are outside the atomic orbital basis $\{\alpha\}$ (see Section 2.2.2), whereas the UW12 geminal $w(r_{12})$ in UW12 hybrids is there to approximate the parts of the correlation hole that are not represented by the semi-local DFT functional. For this reason, it will be interesting in the future to try different forms of the geminal $w(r_{12})$.

It is disappointing that the UW12 hybrid results presented in Table 6.1 for reaction eneriges in the G2RC set are *less* accurate than for the conventional rung-4 hybrids (although of course it is important to remember that B3LYP was parameterized using the molecules in this set). Since the submission of the first draft of this thesis, it has been found that using the frozen-core approximation with UW12 (see Section 3.4) fixes this problem.

6.4.3. Including Orbital Optimization in the Parameterization Procedure

In the same way as for the XCH-BLYP-UW12 functional, the orbitals in a BLYP-osUW12 calculation are optimized fully-self-consistently. However, for fitting the parameters in Ta-

ble 6.1, each ingredient in the energy expression was evaluated using frozen B3LYP orbitals.[6] This simplifies the fitting procedure, but has the disadvantage that the resulting functional will not predict molecular energies as accurately as if the parameters were adjusted in conjunction with the orbital-optimization. In fact, as we see from the lower half of Table 6.1 (the rows labeled "fsc"), re-optimizing the BLYP-osUW12 orbitals after the fitting actually leads to considerably worse performance for the G2RC test set. We see from Table 6.1 that the performance of BLYP-osUW12 for barrier heights is improved upon orbital-optimization, lending further support to the hypothesis that part of the error in barrier-heights is density-driven (see Section 1.15) [63].

In the future, we hope to include orbital-optimization in the parametrization step, as is standard procedure for many double-hybrid functionals [33, 34, 48].[7] Including full orbital optimization in the parameterization step will first require an improvement to the efficiency of the UW12 code, as the prefactor is currently too large to perform a single-point energy calculation including the non-local UW12 correlation term at each point in the parameter space. Double-hybrid functionals avoid this performance bottleneck by simply omitting the non-local MP2 correlation term during the orbital optimization step [34]. This is also an option in the case of UW12, leading to the procedure

1. Fix the value of a_c^{LYP} and optimize the orbitals, omitting the UW12 term

2. Optimize the values of a_c^{LYP}, a_c^{UW12}, r_c with frozen orbitals to minimize Δ_{MSE}^{tot}

3. Return to step 1 with the new value a_c^{LYP}.

4. Repeat until convergence reached.

5. Use the resulting values of the parameters to run a fully-self-consistent UW12 calculation.

---

[6]Note that the orbitals used in the fitting were B3LYP3 orbitals rather than B3LYP5 orbitals (see footnote 6 on page 28).

[7]Although it should be noted that the non-local MP2 correlation term is omitted during the orbital-optimization in most double-hybrids.

Note that there is no guarantee that the above procedure will converge, or will produce lower UW12 energies than using the frozen orbitals.

Table 6.1.: Performance of various hybrid functionals discussed in this chapter. The upper part of the table shows the values of the adjustable parameters. The lower part of the table shows RMSE values (in kcal mol^{-1}) for various test sets. Frozen B3LYP3 (see Footnote 6 on page 28) orbitals were used for all calculations, except for those denoted with "(fsc)" meaning fully-self-consistent. For comparison, literature[34, 7] RMSE values for the rung-5 DSD-BLYP double-hybrid functional (without the empirical dispersion term) are 3.27, 1.41, and 6.97 kcal mol^{-1} for the W4/08, DBH24/08, and SIE4x4 sets respectively. RMSE values in each row are colored from green (smallest RMSE in the row) through red (largest RMSE in the row). The four adjustable parameters in rBLYP-osUW12, and the three adjustable parameters in BLYP-osUW12 were chosen to minimize the sum of the mean-square-errors of the DBH24/08 and W4/08 sets.

	BLYP	PBE0	B3LYP5	rBLYP-osUW12	BLYP-osUW12	PBE-osUW12
$a_{\mathrm{x}}^{\mathrm{HF}}$	0.0	0.25	0.2	0.57	0.75	0.75
$a_{\mathrm{x}}^{\mathrm{S}}$						
$a_{\mathrm{x}}^{\mathrm{B88}}$	1.0		0.72	0.43	0.25	
$a_{\mathrm{x}}^{\mathrm{PBE}}$		0.75				0.25
$a_{\mathrm{c}}^{\mathrm{VWN}}$			0.19			
$a_{\mathrm{c}}^{\mathrm{LYP}}$	1.0		0.81	0.44	0.17	
$a_{\mathrm{c}}^{\mathrm{PBE}}$		1.0				0.16
$a_{\mathrm{c}}^{\mathrm{UW12},s=0}$				0.4	0.58	0.57
r_{c}				3.0	3.0	3.0
W4/08	10.0	5.29	5.86	4.48	5.36	5.64
DBH24/08	8.72	4.49	4.92	1.65	1.52	1.74
DBH24/08(fsc)	8.91	4.55	4.92	1.73	1.36	1.59
G2RC	8.03	8.01	3.86	5.34	8.44	8.88
SIE4x4	27.9	15.9	20.3	8.26	2.45	1.99
$\sqrt{\Delta_{\mathrm{frac}}(5,7)/2}$	20.0	13.8	15.1	6.28	2.23	2.21
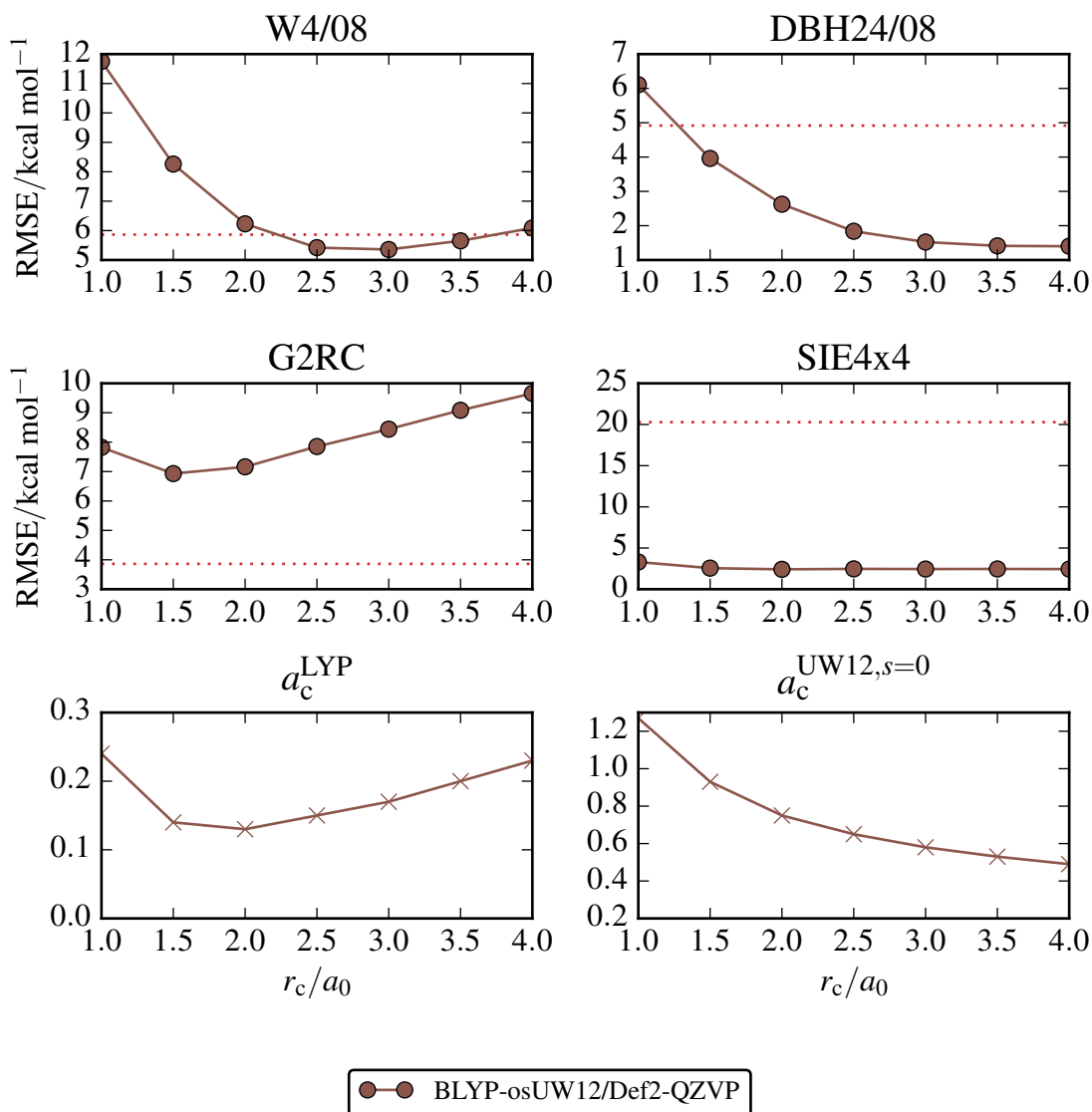
Figure 6.1.: Effect of changing the correlation length scale parameter r_c on the RMSE of various test sets. The upper two sets (W4/08 and DBH24/08) were used to optimize the a_c^{LYP} and a_c^{UW12} parameters. The dotted horizontal line shows the RMSE for B3LYP5 (see Footnote 6 on page 28). Frozen B3LYP3 orbitals were used for all calculations (as opposed to performing fully-self-consistent calculations) in order to reduce computation time. Note that the RMSE for the SIE4x4 set when using BLYP-osUW12 is far below all other DFT methods (see Table 6.1 on the preceding page) for all the values of r_c tested. The lower two panels show the values of the parameters a_c^{LYP} and a_c^{UW12} that were chosen for each r_c value.

6.5. Symmetric Radical Dimers

Let us now turn our attention to the dissociation curves of symmetric dimers with odd numbers of electrons. In these systems, the (de)localization errors present in DFT (see Section 1.17) can be seen clearly [130, 52, 7]. Figs 6.2 and 6.3 show the dissociation curves for four simple dimers. The 16 data points (4 per system) in each figure make up the SIE4x4 test set [7] (see Table 6.1).[8]

We see immediately from Fig 6.2 that B3LYP systematically over-binds molecular cation dimers with many electrons, and that pure Hartree-Fock theory systematically under-binds.[9] We see that the fraction of exact exchange $a_{\mathrm{x}}^{\mathrm{HF}} = 0.75$ in BLYP-osUW12 almost exactly cancels this error for the case of the NH3 and H2O cation dimers, which demonstrates why double-hybrids such as DSD-BLYP and XYG3 are so successful for treating a wide range of problems [13, 7].

Fig 6.3 shows that BLYP-osUW12 even outperforms double-hybrid (rung-5) functionals. The success of BLYP-osUW12 for the SIE4x4 set is quite astonishing. In addition, Fig 6.1 shows that this success is not dependent on the UW12 length scale parameter r_{c} (provided the hybrid parameters are re-optimized for each r_{c}), suggesting that the only purpose of the UW12 model is to "cure" a spurious side-effect of the high exact-exchange fraction $a_{\mathrm{x}}^{\mathrm{HF}}$.

---

[8]Geometries and W2-F12 reference values (with zero-point energies removed) are taken from the Mulliken Center website `http://www.chemie.uni-bonn.de/pctc/mulliken-center/software/GMTKN/gmtkn55`.

[9]Note that HF is exact for the one-electron system $H \ldots H^+$. As discussed in Section 1.17, B3LYP and LDA under-estimate the energy of the state $H^{0.5+} \ldots H^{0.5+}$ relative to $H \ldots H^+$ by 45 kcal mol^{-1} and 60 kcal mol^{-1} respectively. For HF, these two states are equal in energy.
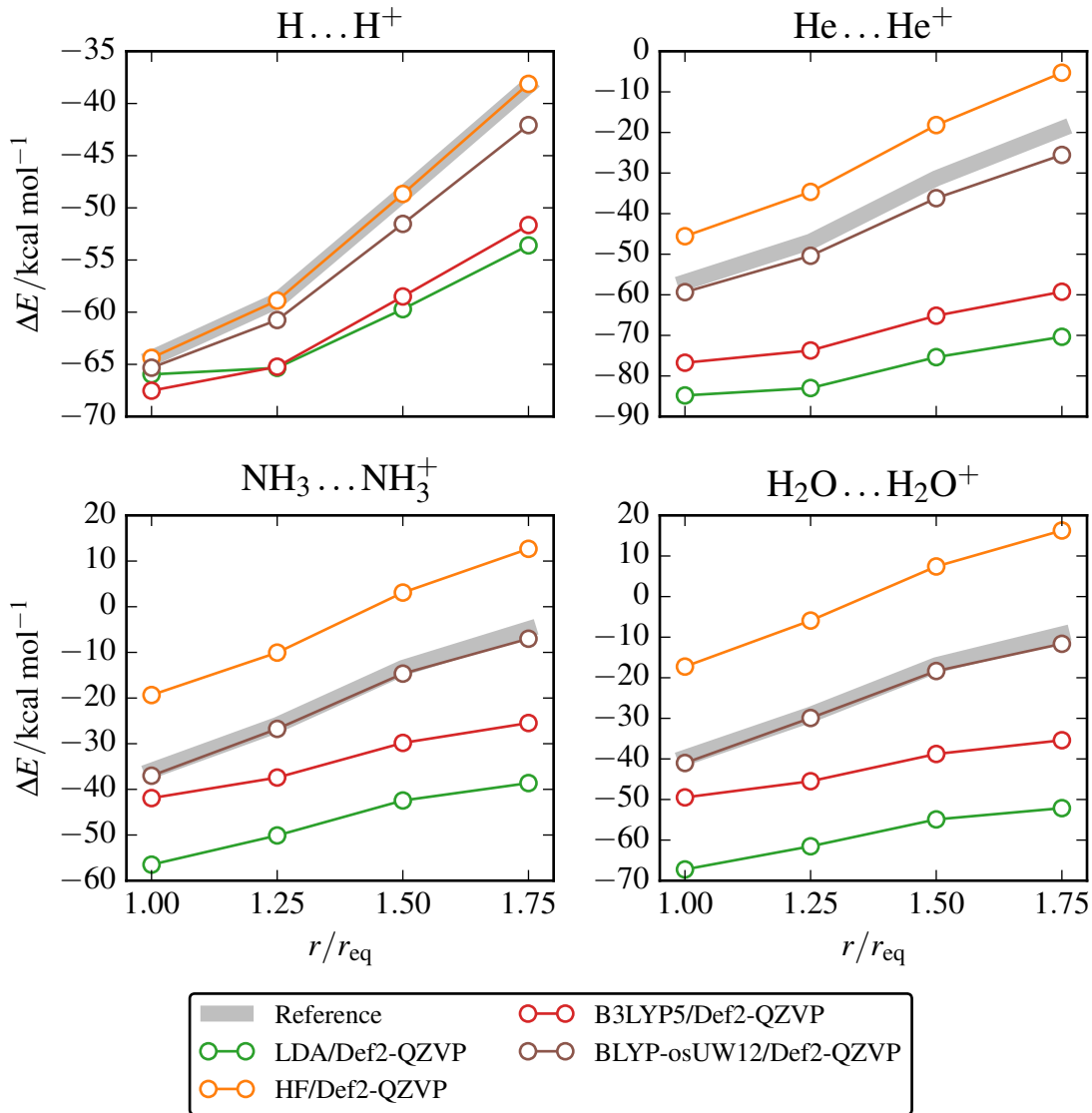
Figure 6.2.: The energy of various molecular cation dimers relative to the dissociated monomers, for rung-2 and rung-4 DFT methods (see Fig 1.1). The equilibrium bond length for each dimer is r_{eq}. All calculations were performed fully-self-consistently. Note that HF is exact for the one-electron system $H\ldots H^+$.
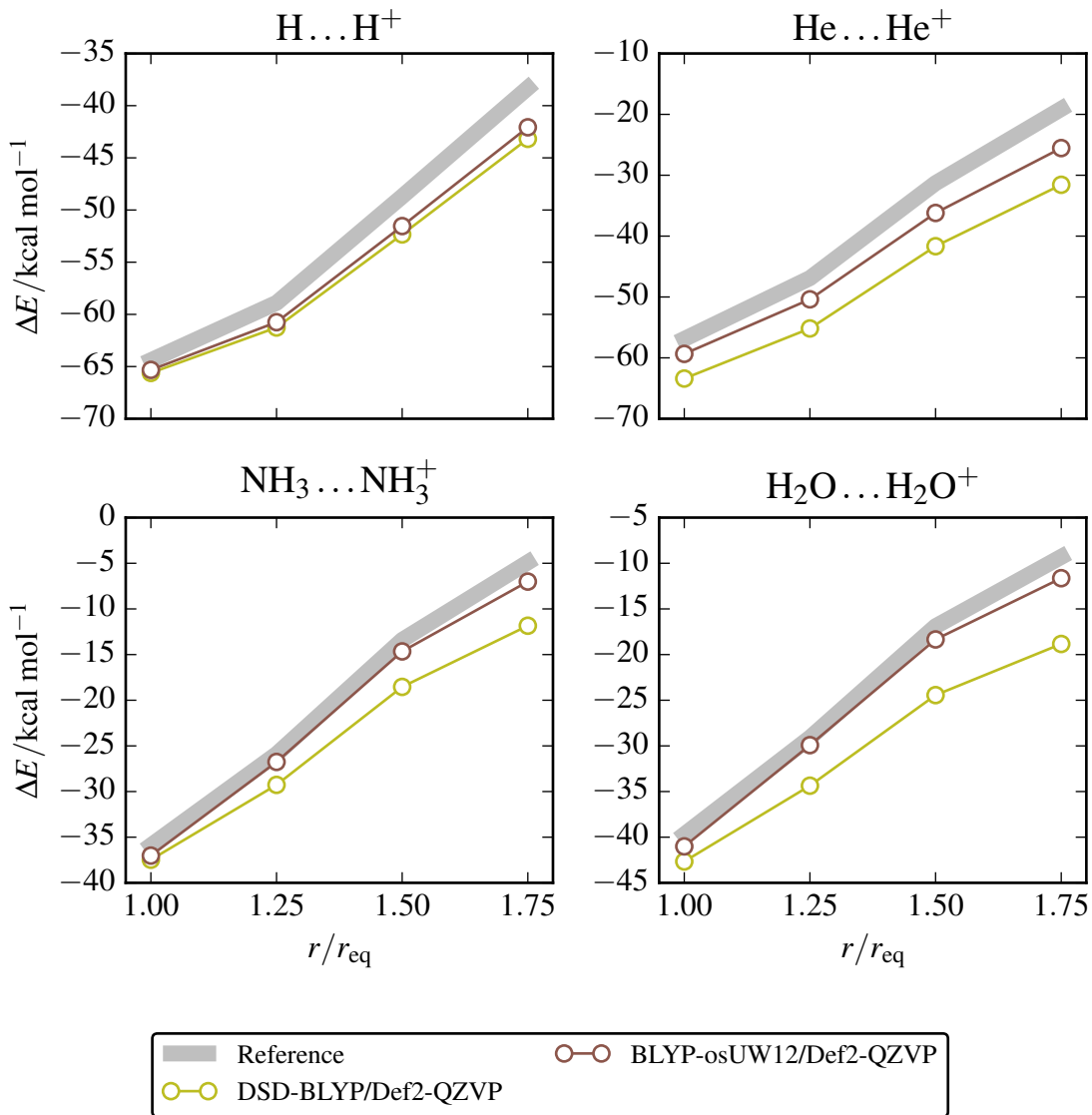
Figure 6.3.: The energy of various molecular cation dimers relative to the dissociated monomers, for rung-4b and rung-5 DFT methods (see Fig 1.1). The equilibrium bond length for each dimer is r_{eq}. The DSD-BLYP results are taken from the supporting information of Ref [7]. The BLYP-osUW12 calculations were performed fully-self-consistently, although Table 6.1 shows that the effect of self-consistent optimization on the SIE4x4 set is negligible (as shown in the literature for the similar SIE11 set [130, 52, 63]). Note that the y-axis scale is different from that in Fig 6.2.

6.6. Non-Integer Number of Electrons

We can quantify the (de)localization error even more simply by considering systems with non-integer numbers of electrons (see Section 1.18). In Figs. 6.4 and 6.5, we plot the energies of atomic ions with non-integer charge. The value of the spin $2S = \left[N_{\mathrm{el},\uparrow} - N_{\mathrm{el},\downarrow} \right]$ for each ion with an integer number of electrons N_{el} was chosen to match the ground-state spin of a neutral atom with N_{el} electrons. The value of $2S$ for ions with non integer charge was chosen as a linear interpolation between ions with integer charge. For the systems studied in this chapter, this is equivalent to allowing only the highest occupied spin-orbital to be fractionally occupied (as prescribed by Janak's theorem [141, 58]). Spherical symmetry of the orbitals was not imposed, and thus the highest occupied spin-orbital was never degenerate with any other orbital. In the lower right-hand panel of Fig 6.4 we can clearly see the deviation from linearity for $C^{0.5+}$ for HF and LDA.

It is well understood that the (de)localization error for the $H^{0.5+}$ ion is density-driven, whereas for $H^{0.5-}$, $C^{0.5+}$, and $C^{0.5-}$ the error is energy-driven [71, 13]. For $C^{0.5+}$, XCH-BLYP-UW12 and rBLYP-osUW12 show deviations from linearity Δ_{lin} (5.5) (defined in Eqn 1.120) of -14 kcal mol^{-1} and -11 kcal mol^{-1} respectively (see Fig 6.5). These values are similar to the value for B2-PLYP quoted in the literature (-14 kcal mol^{-1})[58]. BLYP-osUW12 has a deviation from linearity of -4.6 kcal mol^{-1}, which is similar to the value for XYG3 quoted in the literature (-3.5 kcal mol^{-1}) [58]. The smaller deviation from linearity for BLYP-osUW12 and XYG3 can be attributed to the higher fractions of exact exchange they contain. Thus we have demonstrated that UW12 functionals can be constructed which show the same integer discontinuity behavior as double-hybrid (rung-5) functionals, but which only depend on occupied Kohn-Sham orbitals.

6.6.1. Mean Deviation from Linearity

We can now be more quantitative in our analysis of the deviation from linearity. Values of the mean deviation from linearity $\sqrt{\Delta_{\text{frac}}(5,7)}$ (defined in Eqn 1.121) are shown in Table 6.1. Again, the BLYP-osUW12 functional is the closest to linearity (2.40 kcal mol^{-1}) of all the rung-4 hybrids in Table 6.1, and is thus the functional with the smallest (de)localization error. The four-parameter range-corrected MCY3 functional is a competitor of BLYP-osUW12, with a value for $\sqrt{\Delta_{\text{frac}}(5,7)}$ of 1.98 kcal mol^{-1} according to Ref [78].[10] It will be interesting to compare these two functionals in the future.

---

[10]Note that there is a typographical error in the caption of Table I of Ref [78]: The Δ_{frac} values are in fact given in units of 0.0001 E_h^2 (not 1000 E_h^2 as is erroneously stated). Note also that the authors of Ref [78] use a smaller basis-set for their calculations on the Carbon atom.
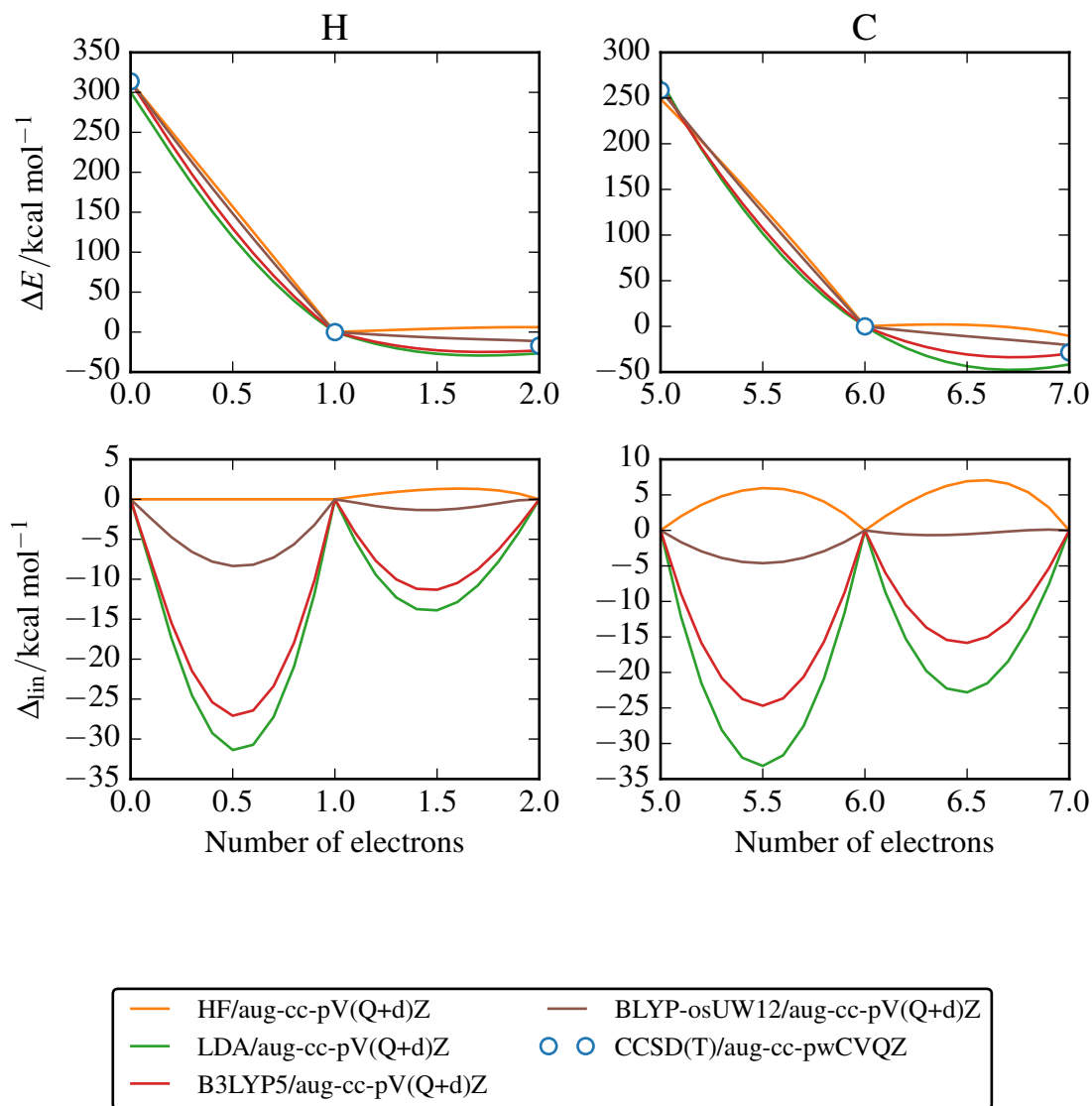
Figure 6.4.: The energies of atoms with non-integer electron number when evaluated with rung-2 and rung-4a methods (see Fig 1.1) and for CCSD(T). In the upper panel we plot the difference between the energy of the ion and the energy of the neutral atom. In the lower panel, we plot the deviation from linearity $\Delta_{\text{lin}}(N_{\text{el}})$. All results are self-consistent. Note that the CCSD(T) results are plotted only for integer numbers of electrons, and are not shown in the lower panel. Note that HF is exact for $N_{\text{el}} \leq 1$.
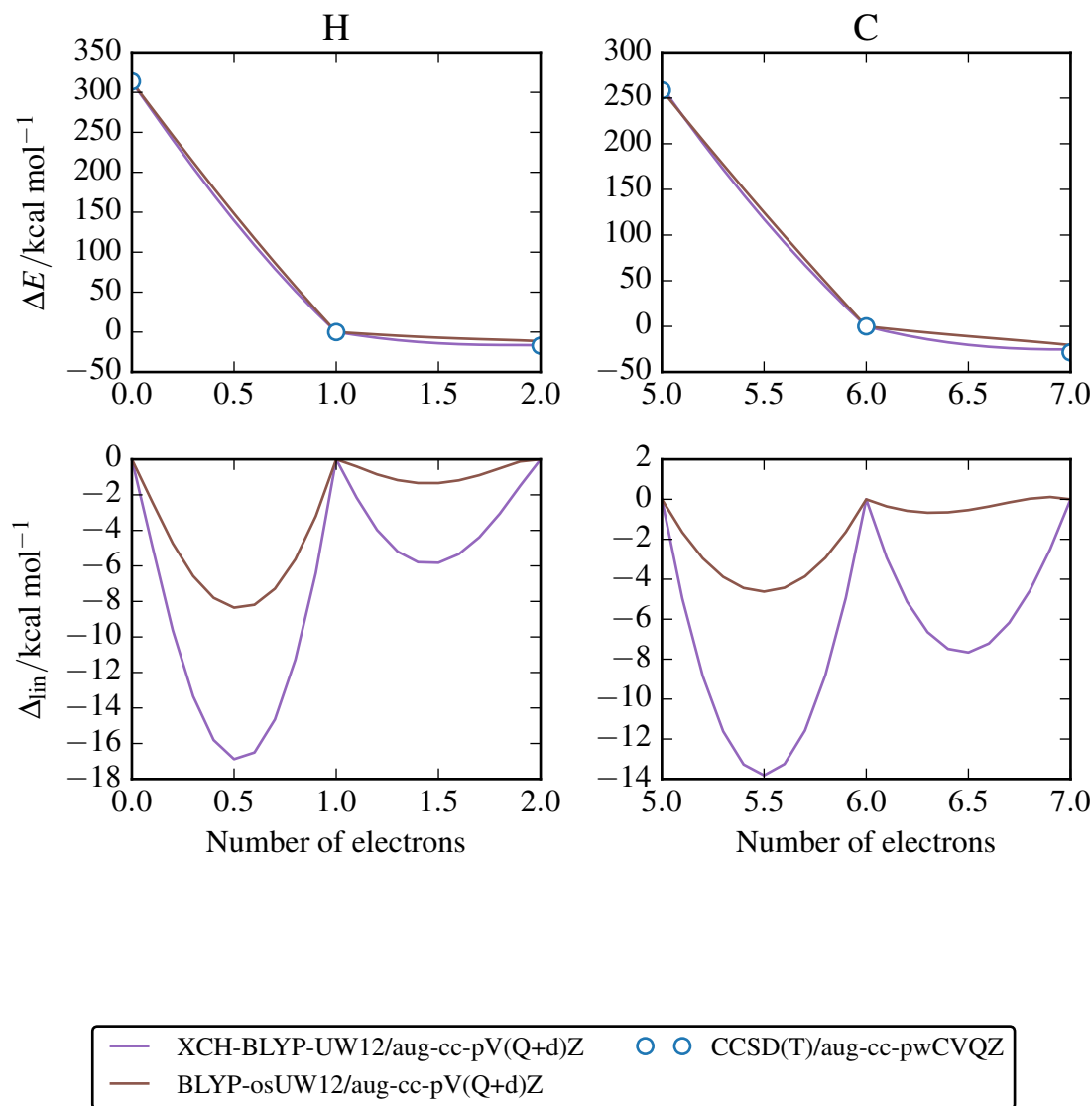
Figure 6.5.: The energies of atoms with non-integer electron number when evaluated with rung-4b methods (see Fig 1.1) and for CCSD(T). In the upper panel we plot the difference between the energy of the ion and the energy of the neutral atom. In the lower panel, we plot the deviation from linearity $\Delta_{lin}(N_{el})$. All results are self-consistent. Note that the CCSD(T) results are plotted only for integer numbers of electrons, and are not shown in the lower panel. Note that the y-axis scale in the lower panel is different from that in Fig 6.4.

6.7. Non-Integer Spin

As a final remark, we note that the high fraction of exact-exchange a_x^{HF} present in double-hybrid functionals is not always advantageous. For instance, double-hybrid functionals have been shown to perform *worse* than those lower down the ladder at problems with a large amount of static correlation, such as predicting the spin-states of transition-metal complexes [142, 7], and dissociating small molecules with high symmetry such as H_2 [11]. It is unlikely that these problems can be remedied by adding in UW12 correlation, which is designed to model short-range (dynamical) correlation. Hence we do not investigate them here. However, we comment that removal of the non-integer spin errors — in addition to the removal of the non-integer charge errors — will be crucial for the accurate DFT functionals of the future [11, 9, 80, 12, 143].

6.8. Chapter Summary

In this chapter, we proposed two new hybrid functionals rBLYP-osUW12 and BLYP-osUW12. These functional have widely different fractions of exact exchange, yet both have similar performance to B3LYP over a modern test set of atomization energies. The functionals reduce the (de)localization error present in the DFT description of molecular cation dimers, and show integer discontinuities for isolated atoms with non-integer charge. The result for BLYP-osUW12 is surprising given that this functional contains no explicit unoccupied orbital information, and only has three adjustable parameters.[11] In the In the future, it may be interesting to apply these new functionals to bond-dissociation of more radical systems. Once

---

[11]In these respects, BLYP-osUW12 is similar to the MCY3 hybrid (rung-4a) functional [78]. MCY3 is a range-separated hybrid functional explicitly constructed in order to satisfy the linearity condition (Eqn 1.118) for the Carbon atom. In the future, it will be interesting to compare the results of MCY3 with BLYP-osUW12. It is known, for instance, that the performance of MCY3 for band gaps degrades as the system size increases [144].

support for periodic boundary conditions is implemented, it will also be possible to analyse the performance of the new functionals for band-gap prediction in solids.

In the next chapter, we summarize the results of this thesis, and make some comments about the future of the field.

7. Conclusions

7.1. Summary

In this thesis, we proposed a new ingredient (known as UW12) for inclusion in hybrid DFT functionals. This ingredient does not fit into any of the categories of ingredients that are currently used in hybrid functionals, and we are thus required to extend the "Jacob's ladder" of functionals in a sideways direction ("rung-4b", see Fig 1.1). UW12 is wavefunction-like in nature, but is an explicit functional of the 1-RDM $\rho(\mathbf{x}|\mathbf{x}')$. UW12 has several advantages over the E_c^{PT2} term used in double hybrids: it has more rapid basis-set convergence, and it can be included fully in the self-consistent optimization. As a result, the gradient theory with respect to nuclear motions — though not developed in this thesis — is straightfoward. These advantages mean that UW12 hybrids may soon surpass double-hybrids in terms of their applicability, performance, and computational efficiency.

We demonstrated that the formal scaling for evaluating the UW12 energy is N^4, where N represents the size of the system.[1] This is equivalent to the formal scaling of density-fitted Hartree-Fock exchange — a component of B3LYP. In addition, we showed that it is possible to compute the UW12 energy and Fock matrix efficiently using machinery (molecular geminal

---

[1] As discussed in Section 3.1.2, achieving N^4 scaling requires that the same-spin $E_{c,s=1}^{UW12}$ component be evaluated using the algorithm presented in Appendix A.2.

integrals and quadrature grids) that is already present in most electronic structure codes. It was thus trivial to implement full self-consistent optimization for UW12 functionals, whereas for double-hybrid functionals this process is far more involved.

We suggested three new UW12 functionals: XCH-BLYP-UW12, rBLYP-osUW12, and BLYP-osUW12. These new functionals estimate reaction barrier-heights with a similar level of accuracy as modern double-hybrid (rung-5) functionals, and have an accuracy similar to that of the existing hybrid (rung-4) functional B3LYP for atomization energies. The three functionals contain fractions of exact exchange between 0.50 and 0.75, and all three reduce (to varying degrees) the (de)localization error present in DFT. Thus they reproduce many of the desirable qualities of double-hybrid functionals, but with a much faster basis-set convergence. The close match between the performance of UW12 functionals and double-hybrid functionals came as something of a suprise, since it has long been supposed that the success of double-hybrid functionals is due to the explicit inclusion of unoccupied orbital information.

7.2. Future Work

The UW12 hybrid functionals presented in this thesis are very much proof-of-concept in nature. To begin with, they are parameterized on a smaller set of molecules than are most modern hybrid and double-hybrid functionals (see Section 6.4). They do not yet make use of the frozen-core approximation; although this work has been started (see Section 3.4) and has been found to improve reaction energy results. Future work would be to re-parameterize the models using more representative benchmark sets, such as those in the GMTKN55 superset [7]. Including self-consistency in the parametrization step would improve the performance across the board.

A further enhancement to the UW12 hybrids would be to replace the exchange energy

$$E_x = a_x^{HF} E_x^{HF} + \left(1 - a_x^{HF}\right) E_x^{DFT} \tag{7.1}$$

with a range-corrected exchange model. This has proved successful for double-hybrid functionals in the past [145, 48], and seems all-the-more natural when using UW12 (which already contains an intrinsic length scale parameter r_c).

We have remarked that the gradient theory with respect to nuclear motions has not yet been implemented for UW12; But that such a gradient theory is a good deal more straightforward than corresponding gradient theories for conventional double-hybrid functionals. Gradient theories for conventional double-hybrid functionals require the definition of a special Lagrangian to optimize the density ρ and density-matrix $\mathbf{D}$ [146], whereas these quantities are already optimized in self-consistent UW12 theory. Neese *et al.* have demonstrated that molecular geometries when using B2-PLYP are more accurate than MP2 and DFT geometries [146], and it will be interesting in the future to see if UW12 hybrids provide the same benefits but with significantly simpler working equations.

It has long been observed that hybrid (rung-4a) functionals containing only semi-local correlation perform poorly for many classes of non-covalent interactions between molecules (even when an empirical dispersion correction term is added). This is true even of the most recent rung-4a functionals [8]. This is yet another motivating factor for adding non-local correlation terms to the energy expression. It will be interesting in the future to apply UW12 hybrids to non-covalently-bound dimers such as the argon-atom dimer [48] and to molecular dimer test sets such as S22 [147]. Since it is common to add an empirical dispersion term to both hybrid and double-hybrid functionals, there is no reason to suggest that such a term should not be added to UW12 hybrids as well [148, 149, 34, 52, 7]. Historically, such empirical dispersion

corrections were only added when estimating properties dominated by van-der-Waals dispersion. However, recent work suggests that other properties (such as atomization energies) can benefit from empirical dispersion correction as well [52, 7]. We suspect that including an empirical dispersion term would improve the atomization energy results given in Section 6.4.

In addition to adjusting the hybrid functional parameters, one could also consider modifying the UW12 correlation model itself. Our chosen model for the geminal $w^s(r_{12})$ in Eqn 2.34 was somewhat arbitrary, and based on the literature for F12 methods. In the future, we hope to try other choices of geminal from the literature (such as those suggested by Grüneis [101]). Alternatively, one could fit $w^s(r_{12})$ to reproduce the exact correlation energy for a model system: for instance, jellium (the uniform electron gas), hookium (two electrons inside a harmonic potential well), 3-spherium (two electrons confined to the surface of a sphere in four dimensions [150]), or the Helium iso-electronic series.

One could also experiment with different length scales r_c for the same-spin (s=1) and opposite-spin (s=0) components of the UW12 energy. The different coalescence cusp conditions (see Eqn 2.35) for same-spin and opposite-spin electron pairs provide a physical motivation for such a formulation [151, 152, 153]. However, since our most accurate hybrid functionals in Chapter 6 do not include any same-spin correlation at all, we do not forsee any major improvement in the accuracy of UW12 functionals resulting from including same-spin UW12 correlation.

Terms which model single-electron-excitations (see Chapter B) could also be added to the theory. However, since most rung-5 double-hybrid functionals do not include such terms, it is difficult to motivate such an approach.

We conclude from this work that wavefunction-like hybrid functionals are worth further investigation. Their performance for many systems that have been a stumbling block for conventional DFT functionals (such as barrier heights and self-interaction-error-dominated systems) is re-

markable, considering that the new functionals do not contain any information about the unoccupied Kohn-Sham orbitals (and hence are still technically rung-4 functionals). Although they are still in the early stages of their development, it is conceivable that they will one day outperform double-hybrid (rung-5) functionals in terms of accuracy (due to orbital optimization), and in terms of computational cost (since smaller basis sets can be used). They represent another exciting step forward in the range of ingredients available to the developers of electronic structure methods, and may soon be put to use in all areas of chemistry.

Appendix

A. Further Algorithms for Evaluating the UW12 Fock Matrix

A.1. Evaluating the Two-Electron Term on a Grid

In some electronic structure programs, the modified electron-repulsion integrals mentioned in Section 4.3 are not available, and the algorithm proposed in Section 3.2.1 is therefore not possible. Instead, one may evaluate the two-electron term using a quadrature grid method similar to that used for the three-electron term in Section 3.2.2. We can express the two-electron $w(r_{12})r_{12}^{-1}$ integrals on a grid as

$$\langle ij|w_{12}r_{12}^{-1}|kl\rangle = \sum_{\lambda} g_{\lambda} \phi_j^{\star}(\mathbf{r}_{\lambda})\phi_l(\mathbf{r}_{\lambda})s_{jl} \, (\mathbf{r}_{\lambda}|w_{12}^{s_{ij}}r_{12}^{-1}|ik) \, . \tag{A.1}$$

The expressions for the two-electron UW12 derivatives are thus

$$\frac{\partial E_{\text{c,2el,+}}^{UW12}}{\partial D_{\alpha\beta}^{\sigma}} = \sum_{j}\langle \alpha j|w_{12}r_{12}^{-1}|\beta j\rangle \tag{A.2}$$

$$= \sum_{\lambda} g_{\lambda} \, \alpha^{\star}(\mathbf{r}_{\lambda}) \sum_{j}(\mathbf{r}_{\lambda}|w_{12}^{\delta_{\sigma_j\sigma}}r_{12}^{-1}|jj)\beta(\mathbf{r}_{\lambda}) \tag{A.3}$$

and

$$\frac{\partial E_{\text{c,2el,-}}^{UW12}}{\partial D_{\alpha\beta}^{\sigma}} = -\sum_{j} \delta_{\sigma_j \sigma} \langle j\alpha | w_{12} r_{12}^{-1} | \beta j \rangle \tag{A.4}$$

$$= -\sum_{\lambda} g_{\lambda} \, \alpha^{\star}(\mathbf{r}_{\lambda}) \sum_{j} \delta_{\sigma_j \sigma} \phi_j^{\star}(\mathbf{r}_{\lambda})(\mathbf{r}_{\lambda} | w_{12}^{1} r_{12}^{-1} | \beta j) \tag{A.5}$$

and we observe that the computational scaling of evaluating $\partial E_{\text{c,2el}}^{UW12}/\partial D_{\alpha\beta}^{\sigma}$ will be[1]

$$N_{\text{grid}} N_{\text{AO}}^{2} \propto N^{3}. \tag{A.6}$$

A.2. Evaluating the Four-Electron Term on a Grid

In this section, we use density-fitting (for the $\langle kl | r_{12}^{-1} | ij \rangle$ integral) and a quadrature grid (for the $\langle ij | w_{12} | kl \rangle$ integral) to evaluate $\partial E_{\text{c,4el}}^{UW12}/\partial D_{\alpha\beta}^{\sigma}$ in a computational time that scales formally as N^4 where N is the size of the system. We obtain the expressions

$$\frac{\partial E_{\text{c,4el,+}}^{UW12}}{\partial D_{\alpha\beta}^{\sigma}} = 2 \sum_{jkl} \langle \alpha j | w_{12} | kl \rangle \langle kl | r_{12}^{-1} | \beta j \rangle \tag{A.7}$$

$$= 2 \sum_{\lambda} g_{\lambda} \, \alpha^{\star}(\mathbf{r}_{\lambda}) \sum_{C} \left[\sum_{jl} (\mathbf{r}_{\lambda} | w_{12}^{\delta_{\sigma_j \sigma}} | jl)(\tilde{C} | r_{12}^{-1} | lj) \right]$$

$$\times \left[\sum_{k} \delta_{\sigma_k \sigma} \phi_k(\mathbf{r}_{\lambda})(k\beta | r_{12}^{-1} | C) \right] \tag{A.8}$$

---

[1]In estimating the slowest step of the calculation, we assume that $N_{\text{grid}} > N_{\text{AO}} > N_{\text{el}}$.

and

$$\frac{\partial E_{\text{c,4el,-}}^{UW12}}{\partial D_{\alpha\beta}^{\sigma}} = -2\sum_{jkl}\delta_{\sigma_j\sigma}\langle\alpha j|w_{12}|kl\rangle\langle lk|r_{12}^{-1}|\beta j\rangle \tag{A.9}$$

$$= -2\sum_{\lambda}g_{\lambda}\,\alpha^{\star}(\mathbf{r}_{\lambda})\sum_{Cl}(l\beta|r_{12}^{-1}|C)$$

$$\sum_{j}(\mathbf{r}_{\lambda}|w_{12}^{1}|jl)\sum_{k}\delta_{\sigma_k\sigma}\phi_k(\mathbf{r}_{\lambda})(\tilde{C}|r_{12}^{-1}|kj) \tag{A.10}$$

and we observe that the computational scaling of evaluating $\partial E_{\text{c,4el}}^{UW12}/\partial D_{\alpha\beta}^{\sigma}$ will be[2]

$$N_{\text{AO}}\,N_{\text{DF}}\,N_{\text{grid}}\,N_{\text{el}} \propto N^4. \tag{A.11}$$

To see this, consider the number of terms in the summation over C and l in Eqn A.10.

It is thus possible to evaluate all the terms in the UW12 energy expression using quadrature grids in a computation time that scales as N^4. As a final remark, we note that one may use standard screening, molecular-orbital localization, and exploiting the short-range nature of the geminal function $w(r_{12})$ to reduce the scaling further (see Section 3.5).

---

[2]In estimating the slowest step of the calculation, we assume that $N_{\text{grid}} > N_{\text{DF}} > N_{\text{AO}} > N_{\text{el}}$.

B. Contributions from Singly-Excited Determinants to the UW12 Energy

If contributions from singly-excited determinants are included, the Unsöld-W12 energy can be written as[1]

$$E_c^{\text{UW12(+singles)}} = \langle 0 | V (1 - |0\rangle \langle 0|) W | 0 \rangle \tag{B.1}$$

where V and W are defined as

$$V = \frac{1}{2} \sum_{pqrs} \langle pq | r_{12}^{-1} | rs \rangle \, a_p^\dagger a_q^\dagger a_s a_r$$

$$W = \frac{1}{2} \sum_{pqrs} \langle pq | w(r_{12}) | rs \rangle \, a_p^\dagger a_q^\dagger a_s a_r \; .$$

Following the derivation of Section 1.13, Eqn B.1 can be written as

$$E_c^{\text{UW12(+singles)}} = E_c^{\text{UW12}} + \sum_{ijka} \left\langle ij \left| w_{12} \right| \overline{aj} \right\rangle \left\langle \overline{ak} \left| r_{12}^{-1} \right| ik \right\rangle \tag{B.2}$$

---

[1] We assume here for simplicity that the singles excitation amplitudes use the same geminal function $w(r_{12})$ as the double excitations. Note that this need not be the case.

where E_c^{UW12} is the Unsöld-W12 energy including contributions from only doubly-excited determinants (defined in Eqn 2.4). Now recognize that

$$\sum_a \left|\overline{aj}\right\rangle\left\langle\overline{ak}\right| = \sum_p \left|\overline{pj}\right\rangle\left\langle\overline{pk}\right| - \sum_l \left|\overline{lj}\right\rangle\left\langle\overline{lk}\right|. \tag{B.3}$$

Substituting Eqn B.3 into Eqn B.2, we obtain

$$\begin{aligned}
E_c^{\text{UW12(+singles)}} =& E_c^{\text{UW12}} + \sum_{ijkp}\left\langle ij\left|w_{12}\right|\overline{pj}\right\rangle\left\langle\overline{pk}\left|r_{12}^{-1}\right|ik\right\rangle \\
& - \sum_{ijkl}\left\langle ij\left|w_{12}\right|\overline{lj}\right\rangle\left\langle\overline{lk}\left|r_{12}^{-1}\right|ik\right\rangle \tag{B.4} \\
=& E_c^{\text{UW12}} + \sum_{ijk}\left\langle\overline{ij}k\left|w_{12}r_{23}^{-1}\right|\overline{ijk}\right\rangle \\
& - \sum_{ijkl}\left\langle ij\left|w_{12}\right|\overline{lj}\right\rangle\left\langle\overline{lk}\left|r_{12}^{-1}\right|ik\right\rangle, \tag{B.5}
\end{aligned}$$

and substituting in Eqns. 2.6, 2.8, 2.11, and 2.13 we obtain

$$\begin{aligned}
E_c^{\text{UW12(+singles)}} =\ & \frac{1}{2}\sum_{ij}\left\langle\overline{ij}\left|w_{12}r_{12}^{-1}\right|ij\right\rangle \\
& + \frac{1}{2}\sum_{ijkl}\left\langle ij\left|w_{12}\right|\overline{kl}\right\rangle\left\langle kl\left|r_{12}^{-1}\right|ij\right\rangle - \sum_{ijkl}\left\langle ij\left|w_{12}\right|\overline{lj}\right\rangle\left\langle\overline{lk}\left|r_{12}^{-1}\right|ik\right\rangle \\
& - \sum_{ijk}\left\langle ijk\left|w_{12}r_{23}^{-1}\right|\overline{ijk}\right\rangle, \tag{B.6}
\end{aligned}$$

where the ket $\left|\overline{ijk}\right\rangle$ is defined as

$$\left|\overline{ijk}\right\rangle = \left|ijk\right\rangle + \left|jki\right\rangle + \left|kij\right\rangle - \left|jik\right\rangle - \left|kji\right\rangle - \left|ikj\right\rangle. \tag{B.7}$$

The contribution from singly-excited determinants to the UW12 energy is currently not imple-

mented in entos. However, we see that it can be calculated using the same algorithms as for the contribution from doubly-excited determinants.

Bibliography

[1] T. C. Wiles and F. R. Manby. Wavefunction-like correlation model for use in hybrid density functionals. *J. Chem. Theory Comput.*, 14:4590–4599, 2018.

[2] A. Urban, D.-H. Seo, and G. Ceder. Computational understanding of Li-ion batteries. *npj Comput. Mater.*, 2:16002, 2016.

[3] L. E. Ratcliff, S. Mohr, G. Huhs, T. Deutsch, M. Masella, and L. Genovese. Challenges in large scale quantum mechanical calculations. *WIREs Comput. Mol. Sci.*, 7:e1290, 2017.

[4] J. Andzelm, B. C. Rinderspacher, A. Rawlett, J. Dougherty, R. Baer, and N. Govind. Performance of DFT methods in the calculation of optical spectra of TCF-Chromophores. *J. Chem. Theory Comput.*, 5:2835–2846, 2009.

[5] K. Raghavachari, G. W. Trucks, J. A. Pople, and M. Head-Gordon. A fifth-order perturbation comparison of electron correlation theories. *Chem. Phys. Lett.*, 157:479–483, 1989.

[6] G. Lever, D. J. Cole, R. Lonsdale, K. E. Ranaghan, D. J. Wales, A. J. Mulholland, C.-K. Skylaris, and M. C. Payne. Large-scale density functional theory transition state searching in enzymes. *J. Phys. Chem. Lett.*, 5:3614–3619, 2014.

[7] L. Goerigk, A. Hansen, C. Bauer, S. Ehrlich, A. Najibi, and S. Grimme. A look at

the density functional theory zoo with the advanced GMTKN55 database for general main group thermochemistry, kinetics and noncovalent interactions. *Phys. Chem. Chem. Phys.*, 19:32184–32215, 2017.

[8] N. Mardirossian and M. Head-Gordon. Thirty years of density functional theory in computational chemistry: an overview and extensive assessment of 200 density functionals. *Mol. Phys.*, 115:2315–2372, 2017.

[9] A. J. Cohen, P. Mori-Sánchez, and W. Yang. Fractional spins and static correlation error in density functional theory. *J. Chem. Phys.*, 129:121104, 2008.

[10] P. Mori-Sánchez, A. J. Cohen, and W. Yang. Localization and delocalization errors in density functional theory and implications for band-gap prediction. *Phys. Rev. Lett.*, 100:146401, 2008.

[11] A. J. Cohen, P. Mori-Sánchez, and W. Yang. Insights into current limitations of density functional theory. *Science*, 321:792–794, 2008.

[12] A. J. Cohen, P. Mori-Sánchez, and W. Yang. Challenges for density functional theory. *Chem. Rev.*, 112:289–320, 2012.

[13] N. Q. Su and X. Xu. The XYG3 type of doubly hybrid density functionals. *WIREs Comput. Mol. Sci.*, 6:721–747, 2016.

[14] A. D. Becke. Perspective: Fifty years of density-functional theory in chemical physics. *J. Chem. Phys.*, 140:18A301, 2014.

[15] N. C. Handy and A. M. Lee. The adiabatic approximation. *Chem. Phys. Lett.*, 252:425–430, 1996.

[16] E. F. Valeev and C. D. Sherrill. The diagonal Born–Oppenheimer correction beyond the Hartree–Fock approximation. *J. Chem. Phys.*, 118:3921–3927, 2003.

[17] A. Karton, E. Rabinovich, J. M. L. Martin, and B. Ruscic. W4 theory for computational thermochemistry: In pursuit of confident sub-kj/mol predictions. *J. Chem. Phys.*, 125(14):144108, 2006.

[18] A. Karton, A. Tarnopolsky, J.-F. Lamère, G. C. Schatz, and J. M. L. Martin. Highly accurate first-principles benchmark data sets for the parametrization and validation of density functional and other approximate methods. derivation of a robust, generally applicable, double-hybrid functional for thermochemistry and thermochemical kinetics. *J. Phys. Chem. A*, 112:12868–12886, 2008.

[19] A. Karton, S. Daon, and J. M. Martin. W4-11: A high-confidence benchmark dataset for computational thermochemistry derived from first-principles W4 data. *Chem. Phys. Lett.*, 510:165–178, 2011.

[20] T. H. Dunning Jr. Gaussian basis sets for use in correlated molecular calculations. I. the atoms boron through neon and hydrogen. *J. Chem. Phys.*, 90:1007–1023, 1989.

[21] R. A. Kendall, T. H. Dunning Jr., and R. J. Harrison. Electron affinities of the first-row atoms revisited. systematic basis sets and wave functions. *J. Chem. Phys.*, 96:6796–6806, 1992.

[22] D. E. Woon and T. H. Dunning Jr. Gaussian basis sets for use in correlated molecular calculations. III. the atoms aluminum through argon. *J. Chem. Phys.*, 98:1358–1371, 1993.

[23] D. E. Woon and T. H. Dunning Jr. Gaussian basis sets for use in correlated molecular calculations. IV. calculation of static electrical response properties. *J. Chem. Phys.*, 100:2975–2988, 1994.

[24] G. E. Scuseria and H. F. Schaefer. Is coupled cluster singles and doubles (ccsd) more

computationally intensive than quadratic configuration interaction (qcisd)? *J. Chem. Phys.*, 90(7):3700–3703, 1989.

[25] Z. Rolik, L. Szegedy, I. Ladjánszki, B. Ladóczki, and M. Kállay. An efficient linear-scaling ccsd(t) method based on local natural orbitals. *J. Chem. Phys.*, 139(9):094105, 2013.

[26] W. Kohn, A. D. Becke, and R. G. Parr. Density functional theory of electronic structure. *J. Phys. Chem.*, 100(31):12974–12980, 1996.

[27] S. H. Vosko, L. Wilk, and M. Nusair. Accurate spin-dependent electron liquid correlation energies for local spin density calculations: a critical analysis. *Can. J. Phys.*, 58:1200–1211, 1980.

[28] K. Capelle. A bird's-eye view of density-functional theory. *Braz. J. Phys.*, 36:1318–1343, December 2006.

[29] J. P. Perdew, K. Burke, and M. Ernzerhof. Generalized gradient approximation made simple. *Phys. Rev. Lett.*, 77:3865–3868, October 1996.

[30] Y. Zhao and D. G. Truhlar. A new local density functional for main-group thermochemistry, transition metal bonding, thermochemical kinetics, and noncovalent interactions. *J. Chem. Phys.*, 125(19):194101, 2006.

[31] C. Lee, W. Yang, and R. G. Parr. Development of the Colle-Salvetti correlation-energy formula into a functional of the electron density. *Phys. Rev. B*, 37:785–789, 1988.

[32] A. D. Becke. Density-functional exchange-energy approximation with correct asymptotic behavior. *Phys. Rev. A*, 38:3098–3100, 1988.

[33] S. Grimme. Semiempirical hybrid density functional with perturbative second-order correlation. *J. Chem. Phys.*, 124:034108, 2006.

[34] S. Kozuch and J. M. L. Martin. Spin-component-scaled double hybrids: An extensive search for the best fifth-rung functionals blending DFT and perturbation theory. *J. Comput. Chem.*, 34:2327–2344, 2013.

[35] A. D. Becke. Densityfunctional thermochemistry. III. the role of exact exchange. *J. Chem. Phys.*, 98:5648–5652, 1993.

[36] Y.-S. Lin, G.-D. Li, S.-P. Mao, and J.-D. Chai. Long-range corrected hybrid density functionals with improved dispersion corrections. *J. Chem. Theory Comput.*, 9(1):263–272, 2013. PMID: 26589028.

[37] J. Sun, A. Ruzsinszky, and J. P. Perdew. Strongly constrained and appropriately normed semilocal density functional. *Phys. Rev. Lett.*, 115:036402, July 2015.

[38] Y. Zhang and W. Yang. Comment on "generalized gradient approximation made simple". *Phys. Rev. Lett.*, 80:890–890, January 1998.

[39] J. P. Perdew and K. Schmidt. Jacob's ladder of density functional approximations for the exchange-correlation energy. *AIP Conf. Proc.*, 577:1–20, 2001.

[40] N. Mardirossian and M. Head-Gordon. ωB97X-V: A 10-parameter, range-separated hybrid, generalized gradient approximation density functional with nonlocal correlation, designed by a survival-of-the-fittest strategy. *Phys. Chem. Chem. Phys.*, 16:9904–9924, 2014.

[41] O. A. Vydrov and T. Van Voorhis. Nonlocal van der waals density functional: The simpler the better. *J. Chem. Phys.*, 133(24):244103, 2010.

[42] `entos`, an electronic structure program designed by F.R. manby and T.F. miller, 2017.

[43] R. S. Mulliken. Electronic structures of polyatomic molecules and valence. *Phys. Rev.*, 40:55–62, April 1932.

[44] R. S. Mulliken. Electronic structures of polyatomic molecules and valence. ii. general considerations. *Phys. Rev.*, 41:49–71, July 1932.

[45] A. D. Becke. A new mixing of Hartree-Fock and local density-functional theories. *J. Chem. Phys.*, 98:1372–1377, 1993.

[46] P. M. W. Gill, B. G. Johnson, J. A. Pople, and M. J. Frisch. An investigation of the performance of a hybrid of Hartree-Fock and density functional theory. *Int. J. Quantum Chem.*, 44:319–331, 1992.

[47] K. Burke. Perspective on density functional theory. *J. Chem. Phys.*, 136:150901, 2012.

[48] L. Goerigk and S. Grimme. Double-hybrid density functionals. *WIREs Comput. Mol. Sci.*, 4:576–600, 2014.

[49] E. Ruiz, D. R. Salahub, and A. Vela. Charge-transfer complexes: stringent tests for widely used density functionals. *J. Phys. Chem.*, 100:12265–12276, 1996.

[50] K. Sharkas, J. Toulouse, and A. Savin. Double-hybrid density-functional theory made rigorous. *J. Chem. Phys.*, 134:064113, 2011.

[51] Y. Zhao, N. E. Schultz, and D. G. Truhlar. Design of density functionals by combining the method of constraint satisfaction with parametrization for thermochemistry, thermochemical kinetics, and noncovalent interactions. *J. Chem. Theory Comput.*, 2:364–382, 2006.

[52] L. Goerigk and S. Grimme. A thorough benchmark of density functional methods for general main group thermochemistry, kinetics, and noncovalent interactions. *Phys. Chem. Chem. Phys.*, 13:6670–6688, 2011.

[53] C. Møller and M. S. Plesset. Note on an approximation treatment for many-electron systems. *Phys. Rev.*, 46:618–622, 1934.

[54] A. Görling and M. Levy. Correlation-energy functional and its high-density limit obtained from a coupling-constant perturbation expansion. *Phys. Rev. B*, 47:13105–13113, 1993.

[55] A. Görling and M. Levy. Exact Kohn-Sham scheme based on perturbation theory. *Phys. Rev. A*, 50:196–204, 1994.

[56] Y. Zhao, B. J. Lynch, and D. G. Truhlar. Doubly hybrid meta DFT: New multi-coefficient correlation and density functional methods for thermochemistry and thermochemical kinetics. *J. Phys. Chem. A*, 108:4786–4791, 2004.

[57] Y. Zhang, X. Xu, and W. A. Goddard. Doubly hybrid density functional for accurate descriptions of nonbond interactions, thermochemistry, and thermochemical kinetics. *Proc. Natl. Acad. Sci.*, 106:4963–4968, 2009.

[58] N. Q. Su, W. Yang, P. Mori-Sánchez, and X. Xu. Fractional charge behavior and band gap predictions with the XYG3 type of doubly hybrid density functionals. *J. Phys. Chem. A*, 118:9201–9211, 2014.

[59] W. Kurlancheek and M. Head-Gordon. Violations of N-representability from spin-unrestricted orbitals in møller–plesset perturbation theory and related double-hybrid density functional theory. *Mol. Phys.*, 107:1223–1232, 2009.

[60] R. C. Lochan and M. Head-Gordon. Orbital-optimized opposite-spin scaled second-order correlation: An economical method to improve the description of open-shell molecules. *J. Chem. Phys.*, 126:164101, 2007.

[61] F. Neese, T. Schwabe, S. Kossmann, B. Schirmer, and S. Grimme. Assessment of orbital-optimized, spin-component scaled second-order many-body perturbation theory for thermochemistry and kinetics. *J. Chem. Theory Comput.*, 5:3060–3073, 2009.

[62] R. Peverati and M. Head-Gordon. Orbital optimized double-hybrid density functionals. *J. Chem. Phys.*, 139:024110, 2013.

[63] J. C. Sancho-García, A. J. Pérez-Jiménez, M. Savarese, E. Brémond, and C. Adamo. Importance of orbital optimization for double-hybrid density functionals: Application of the OO-PBE-QIDH model for closed- and open-shell systems. *J. Phys. Chem. A*, 120:1756–1762, 2016.

[64] S. Śmiga, O. Franck, B. Mussard, A. Buksztel, I. Grabowski, E. Luppi, and J. Toulouse. Self-consistent double-hybrid density-functional theory using the optimized-effective-potential method. *J. Chem. Phys.*, 145:144102, 2016.

[65] Y. Jin, D. Zhang, Z. Chen, N. Q. Su, and W. Yang. Generalized optimized effective potential for orbital functionals and self-consistent calculation of random phase approximations. *J. Phys. Chem. Lett.*, 8:4746–4751, 2017.

[66] T. W. Hollins, S. J. Clark, K. Refson, and N. I. Gidopoulos. Optimized effective potential using the hylleraas variational method. *Phys. Rev. B*, 85:235126, June 2012.

[67] T. Hollins, S. Clark, N. Gidopoulos, and Condensed Matter Theory Group Team. The local fock exchange potential in kohn sham theory. In *APS March Meeting Abstracts*, page P1.358, 2014.

[68] A. I. Blair, A. Kroukis, and N. I. Gidopoulos. A correction for the hartree-fock density of states for jellium without screening. *J. Chem. Phys.*, 142(8):084116, 2015.

[69] T. W. Hollins, S. J. Clark, K. Refson, and N. I. Gidopoulos. A local fock-exchange potential in kohn–sham equations. *J. Phys. Condens. Matter*, 29(4):04LT01, November 2016.

[70] S. J. Clark, T. W. Hollins, K. Refson, and N. I. Gidopoulos. Self-interaction free local ex-

change potentials applied to metallic systems. *J. Phys. Condens. Matter*, 29(37):374002, August 2017.

[71] J. P. Perdew, R. G. Parr, M. Levy, and J. L. Balduz. Density-functional theory for fractional particle number: Derivative discontinuities of the energy. *Phys. Rev. Lett.*, 49:1691–1694, 1982.

[72] W. Yang, Y. Zhang, and P. W. Ayers. Degenerate ground states and a fractional number of electrons in density and reduced density matrix functional theory. *Phys. Rev. Lett.*, 84:5172–5175, 2000.

[73] B. G. Janesko and G. E. Scuseria. Hartree–Fock orbitals significantly improve the reaction barrier heights predicted by semilocal density functionals. *J. Chem. Phys.*, 128:244112, 2008.

[74] M.-C. Kim, E. Sim, and K. Burke. Ions in solution: Density corrected density functional theory (DC-DFT). *J. Chem. Phys.*, 140:18A528, 2014.

[75] M.-C. Kim, E. Sim, and K. Burke. Understanding and reducing errors in density functional calculations. *Phys. Rev. Lett.*, 111:073003, 2013.

[76] M.-C. Kim, E. Sim, and K. Burke. Communication: Avoiding unbound anions in density functional calculations. *J. Chem. Phys.*, 134:171103, 2011.

[77] M.-C. Kim, H. Park, S. Son, E. Sim, and K. Burke. Improved DFT potential energy surfaces via improved densities. *J. Phys. Chem. Lett.*, 6:3802–3807, 2015.

[78] A. J. Cohen, P. Mori-Sánchez, and W. Yang. Development of exchange-correlation functionals with minimal many-electron self-interaction error. *J. Chem. Phys.*, 126:191109, 2007.

[79] R. G. Parr and W. Yang. *Density-Functional Theory of Atoms and Molecules*, volume 16

of *International series of monographs on chemistry*. Oxford University Press, New York, 1989.

[80] A. J. Cohen, P. Mori-Sánchez, and W. Yang. Second-order perturbation theory with fractional charges and fractional spins. *J. Chem. Theory Comput.*, 5:786–792, 2009.

[81] I. Y. Zhang, X. Xu, Y. Jung, and W. A. Goddard. A fast doubly hybrid density functional method close to chemical accuracy using a local opposite spin ansatz. *Proc. Natl. Acad. Sci.*, 108:19896–19900, 2011.

[82] F. Weigend. Hartree-Fock exchange fitting basis sets for H to Rn. *J. Comput. Chem.*, 29:167–175, 2008.

[83] J. L. Whitten. Coulombic potential energy integrals and approximations. *J. Chem. Phys.*, 58:4496–4501, 1973.

[84] B. I. Dunlap, J. W. D. Connolly, and J. R. Sabin. On some approximations in applications of Xα theory. *J. Chem. Phys.*, 71:3396–3402, 1979.

[85] O. Vahtras, J. Almlöf, and M. Feyereisen. Integral approximations for LCAO-SCF calculations. *Chem. Phys. Lett.*, 213:514–518, 1993.

[86] Y. Jung, A. Sodt, P. M. W. Gill, and M. Head-Gordon. Auxiliary basis expansions for large-scale electronic structure calculations. *Proc. Natl. Acad. Sci.*, 102:6692–6697, 2005.

[87] A. D. Becke. A multicenter numerical integration scheme for polyatomic molecules. *J. Chem. Phys.*, 88(4):2547–2553, 1988.

[88] G. te Velde and E. Baerends. Numerical integration for polyatomic systems. *J. Comput. Phys.*, 99(1):84–98, 1992.

[89] C. W. Murray, N. C. Handy, and G. J. Laming. Quadrature schemes for integrals of density functional theory. *Molecular Physics*, 78(4):997–1014, 1993.

[90] A. Unsöld. Quantentheorie des Wasserstoffmolekülions und der Born-Landéschen Abstoßungskräfte. *Zeitschrift für Physik*, 43:563–574, 1927.

[91] W. Klopper and W. Kutzelnigg. Møller-Plesset calculations taking care of the correlation cusp. *Chem. Phys. Lett.*, 134:17–22, 1987.

[92] W. Kutzelnigg and W. Klopper. Wave functions with terms linear in the interelectronic coordinates to take care of the correlation cusp. I. general theory. *J. Chem. Phys.*, 94:1985–2001, 1991.

[93] S. F. Boys and N. C. Handy. The determination of energies and wavefunctions with full electronic correlation. *Proc. R. Soc. Lon. Ser. A*, 310:43–61, 1969.

[94] S. Ten-no. Explicitly correlated second order perturbation theory: Introduction of a rational generator and numerical quadratures. *J. Chem. Phys.*, 121:117–129, 2004.

[95] H.-J. Werner, T. B. Adler, and F. R. Manby. General orbital invariant MP2-F12 theory. *J. Chem. Phys.*, 126:164102, 2007.

[96] F. Della Sala and A. Görling. Asymptotic behavior of the Kohn-Sham exchange potential. *Phys. Rev. Lett.*, 89:033003, 2002.

[97] D. M. Wilkins, A. Grisafi, Y. Yang, K. U. Lao, R. A. DiStasio, and M. Ceriotti. Accurate molecular polarizabilities with coupled cluster theory and machine learning. *Proc. Natl. Acad. Sci. U.S.A.*, 116:3401–3406, 2019.

[98] F. Della Sala and A. Görling. Efficient localized Hartree–Fock methods as effective exact-exchange Kohn–Sham methods for molecules. *J. Chem. Phys.*, 115:5718–5732, 2001.

[99] O. V. Gritsenko and E. J. Baerends. Orbital structure of the Kohn-Sham exchange potential and exchange kernel and the field-counteracting potential for molecules in an electric field. *Phys. Rev. A*, 64:042506, 2001.

[100] M. Grüning, O. V. Gritsenko, and E. J. Baerends. Exchange potential from the common energy denominator approximation for the Kohn–Sham Green's function: Application to (hyper)polarizabilities of molecular chains. *J. Chem. Phys.*, 116:6435–6442, 2002.

[101] A. Grüneis. Efficient explicitly correlated many-electron perturbation theory for solids: Application to the Schottky defect in mgo. *Phys. Rev. Lett.*, 115:066402, 2015.

[102] W. Klopper, F. R. Manby, S. Ten-No, and E. F. Valeev. R12 methods in explicitly correlated molecular electronic structure theory. *Int. Rev. Phys. Chem.*, 25:427–468, 2006.

[103] L. Kong, F. A. Bischoff, and E. F. Valeev. Explicitly correlated R12/F12 methods for electronic structure. *Chem. Rev.*, 112:75–107, 2012.

[104] S. Ten-no. Initiation of explicitly correlated Slater-type geminal theory. *Chem. Phys. Lett.*, 398:56–61, 2004.

[105] D. P. Tew and W. Klopper. New correlation factors for explicitly correlated electronic wave functions. *J. Chem. Phys.*, 123(7):074101, 2005.

[106] P. M. Gill, B. G. Johnson, and J. A. Pople. A standard grid for density functional calculations. *Chem. Phys. Lett.*, 209:506–512, 1993.

[107] J. Reinders. *Intel threading building blocks: outfitting C++ for multi-core processor parallelism.* " O'Reilly Media, Inc.", 2007.

[108] K. L. Bak, J. Gauss, P. Jørgensen, J. Olsen, T. Helgaker, and J. F. Stanton. The accurate determination of molecular equilibrium structures. *J. Chem. Phys.*, 114:6548–6556, 2001.

[109] F. Weigend. A fully direct RI-HF algorithm: Implementation, optimised auxiliary basis sets, demonstration of accuracy and efficiency. *Phys. Chem. Chem. Phys.*, 4:4285–4291, 2002.

[110] J. G. Hill and J. A. Platts. Auxiliary basis sets for density fitting–MP2 calculations: Nonrelativistic triple-ζ all-electron correlation consistent basis sets for the 3d elements sc–zn. *J. Chem. Phys.*, 128:044104, 2008.

[111] M. Head-Gordon, J. A. Pople, and M. J. Frisch. MP2 energy evaluation by direct methods. *Chem. Phys. Lett.*, 153:503–506, 1988.

[112] M. Häser and R. Ahlrichs. Improvements on the direct SCF method. *J. Comput. Chem.*, 10:104–111, 1989.

[113] D. S. Lambrecht, B. Doser, and C. Ochsenfeld. Rigorous integral screening for electron correlation methods. *J. Chem. Phys.*, 123:184102, 2005.

[114] J. C. Womack. *Evaluating many-electron molecular integrals for quantum chemistry*. PhD thesis, University of Bristol, 2015.

[115] S. Obara and A. Saika. Efficient recursive computation of molecular integrals over cartesian Gaussian functions. *J. Chem. Phys.*, 84:3963–3974, 1986.

[116] T. Yanai, D. P. Tew, and N. C. Handy. A new hybrid exchange–correlation functional using the Coulomb-attenuating method (CAM-B3LYP). *Chem. Phys. Lett.*, 393:51–57, 2004.

[117] L. E. McMurchie and E. R. Davidson. One- and two-electron integrals over cartesian gaussian functions. *J. Chem. Phys.*, 26(2):218–231, 1978.

[118] J. A. Pople and W. J. Hehre. Computation of electron repulsion integrals involving contracted gaussian basis functions. *J. Chem. Phys.*, 27(2):161–168, 1978.

[119] A. J. May. *Density fitting in explicitly correlated electronic structure theory*. PhD thesis, University of Bristol, 2006. The auxiliary integral definitions can be found on Page 69 of Andrew May's thesis.

[120] J. Toulouse, K. Sharkas, E. Brémond, and C. Adamo. Communication: Rationale for a new class of double-hybrid approximations in density-functional theory. *J. Chem. Phys.*, 135:101102, 2011.

[121] E. Brémond and C. Adamo. Seeking for parameter-free double-hybrid functionals: The PBE0-DH model. *J. Chem. Phys.*, 135:024106, 2011.

[122] J.-D. Chai and S.-P. Mao. Seeking for reliable double-hybrid density functionals without fitting parameters: The PBE0-2 functional. *Chem. Phys. Lett.*, 538:121–125, 2012.

[123] T. H. Dunning Jr., K. A. Peterson, and A. K. Wilson. Gaussian basis sets for use in correlated molecular calculations. X. the atoms aluminum through argon revisited. *J. Chem. Phys.*, 114:9244–9253, 2001.

[124] F. Weigend and R. Ahlrichs. Balanced basis sets of split valence, triple zeta valence and quadruple zeta valence quality for H to Rn: Design and assessment of accuracy. *Phys. Chem. Chem. Phys.*, 7:3297–3305, 2005.

[125] B. J. Lynch and D. G. Truhlar. Small representative benchmarks for thermochemical calculations. *J. Phys. Chem. A*, 107:8996–8999, 2003.

[126] A. Karton and J. M. L. Martin. Basis set convergence of explicitly correlated double-hybrid density functional theory calculations. *J. Chem. Phys.*, 135:144119, 2011.

[127] B. Chan and L. Radom. Obtaining good performance with triple-ζ-type basis sets in double-hybrid density functional theory procedures. *J. Chem. Theory Comput.*, 7:2852–2863, 2011.

[128] P. L. Fast, J. Corchado, M. L. Sanchez, and D. G. Truhlar. Optimized parameters for scaling correlation energy. *J. Phys. Chem. A*, 103:3139–3143, 1999.

[129] J. Zheng, Y. Zhao, and D. G. Truhlar. The DBH24/08 database and its use to assess

electronic structure model chemistries for chemical reaction barrier heights. *J. Chem. Theory Comput.*, 5:808–821, 2009.

[130] L. Goerigk and S. Grimme. A general database for main group thermochemistry, kinetics, and noncovalent interactions − assessment of common and reparameterized (meta-)GGA density functionals. *J. Chem. Theory Comput.*, 6:107–126, 2010.

[131] J. T. Margraf, D. S. Ranasinghe, and R. J. Bartlett. Automatic generation of reaction energy databases from highly accurate atomization energy benchmark sets. *Phys. Chem. Chem. Phys.*, 19:9798–9805, 2017.

[132] T. Benighaus, R. A. DiStasio, R. C. Lochan, J.-D. Chai, and M. Head-Gordon. Semiempirical double-hybrid density functional with improved description of long-range correlation. *J. Phys. Chem. A*, 112:2702–2712, 2008.

[133] F. Jensen. Polarization consistent basis sets: Principles. *J. Chem. Phys.*, 115:9113–9125, 2001.

[134] F. Jensen. Polarization consistent basis sets. II. estimating the Kohn–Sham basis set limit. *J. Chem. Phys.*, 116:7372–7379, 2002.

[135] F. Jensen. Polarization consistent basis sets. III. the importance of diffuse functions. *J. Chem. Phys.*, 117:9234–9240, 2002.

[136] F. Jensen and T. Helgaker. Polarization consistent basis sets. V. the elements Si–Cl. *J. Chem. Phys.*, 121:3463–3470, 2004.

[137] F. Jensen. Polarization consistent basis sets. 4: the elements He, Li, Be, B, Ne, Na, Mg, Al, and Ar. *J. Phys. Chem. A*, 111:11198–11204, 2007.

[138] A. Schäfer, C. Huber, and R. Ahlrichs. Fully optimized contracted Gaussian basis sets of triple zeta valence quality for atoms Li to Kr. *J. Chem. Phys.*, 100:5829–5835, 1994.

[139] I. Y. Zhang, N. Q. Su, É. A. G. Brémond, C. Adamo, and X. Xu. Doubly hybrid density functional xDH-PBE0 from a parameter-free global hybrid model PBE0. *J. Chem. Phys.*, 136:174103, 2012.

[140] E. F. Valeev. Combining explicitly correlated r12 and gaussian geminal electronic structure theories. *J. Chem. Phys.*, 125(24):244106, 2006.

[141] J. F. Janak. Proof that $\frac{\partial e}{\partial n_i} = \epsilon$ in density-functional theory. *Phys. Rev. B*, 18:7165–7168, 1978.

[142] P. Verma, Z. Varga, J. E. M. N. Klein, C. J. Cramer, L. Que, and D. G. Truhlar. Assessment of electronic structure methods for the determination of the ground spin states of Fe(ii), Fe(iii) and Fe(iv) complexes. *Phys. Chem. Chem. Phys.*, 19:13049–13069, 2017.

[143] I. Y. Zhang, P. Rinke, and M. Scheffler. Wave-function inspired density functional applied to the H_2/H_2^+ challenge. *New J. Phys.*, 18:073026, 2016.

[144] X. Zheng, A. J. Cohen, P. Mori-Sánchez, X. Hu, and W. Yang. Improving band gap prediction in density functional theory from molecules to solids. *Phys. Rev. Lett.*, 107:026403, 2011.

[145] J.-D. Chai and M. Head-Gordon. Long-range corrected double-hybrid density functionals. *J. Chem. Phys.*, 131:174105, 2009.

[146] F. Neese, T. Schwabe, and S. Grimme. Analytic derivatives for perturbatively corrected "double hybrid" density functionals: Theory, implementation, and applications. *J. Chem. Phys.*, 126(12):124115, 2007.

[147] M. S. Marshall, L. A. Burns, and C. D. Sherrill. Basis set convergence of the coupled-cluster correction, δMP2CCSD(T): Best practices for benchmarking non-covalent in-

teractions and the attendant revision of the S22, NBC10, HBC6, and HSG databases. *J. Chem. Phys.*, 135:194102, 2011.

[148] S. Grimme, J. Antony, S. Ehrlich, and H. Krieg. A consistent and accurate ab initio parametrization of density functional dispersion correction (DFT-D) for the 94 elements H-Pu. *J. Chem. Phys.*, 132:154104, 2010.

[149] G. Stefan, E. Stephan, and G. Lars. Effect of the damping function in dispersion corrected density functional theory. *J. Comput. Chem.*, 32:1456–1465, 2011.

[150] P.-F. Loos and P. M. Gill. Excited states of spherium. *Mol. Phys.*, 108:2527–2532, 2010.

[151] T. Kato. On the eigenfunctions of many-particle systems in quantum mechanics. *Commun. Pure Appl. Math.*, 10:151–177, 1957.

[152] R. T. Pack and W. B. Brown. Cusp conditions for molecular wavefunctions. *J. Chem. Phys.*, 45:556–559, 1966.

[153] W. Kutzelnigg and J. D. Morgan. Rates of convergence of the partial-wave expansions of atomic correlation energies. *J. Chem. Phys.*, 96:4484–4508, 1992.

List of Corrections

Correction Number	Action Completed and Location in Revised Thesis
1.1	Chapters 1 and 2 in original thesis combined and re-titled. Chapter 3 in original thesis renumbered as Chapter 2
1.2	Added Section 1.12.1 on page 29
1.3	Added Section 1.20 on page 53
2.1	Moved footnotes into text, especially in Section 1.5, Section 1.6, and Section 1.8
2.2	Clarified text in Chapter 1 to avoid assumed knowledge
2.3	Chapter 1 lengthened significantly
2.4	Copyright notice removed from the start of each chapter
2.5	Added Section 3.1.1 on page 67, including a table showing the number of lines of code added
2.6	Turned bold information note into a sentence at the start of Section 1.2 on page 2
2.7	Added Section 1.3 on page 5
2.8	Added Section 1.4 on page 5
2.9	Added critical analysis to Section 1.4 on page 5

2.10	Added equation numbers to all equations
2.11	Removed $U_{n,n}$ from the definition of H_{el} (Eqn 1.2 on page 2)
2.12	Notation $V_n(\boldsymbol{r})$ changed to $V_{el,n}(\boldsymbol{r})$
2.13	Added discussion after Eqn 1.28 on page 10 and added a full discussion to Section 1.17
2.14	Added description of the first Hohenberg-Kohn theorem to Section 1.5
2.15	Added description of the second Hohenberg-Kohn theorem to Section 1.5
2.16	Added a final remark to Section 1.6 about how the Kohn-Sham method is exact in principle
2.17	Added Eqn 1.33 on page 12 and added more text to end of Section 1.6 to clarify
2.18	Added Section 1.7
2.19	Added description of the uniform-electron-gas to Section 1.7
2.20	Included a note on formal-scaling at the end of Section 1.4
2.21	Added some text about GEAs and GGAs to Section 1.8
2.22	Changed PBE0 reference to PBE as suggested. Added citations for PBE and M06-L to Section 1.8. Added some text about GGAs to Section 1.8.
2.23	Added sentences to Section 1.8 clarifying local / semi-local / non-local
2.24	Added Section 1.9 on page 22 about Gaussian basis-sets. Decided not to include r12/F12 theories as we do not make use of them.
2.25	Added Footnote 2 on page 21
2.26	Added Section 1.6.1 on page 14 and expanded Section 1.10 on page 23
2.27	Added a note about OEP to the end of Section 1.14.1

2.28	Moved discussion of density fitting to here (added Section 1.19.1 on page 48) as suggested
2.29	Added Section 1.19.2 on page 52 about quadrature, with citations
2.30	Added note on convergence criteria to Section 1.10
2.31	Extended Section 1.15 and clarified
2.32	Added Section 1.16 on page 42 introducing non-integer spin errors
2.33	Changed notation for $\rho(\mathbf{x}|\mathbf{x}')$ in Section 1.18 to be consistent with the rest of the thesis
2.34	Added a reference to Fig 6.4 on page 147 to Section 1.18. Decided not to introduce Janak's theorem and derivative gaps as we don't calculate them, and they can don't add any information that isn't captured in Δ_{frac} for the systems we studied.
2.35	Corrected spelling and added references to Mulliken's 1932 papers after Eqn 1.77
2.36	Mulliken notation corrected in Eqn 1.77 on page 26, Eqn 2.9 on page 58, Eqn 2.12 on page 58 and Eqn 2.14 on page 58
2.37	Added a note on the adiabatic connection to the beginning of Section 1.12
2.38	Added references to Görling-Levy perturbation theorty to the start of Section 1.14. Added a note that F is the Fock operator after Eqn 1.89.
2.39	Added a note on range-separated double-hybrids to the end of Section 1.14
2.40	Added more detail and reference to Section 1.14
2.41	Added a note about Janak's theorem, and lengthened Section Section 1.14.1

2.42	Gave a backgroud to OEP in Section 1.14.1 and discussed orbital optimization
2.43	Added a clear definition or reference for each functional in Table 1.1 on page 20. Included benchmark values. Also included discussion with values in Section 1.12.1.
2.44	Added discussion of self-consistent optimization of PT2 to Section 1.14.1
3.1	Added Section 2.1.1 on page 55
3.2	Added Section 2.1.1 on page 55
3.3	Added Section 3.1.1 on page 67, and Section 4.1.1 on page 88
3.4	Added Section 2.2.3 on page 61, and Section 2.2.4 on page 63
3.5	Added a reference to the new Section 1.9 into Section 1.14, and into Section 2.1
3.6	Corrected Eqn 2.10 on page 58
3.7	Added Footnote 2 on page 59
3.8	Corrected typo just after Eqn 2.36
4.1	Added Section 3.1.2 on page 70
4.2	Added text above Eqn 1.131
4.3	Added a brief note about robust density fitting to Section 1.19.1
4.4	Added Eqn 1.134 on page 50
4.5	Corrected Eqn 1.134 on page 50
4.6	Added Section 3.4 on page 84 and Section 3.5 on page 84
4.7	Added notes on future work to Sections 3.2.2.1 and 3.5
4.8	Added Section 4.1.1 on page 88

4.9	Adjusted line spacing in Listing 4.1 on page 90, and Listing 4.2 on page 107, and Listing 4.3 on page 110. Code comments were all deemed necessary.
4.10	Added explanation around Eqn 3.5 on page 72
4.11	Added explanation around Eqn 3.5 on page 72
4.12	Corrected Eqn 3.9 on page 73
4.13	Added notes about choice of density fitting kernel after Eqns 3.13, 3.32, and 3.33.
4.14	Added Section 4.1.1 on page 88
4.15	Changed w_λ to g_λ throughout for clarity for the grid weights
4.16	Added Section 3.2.2.1 on page 76
4.17	Added more discussion and concluding remarks to Section 3.3.1
4.18	Added Footnote 3 on page 70
4.19	Added Footnote 11 on page 82
4.20	Moved all table captions above tables
4.21	Rebalanced discussion between text and caption of Table 3.2 on page 81
4.22	Added Footnote 10 on page 82
4.23	Added Section 3.3.2 on page 82
5.1	Added Section 4.1.1 on page 88 and expanded Section 4.3.2.1 on page 101
5.2	Added Section 4.1.1 on page 88 and Section 4.3.6 on page 111
5.3	Added paragraph on calculating and passing of $c_{s\gamma}$ coefficients to Section 4.2
5.4	Added Eqn 4.12 on page 92 and some text about setting exponents to zero
5.5	Added a derivation to Section 4.3.1. Added Footnote 3 on page 93

5.6	Cited Andrew May's thesis properly in Section 4.3.2.1
5.7	Added a note about the significance of the choice of formalism to Section 4.3.2.1
5.8	Added a paragraph to Section 4.3.2.1 about how the code is affected
5.9	Added discussion of Obara-Saika advantages to Section 4.3
5.10	Added a sentence to Section 4.1.1 about how the Coulomb-attentuated integrals were used and another sentence to Section 4.3.5
5.11	Coulomb-attentuated integrals are mentioned in passing but are not used in the project, so a literature comparison of different evaluation methods was not done
5.12	Added a reference to the expanded Section 3.5
5.13	Added Section 3.2.5 on page 79
6.1	Added further discussion of results. Chapters 5 and 6 lengthened significantly.
6.2	Extended Section 6 with a discussion of modern test sets
6.3	Added note about UW12 fraction to the start of Section 5.2
6.4	Added a note on r_c scaling to Section 2.3 and to the start of Section 5.2
6.5	Added Fig 5.3 on page 126, and additional discussion of the individual BH6 errors to Section 5.4
6.6	Added more detailed explanation of basis-set convergence figure to Section 5.4.
7.1	Added Section 6.2.1 on page 132
7.2	Added discussion of functional prefixes after Eqn 6.1
7.3	Added Section 6.4.2 on page 136 and Fig 6.1 on page 141

7.4	Added Section 6.4.3 on page 137
7.5	Added Footnote 7 on page 138
7.6	Added reference to footnote about VWN variant in caption of Table 6.1 on page 140
7.7	Changed references to Figs 6.2 and 6.3 in Section 6.5
8.1	Lengthened Footnote 1 on page 151
8.2	Added critical analysis of future work to Section 7.2
8.3	Added a new paragraph to Section 7.2 containing a reference to Neese et al's Journal of Chemical Physics paper
B.1	All bras now match their corresponding kets in height in Appendices A and B
R.1	Removed PMID from all bibliography entries
R.2	Removed month from all bibliography entries
R.3	Removed "review article" note from all bibliography entries
R.4	Removed issue number from all bibliography entries
R.5	Used initials-only format for all bibliography entries
R.6	Fixed capitalisation errors in chemical formulae, surnames, and abbreviations in article titles